Fakultät für Medizin, Technische Universität München

The role of HNF1B in pancreatic cancer initiation and progression

Suyang Zhong

Vollständiger Abdruck der von der Fakultät für Medizin der Technischen Universität München zur Erlangung des akademischen Grades eines

Doktors der Naturwissenschaften (**Dr. rer. nat.**)

genehmigten Dissertation.

Vorsitzender: Prof. Dr. Radu Roland Rad

Prüfer/-in der Dissertation:

1. Priv.-Doz. Dr. Guido von Figura
2. Prof. Dr. Angelika Schnieke

Die Dissertation wurde am 16.11.2020 bei der Technischen Universität München eingereicht und durch die Fakultät für Medizin am 09.03.2021 angenommen.

Table of Contents

List of Figures

List of Tables

Abstract

Pancreatic ductal adenocarcinoma (PDAC) is an exocrine pancreatic cancer characterized by a dismal prognosis. PDAC develops by multistep progression from precursor lesions acinar-to-ductal metaplasia (ADM) to pancreatic intraepithelial neoplasia (PanIN) and finally invasive cancer. Mutations or dysregulation of some transcription factors (TFs) affect cancer progression and hallmark characteristics of PDAC.

Hepatocyte nuclear factor-1 beta (HNF1B) is a homeodomain-containing TF which is essential for the embryonic development of the organs derived from endoderm including pancreas. More importantly, HNF1B is associated with human pancreatic cancer risk, tumor differentiation and prognosis. However, the role of HNF1B in pancreatic carcinogenesis and maintenance of pancreatic cancer has not been fully elucidated.

Since PDAC can originate from acinar cells, in current project we investigated the contribution of murine Hnf1b from mature acinar cells to carcinogenesis. To do so, Kras^{G12D} expression and *Hnf1b* ablation was induced in the pancreata of adult mice (i.e., *ptf1aCreER; Kras^{G12D}; Hnf1b$^{fl/fl}$*). It is shown that ablation of *Hnf1b* in mature acinar cells significantly inhibited PanIN formation. In combination with cerulein-induced acute pancreatitis, *Hnf1b* ablation also ameliorated the inflammation and pre-cancerous lesions.

In vitro culture of acinar cells revealed that Hnf1b was dispensable for the initiation of ADM, but was required for the proliferation of metaplasia cells. Consistently, *in vivo* staining showed fewer proliferative (Ki67$^+$) metaplasia cells in *Hnf1b*-deficient acinar cells.

In human PDAC cell lines, HNF1B expressed in well-differentiated PDAC cell lines but not in poorly-differentiated cells. Interestingly, knockout of *HNF1B* by CRISPR-Cas9 did not affect epithelial-mesenchymal transition (EMT) or morphology of PDAC cells. However, knockout of *HNF1B* suppressed the proliferation and colony formation of

CFPAC-1 cells via regulation of potential target genes including *PPP2R5C*, which resulted in attenuated activation of Akt.

In murine PDAC cells, Hnf1b was expressed in epithelial cell lines, but significantly decreased in mesenchymal cell lines. However, knockout of *Hnf1b* did not lead to EMT, but promoted the proliferation of murine cancer cells, indicating *Hnf1b* is a tumor suppressor gene in murine PDAC.

In conclusion, Hnf1b is a mediator for Kras^{G12D}-driven PanIN formation in the mouse model. Human HNF1B is required for cell proliferation in well-differentiated PDAC cells, while murine Hnf1b inhibits the proliferation of epithelial PDAC cells. Taken together, this project reveals the role of Hnf1b in carcinogenesis, and highlights the versatile roles of the same gene under different conditions.

Zusammenfassung

Das duktale Adenokarzinom des Pankreas (PDAC) ist gekennzeichnet durch eine schlechte Prognose. PDAC entwickelt sich schrittweise aus azino-duktale Metaplasie (ADM), aus welchen pankreatische intraepitheliale Neoplasien (PanIN) und schliesslich invasives Karzinom entsteht. Es gibt Hinweise auf mehrere Transkriptionsfaktoren (TF), die eine entscheidende Rolle bei der Karzinomentstehung spielen und als Marker für PDAC-Subtypisierungen etabliert wurden.

Hepatocyte nuclear factor-1 beta (HNF1B) ist ein homeodomain-enthaltender TF, der essential für die Embryonalentwicklung von Organen des Endoderms also auch des Pankreas ist. Interessanterweise ist HNF1B mit einem erhöhten Pankreaskarzinomrisiko, Tumordifferenzierung und Prognose assoziiert. Allerdings ist die exakte Rolle von HNF1B in der Pankreaskarzinomentstehung und –progression bislang nicht geklärt.

Da PDAC aus Azinuszellen entstehen kann, wurde in der vorliegenden Arbeit untersucht, welche Rolle Hnf1b in adulten Azinuszellen bei der Karzinogenese spielt. Hierfür wurden Mäuse, die eine Kras^{G12D} Expression und *Hnf1b* Ablation im Pankreas adulter Tiere erlauben, verwendet (*ptf1aCreER; Kras^{G12D}; Hnf1b$^{fl/fl}$*). Es konnte gezeigt werden, dass eine *Hnf1b* Ablation in adulten Azinuszellen die PanIN Entstehung signifikant inhibierte. In Kombination mit einer Cerulein-induzierten akuten Pankreatitis führte eine *Hnf1b* Ablation zu einer verminderten Inflammation und Ausbildung von PDAC-Vorläuferläsionen.

In vitro Kultur von Azinuszellen zeigte, dass Hnf1b für die Initiierung von ADM nicht notwendig aber für die Proliferation metaplastischer Zellen essentiell war. *In vivo* Färbung zeigte hier eine geringere Anzahl Ki67^{+} metaplastischer Zellen in *Hnf1b*-defizienten Azinuszellen.

In humanen PDAC Zelllinien konnte gezeigt werden, dass HNF1B in gut differenzierten, nicht aber in schlecht differenzierten PDAC-Zelllinien exprimiert war. Interessanterweise beeinflusste eine Ablation von HNF*1B* mittels CRISPR-Cas9 weder die epithelial-mesenchymale Transition (EMT) noch die Morphologie von PDAC

Zellen. Allerdings führte der Knockout von *HNF1B* zu einer verminderte Proliferation und Kolonieformation von CFPAC-1 Zellen mutmaßlich über die Regulation potentieller Targetgene wie *PPP2R5C*, was in einer verminderten Aktivierung von Akt resultierte.

In murinen PDAC Zelllinien zeigte sich eine Hnf1b Expression in epithelial differentierten Zelllinien, jedoch wiesen mesenchymal differentierte Zelllinien eine signifikant verminderte Expression auf. Interessanterweise führte ein Knockout von *Hnf1b* nicht zu EMT sondern verstärkte die Proliferation muriner PDAC Zellen, was darauf hinweist, dass *Hnf1b* als Tumorsuppressor in murinem PDAC fungiert.

Zusammenfassend zeigte sich, dass Hnf1b eine wichtige Funktion in der Kras^{G12D} vermittelten Entstehung von PanINs spielt. Humanes HNF1B ist essentiell für Zellproliferation gut differenzierte PDAC Zellen, wohingegen murines Hnf1b die Zellproliferation epithelialer PDAC Zellen vermindert. Somit konnte in dieser Arbeit die entscheidende Rolle von Hnf1b in der Pankreaskarzinomentstehung und die Kontext-abhängigen Funktionen dieses Gens in verschiedenen Zelllinien aufgezeigt werden.

1 Introduction

1.1 Exocrine pancreas and pancreatic ductal adenocarcinoma

1.1.1 Structure and functions of exocrine pancreas

The pancreas is divided into the endocrine (islets of Langerhans) and exocrine compartments. The islets of Langerhans consist of glucagon-producing α-cells, insulin producing β-cells, with the remainder δ-cells (somatostatin-producing), γ- or PP cells (pancreatic polypeptide-producing), and ε-cells (ghrelin-producing) [1]. The exocrine pancreas mainly contains two major cell types: acinar cells and ductal cells. The acinar cells are formed into a unit called acinus [2]. An acinus and its draining ductule compose the functional unit of the exocrine pancreas. A ductule from the acinus drains into interlobular ducts, which then drain into the main pancreatic duct. In mice, the major pancreatic duct joins the common bile duct before it enters the duodenum [3].

The exocrine pancreas has two major physiologic functions. Firstly, it supplies the enzymes and zymogens (from acinar cells) that are needed for digesting dietary lipids, carbohydrates, and proteins. Secondly, it secretes a bicarbonate-rich fluid (from ductal cells) that neutralizes gastric acid and facilitates digestion by pancreatic enzymes [4]. The acinar cell synthesizes, stores and secretes digestive enzymes, including proteinases, phospholipases and colipases as zymogens, as well as amylase, lipases and ribonucleases in active forms [5]. In addition, the acinar cell also expresses some proteinase inhibitors such as pancreatic secretory trypsin inhibitor (encoded by *SPINK1* gene) to protect the pancreas from the damage by premature activation of trypsin [5].

Some highly expressed enzymes such as amylase, carboxypeptidase A, and elastase, as well as transcription factors including Ptf1a, Mist1 and Rbpjl are frequently recognized as acinar cell-specific markers. The protein and mRNA levels of these enzymes and transcription factors are examined by immunohistochemistry (IHC) staining and reverse transcription polymerase chain reaction (RT-PCR) respectively to assess the cellular identity/injury of acinar cells.

Duct cells form the ductal epithelial tree to secrete bicarbonate-rich fluid and drain the proteins secreted by acinar cells. Ductal cells contain abundant mitochondria to provide energy products (ATPs) needed for ion transport [2]. Ductal markers used to label and identify ductal epithelium include carbonic anhydrase II (CAII), mucin 1, cystic

fibrosis transmembrane receptor (CFTR), and various cytokeratins (for example CK19). In addition, duct-specific transcription factors including Hnf1β, Hnf6 and Sox9 express throughout the ductal epithelial tree [6] and are also recognized as ductal markers. Beside of acinar cells and ductal cells, centroacinar cells (CACs) locate in the center of a secretory acinus and bridge the acinus and terminal ductal epithelium (**Figure 1-1**). These cells are considered as specialized ductal cells because they express ductal markers including CAII [7] and CFTR [8]. However, the role of centroacinar cells in response to injury and carcinogenesis, and whether CACs are progenitors in adult mammals is still not fully understood [9].

Pancreatic stellate cells (PSCs) comprise approximately 4% of all pancreatic cells [10]. Under normal physiological condition, PSCs are quiescent. In chronic pancreatitis and pancreatic cancer, PSCs are stimulated into a proliferating myofibroblastic cell type that synthesizes and secretes extracellular matrix proteins, pro-inflammatory cytokines and growth factors, thus promoting the inflammation and fibrosis during both chronic pancreatitis and pancreatic cancer [2].
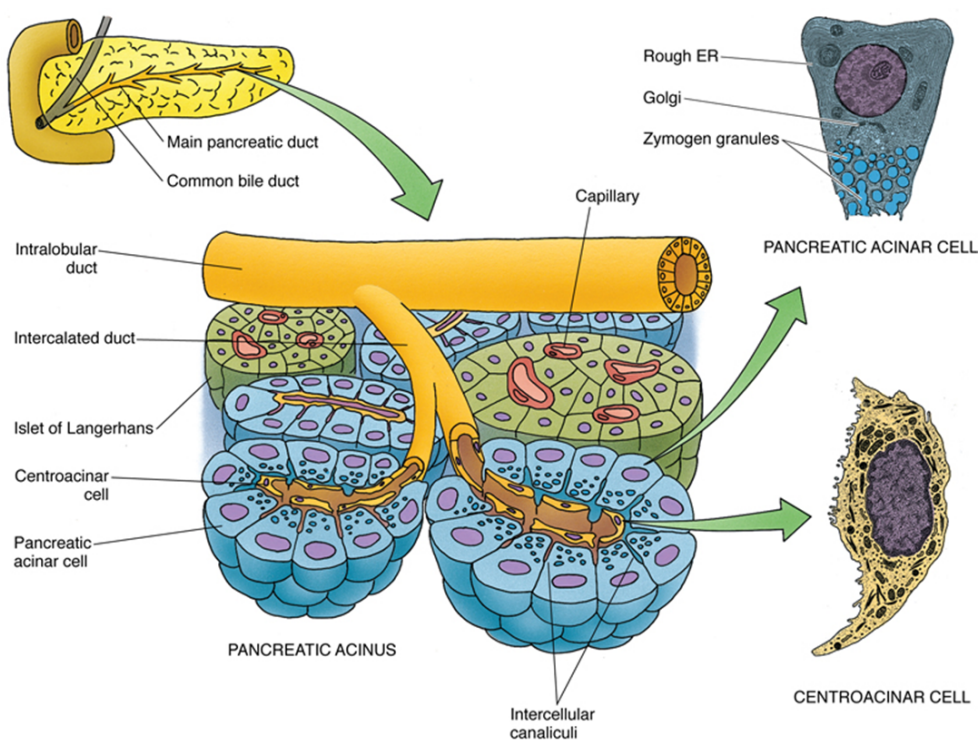
Figure 1-1: Structure of pancreas.
The basic secretory unit is composed of an acinus and an intercalated duct. Intercalated ducts merge to form intralobular ducts, interlobular ducts, and then the main pancreatic duct. The acinar cell is abundant in rough endoplasmic reticulum (rough ER) and specialized for protein secretion. Adopted from [11].

1.1.2 Pancreatic ductal adenocarcinoma as a type of exocrine pancreatic cancer

Pancreatic ductal adenocarcinoma (PDAC) develops from exocrine cells, accounts for ~80% of all pancreatic cancers and remains a malignancy with poor prognosis [12]. Fortunately, a recent comprehensive overview of cancer survival across seven high-income countries showed that the 5-year survival of PDAC has increased from 3.2%-8.8% in 1995–1999 to 7.9%-14.6% in 2010–2014 time period [13]. However, PDAC is still the most fatal cancer.

Failure to early diagnosis is a limitation to the treatment of PDAC patients, as most of the PDAC cases are already in an advanced stage when they are diagnosed. This is supported by experimental tracing in a mouse model for PDAC (*Pdx1-Cre; LSL-Kras^{G12D}; p53$^{fl/+}$; Rosa-LSL-YFP*), where only the pancreatic cells of epithelial origin were genetically labeled with yellow fluorescent protein (YFP). Using this model, it was shown that mice with PanIN (a precursor lesion which will be introduced in next chapters) but without macro- or micro-metastases already harbor liver seeding of YFP$^+$ cells in a subset of mice, indicating circulating pancreatic epithelial cells can spread *before* obvious tumor formation [14]. The computational analysis of mutation profiles of human specimens revealed that precancerous neoplastic cell can move through the pancreatic ductal system and clonally expand to form one or more lesions, and eventually lead to an invasive pancreatic cancer [15]. This reframes the step-wise progression model of pancreatic cancer, suggesting that the detectable high-grade pancreatic precursor lesions mean that there are already neoplasias colonized in pancreas. On the other hand, these findings underscore the importance of precursor lesions of PDAC.

1.1.3 Precursor lesions of PDAC

The carcinogenesis of PDAC is a multistep progression characterized by increasing degrees of morphological and cytological atypia. PDAC arises from noninvasive precursor lesions, which include noncystic lesions [pancreatic intraepithelial neoplasia (PanIN) and atypical flat lesions (AFLs) [16] and cystic lesions [intraductal papillary mucinous neoplasm (IPMN), intraductal tubulopapillary neoplasm (ITPN), and mucinous cystic neoplasm (MCN)] [17].

Based on the 2010 World Health Organization classification, PanIN, IPMN, and MCN are divided into three grades of dysplasia: low, intermediate, and high grade. However, according to the updated classification, these 3 precursor lesions are now classified into two tiers of dysplasia (low and high), based on the highest grade of dysplasia detected [18].

Among these precursor lesions, PanIN has gained more attention because it gives rise to most of PDAC cases and the PDAC derived from PanIN is the most malignant [19]. For example, those patients who had IPMN associated pancreatic cancer (n=20) had better progression-free survival (PFS) and overall survival (OS), compared to patients with PanIN associated pancreatic cancer (n=52) [19]. In addition, cystic lesions are usually bigger than non-cystic lesions and can be diagnosed by radiological examinations, whereas PanINs are diagnosed microscopically in pancreatic resection or biopsy specimens. This limits the possibility of detecting PanIN, and further emphasizes the importance of understanding PanIN in more details on molecular level.

1.1.4 Genetic alternations in PanIN and PDAC

During the progression from PanIN to invasive cancer, early genetic alternations include telomere shortening and *KRAS* (Kirsten RAS, also known as KRAS2) mutations, followed by the inactivation of p16/CDKN2A, and finally the inactivation of TP53 and SMAD4 (typically in PanIN-3 lesions) [20] (**Figure 1-2**).

Mutations of oncogenes enhance carcinogenesis. Point mutations in ***KRAS*** gene is the most common mutation for PDAC. The *KRAS* gene encodes a protein as a member of the small GTPase superfamily. A single amino acid substitution from G to D (or V) at codon 12 (accounting for 98% of *KRAS* mutations [21]) is responsible for a constitutive activation observed in approximately 90% of PDAC. A meta-analysis of PCR-based examinations showed that *KRAS* mutations were found in 36%, 44%, and 87% of PanIN-1a, 1b, and 2–3 lesions, respectively (trend statistic p <0.001) [22]. However, a study using a more sensitive mutation detection method (pyrosequencing) revealed that the *KRAS* mutations in low-grade PanIN were already very prevalent, as *KRAS* codon 12 mutations were detected in 46 of 50 (92.0%) PanIN-1A, 48 of 52 (92.3%) PanIN-1B, 42 of 45 (93.3%) PanIN-2, and 21 of 22 (95.4%) PanIN-3 lesions;

but the authors noted that the average concentration of mutant *KRAS* alleles in PanINs increased significantly with increasing grade of PanIN [23]. This suggests that *KRAS* mutation is a very early event during pancreatic carcinogenesis, and that *KRAS* mutation facilitates the progression from low-grade to high-grade PanINs and possibly initiates PanINs.

Another oncogenic mutation is *BRAF* mutation. Activated KRAS binds and activates RAF family kinases; activated RAFs phosphorylate and activate MEK1/2 kinases, which in turn phosphorylate and activate ERK1/ERK2 kinases (known as Ras-Raf-MEK-ERK pathway). *BRAF* mutations are observed in ~3% of PDAC [24],[25]. It was proposed that *KRAS* and *BRAF* mutation are exclusive in PDAC, indicating that *BRAF* mutation provides an alternative activation of MAPK cascade in the absence of *KRAS* mutation. The *BRAF* mutation in PanINs is rarely reported. Only one study showed that 1.9% (1/52) PanIN1b and 4.5% (1/22) PanIN3 harbored *BRAF^{V600E}* mutation.

Mutations of tumor suppressor genes

CDKN2A (encoding the p16^{INK4} and p14^{ARF}) is the most frequently inactivated tumor suppressor gene in PDAC and is observed in up to 95% of patients [26]. p16^{INK4} inhibits cyclin-dependent kinases 4 and 6 (CDK4 and CDK6) and thereby activates Rb protein, which blocks the G1/S transition. Therefore, the loss of function of p16^{INK4} leads to entry in cell cycle and uncontrollable cell proliferation. The inactivating modifications of *CDKN2A* (deletion, mutation and promoter methylation) arise at late stages of PanINs (30%-44% for PanIN-1, 80% for PanIN-2, and 92%-100% for PanIN-3) [27].

TP53 (also known as p53) is a tumor suppressor gene mutated in 70% of pancreatic cancers [24]. Notably, the p53 mutations frequently result in expression of a stable mutant protein p53^{R172H} rather than loss of protein. p53^{R172H} promotes chromosomal instability and widely metastasis [28], while overcomes Kras^{G12D}-induced senescence/growth arrest [29]. Consistently, *TP53* mutation is a very late event in PDAC, as genetic alteration of *TP53* was rarely detectable in high-grade PanINs. Moreover, it was found that *TP53* mutations were more prevalent in basal-like subtype tumors, whereas *GNAS* mutations were enriched in classical subtype tumors [24]. These two subtypes were also distinguished by differential regulation of gene

expression via miRNA and DNA methylation.

SMAD4 (Mothers against decapentaplegic homolog 4) is a central mediator of transforming growth factor beta (TGF-β) signaling pathway. It is subjected to frequent deletion or intragenic mutation in PDAC. Loss of SMAD4 leads to uncontrolled proliferation [27]. SMAD4 inactivation was reported in 31% of PanIN-3 [30], and in about 30% of PDAC [24].
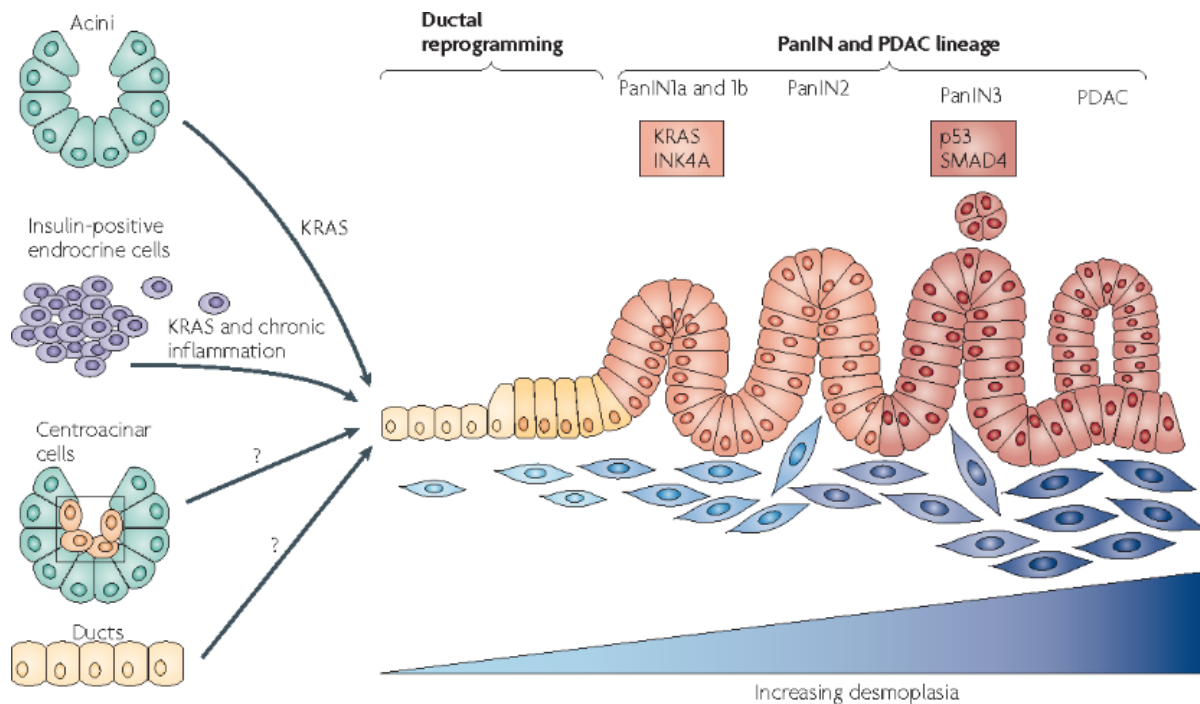
Figure 1-2: KRAS is a master regulator of pancreatic ductal adenocarcinoma initiation and progression.
Constitutively active KRAS is sufficient to initiate the development of pancreatic intraepithelial neoplasia (PanIN) and pancreatic ductal adenocarcinoma (PDAC). PanINs are classified into three stages, and mutations are indicated in boxes. Changes in the epithelium are matched by desmoplastic changes in the stroma. In mouse models, the human PanIN spectrum followed by progression to PDAC has been recapitulated by activating mutant KRAS in embryonic pancreatic progenitors. Eliminating tumour suppressors commonly inactivated in the human disease dramatically decreases PDAC latency. Figure is adopted from [31].

1.1.5 Genetically engineered mouse models (GEMM) for PDAC

Genetically engineered mouse models (GEMM) have been developed to recapitulate key aspects of PDAC. Because activating Kras mutations are the predominant mutations in PDAC and its precursor lesions [32], the most commonly used models are based on the expression of mutant Kras mediated by Cre-LoxP system. In murine embryonic pancreata, when a Kras^{G12D} knocked-in allele with *LoxP*-floxed STOP transcriptional cassette (*LSL-Kras^{G12D}*) was activated by Cre recombinase under the control of either the *Pdx1* or the *Ptf1a* promoters (designated as *Pdx1-Cre; LSL-Kras^{G12D}* and *Ptf1a-Cre; LSL-Kras^{G12D}*), the Kras^{G12D} oncogene expressed in *all* pancreatic lineages from early embryonic development [33]. These compound strains develop the full spectrum of PanIN lesions which histologically recapitulate human PanINs, and progress with long latencies to PDAC at low frequency [34].

Additionally, to accelerate cancer development, mutation or inactivation of the tumour suppressor genes especially *TP53* is further incorporated into the Kras^{G12D} model. Another common strategy to accelerate the progression of PDAC is cerulein-induced acute pancreatitis or chronic pancreatitis [35].

1.1.6 Acinar cell can be the origin of oncogenic Kras-driven carcinogenesis

PDAC is characterized by its ductal and glandular morphology, but the cellular origin of PDAC is still controversial. When *Kras^{G12D}* was knocked into about 12% of ductal cells by Sox9Cre^{ER} on postnatal day 10, these mice rarely developed PanIN lesions between the ages of 8 and 17 months [35]. Ck19Cre^{ERT} activated Kras^{G12D} expression in pancreatic ductal cells between the ages of 6 and 8 weeks only exhibited few sparse PanIN lesions instead of penetrating lesions in the whole pancreas at the age of 6 months [36]. These studies showed ductal cells are resistant to the oncogenic transformation by Kras^{G12D}, indicating that *Kras^{G12D}*-driven PDAC may not be derived from ductal cells. On the contrary, one of the most striking discoveries from mouse model of PDAC in the past decades is that PDAC can readily originate from mature acinar cells. Knockin of *Kras^{G12D}* allele in the *Elastase*- and *Mist1*-expressing mature acinar compartment resulted in the spontaneous PanIN lesions of all histological grades. The lineage tracing in reporter mice confirmed that the PanINs were derivatives of differentiated acinar cells [37]. This study showed that the differentiated

acinar cells in adult mice retain their susceptibility for spontaneous transformation into mPanIN lesions. Moreover, the oncogenic Kras-expressing adult mice could develop the full spectrum of PanINs and invasive PDAC, if they were challenged with cerulein-induced pancreatitis [38].

After that, acinar cells have become the central character of the PDAC carcinogenesis. Research focus is on the response of acinar cells to different stimuli (especially inflammation) and communications with other cell populations, and roles of different tumor suppressor genes, oncogenes, TFs in PDAC progression have been intensively investigated in acinar cells.

1.1.7 Importance of acinar-to-ductal metaplasia (ADM)

Metaplasia is the conversion of one differentiated cell type into another type in the same tissue [39]. During ADM, acinar cells at first dedifferentiate into progenitor-cell status (indicated by re-expression of progenitor marker genes such as Pdx1, Hes1, and Sox9, as well as dramatic change in cellular morphology due to release of zymogens), and then transdifferentiate into duct-like cells (indicated by up-regulation of ductal genes such as *Krt19*).

ADM is frequently observed *in vivo* in mouse models under stress conditions such as acute and chronic pancreatitis, but ADM *in vivo* is reversible when the inflammation resolves (i.e. reestablishment of acinar structure and functions, called "regeneration"). However, in the presence of mutant Kras, ADM may proceed to PanIN, and may develop PDAC [40] if genetic mutations and epigenetic disorder are accumulated. Therefore, ADM is the perquisite for early carcinogenesis in the presence of oncogenic Kras, and understanding the mechanisms of metaplasia could help identify early interventions for pancreatitis and pancreatic carcinogenesis.

1.1.8 Pathways important for ADM and PanIN

Both acinar cell autonomous and non-autonomous factors can contribute to ADM and PanIN formation. Compared to human acinar cells, the murine acinar cells are highly plastic. For example, among a panel of inflammation- or cancer-associated cytokines and growth factors, only TGF-β1 efficiently converted human acinar cells *in vitro* to

duct-like cells in a SMAD-dependent manner [41]. In contrast, various factors including EGFR ligands EGF and TGF-α, and pro-inflammatory cytokines, such as TNF-α, IL-6, and IL-1α, all can induce ADM of murine cells. Extracellular signals that act on acinar cells to affect the formation of ADM and PanIN are reviewed in the following section.

Epidermal growth factor receptor (EGFR) and EGF family

Transforming growth factor-alpha (TGF-α) is a member of the epidermal growth factor (EGF) family, which acts in autocrine and paracrine fashions by binding to the EGFR to regulate cell proliferation, differentiation, transformation, and migration [42]. It had been reported that the EGFR, EGF and TGF-α were found in the normal human exocrine pancreas, but pancreatic tumors exhibited increased mRNA levels and higher protein levels of these genes [43]. These findings suggest that overexpression of the EGFR and its ligands may contribute to the pathophysiological processes in human pancreatic cancer. In transgenic mice, overexpression of TGF-α under the control of *Elastase* promoter showed hyperplasia, fibrosis and ADM in adult pancreata, indicating an oncogenic role of TGF-α and EGFR [44]. On the other hand, Kras^{G12D}-mediated tumorigenesis was inhibited in pancreatic *Egfr* knockouts (*Ptf1aCre$^{/+}$; LSL-Kras$^{G12D/+}$; Egfr$^{fl/fl}$*) because Kras requires EGFR to robustly activate ERK, which is necessary for tumorigenesis [45]. In addition, pancreatic *Egfr* knockouts resist ADM *in vitro* and *in vivo* [46]. Consistently, Kras^{G12V}-driven metaplasia was still largely dependent on activation of EGFR because addition of their cognate ligands EGF or TGF-α, effectively increased the number of metaplasia [47].

Transforming growth factor beta (TGF-β) pathway

TGF-β is a multifunctional cytokine that has been implicated in carcinogenesis and cancer progression. TGF-β pathway is supposed to maintain homeostasis of tissue and inhibits epithelial growth, but it appears to promote the progression of advanced tumors [48].

The canonical pathway is initiated with that TGF-β binds to the type 2 TGF-β receptor (TGFBR2) that recruits the type 1 TGF-β receptor (TGFBR1), leading to the phosphorylation of SMAD2 and SMAD3 by TGFBR1. The phosphorylated SMAD proteins dissociate from the SMAD anchor for receptor activation (SARA) protein,

hetero-oligomerize with SMAD4, and translocate to the nucleus, interacting with myriad transcriptional coregulators to mediate target gene expression or repression [49]. Besides, TGF-β signaling can also be transduced through the Smad-independent pathways, including phosphatidylinositol-3 kinase (PI3K)/protein kinase B (AKT) pathway, JNK pathway, mitogen-activated protein kinase (MAPK) pathway, and Rho-like GTPases (RhoA and Cdc42) [50].

Combined with the activated $Kras^{G12D}$ allele, Smad4 deficiency accelerated the progression of KRAS^{G12D}-initiated neoplasms. While Kras^{G12D} alone elicited premalignant PanINs that progressed slowly to carcinoma, the combination of Kras^{G12D} and Smad4 deficiency resulted in a rapid development of tumors resembling intraductal papillary mucinous neoplasia (IPMN), another precursor to PDAC. SMAD4 deficiency also accelerated PDAC development of $Pdx1\text{-}Cre; Kras^{G12D}; Ink4a/Arf^{lox/lox}; Smad4^{lox/lox}$ mice with a small number of them also have IPMN [51]. In addition, knockdown of $Smad4$ in KRAS^{G12V}-expressing human pancreatic ductal cells failed to cause tumorigenic transformation, but KRAS^{G12V}-mediated malignant transformation occurred in a new TGF-β-resistant human ductal cell line avoid of Smad4 protein expression [52]. These results demonstrate that Smad4 is a tumor suppressor to block the Kras^{G12D}-initiated pancreatic neoplasms. However, it is unclear how Smad4 deletion alters the precursor lesion phenotype from PanIN to IPMN. It is known that pancreas-specific KRAS^{G12D} activation alone generated intraepithelial neoplasia within one year. In contrast, the $Tgfbr2$ knockout combined with Kras^{G12D} expression developed well-differentiated PDAC with 100% penetrance in mice with a median survival of 59 days. Heterozygous deletion of $Tgfbr2$ with Kras^{G12D} expression also developed PDAC, indicating a haploinsufficiency of TGF-β signaling [53]. Only 50% of $Elastase\text{-}Cre; Kras^{G12D+/-}; Tgfbr1^{+/-}$ mice developed preinvasive lesions compared with 100% of $Elastase\text{-}Cre; Kras^{G12D+/-}$ mice. The frequency of precancerous lesions was significantly lower in $Tgfbr1$-haploinsufficient mice. Yet, the mitotic index of precancerous cells and the observable levels of fibrosis, lipoatrophy, and lymphocytic infiltration were reduced in $Elastase\text{-}Cre; Kras^{G12D+/-};Tgfbr1^{+/-}$ mice [54]. In accordance, expression of an active Tgfbr1 induced ADM, eventually facilitating the onset of Kras^{G12D}-induced pre-cancerous PanINs [55]. Therefore, Tgfbr1 signaling promotes the development of precancerous lesions in mice, which is contrary to the tumor-

suppressive role of Smad4 and Tgfbr2.

Canonical Wnt signaling pathway

The Wnt signaling consists of canonical (β-catenin dependent) and non-canonical (β-catenin independent) pathways. The canonical pathway is activated by Wnt family ligands binding to Frizzled/LRP receptor complexes, leading to a block in β-catenin phosphorylation by glycogen synthase kinase 3 (GSK3) complex (consisting of Axin, APC and GSK-3) [56]. Hypophosphorylated β-catenin accumulates in the cytoplasm and is translocated to the nucleus where it regulates target gene expression through partnerships with the T cell-specific transcription factor/lymphoid enhancer-binding factor 1 (TCF/LEF) family of transcription factors [57].

Activation of the canonical Wnt/β-catenin pathway is required to initiate pancreatic cancer. In *Ptf1a-Cre; LSL-Kras$^{G12D+/-}$; β-catenin$^{f/f}$* mice, β-catenin null cells were incapable of undergoing ADM and did not contribute to Kras driven PanIN lesions. On the other hand, inducible expression of Dkk1, an endogenous secreted inhibitor of the canonical Wnt pathway, inhibited PanIN development and progression. Lastly, when *Ptf1a-Cre; LSL-Kras$^{G12D+/-}$* mice were treated with a therapeutic antibody that interacts with multiple Frizzled receptors, they showed a prevalence of normal acini and ADM, and fewer lesions. Moreover, in dissected tissues, phospho-β-catenin accumulated, whereas the mRNA levels of Wnt target genes *Axin2*, *Lef1* and *MMP7* declined, and phospho-ERK 1/2 and Ki67-positive cells significantly decreased [58]. A recent publication confirmed that overexpression of active β-catenin or Wnt1 accelerates pancreatic carcinogenesis in *Ptf1a-Cre;LSL-Kras^{G12D}* mice [59]. In contrast, it is also reported that β-catenin blocks Kras-dependent reprogramming of acini into pancreatic cancer precursor lesions in mice [60]. It is found that β-catenin is required for efficient acinar regeneration following cerulein-induced acute pancreatitis, and the regeneration-associated reactivation of β-catenin signaling is inhibited during Kras^{G12D}-induced ADM reprogramming. These seemingly contradictory findings indicate that the role of canonical Wnt pathway in PDAC initiation is context-dependent, and also there is a profound impact of cerulein-induced pancreatitis on Kras^{G12D}-driven carcinogenesis.

1.1.9 Acinar transcription factors inhibit Kras-driven carcinogenesis

According to lineage tracing in mouse models, PDAC and one of its precursor lesions PanIN can derive from acinar cells. Therefore, Ptf1a as a master regulator of acinar differentiation and homeostasis plays a suppressive role in PDAC initiation. Knockout of *Ptf1a* in acinar cells alone is sufficient to induce ADM, and Ptf1a-deficient acinar cells are dramatically sensitized to mutant Kras-driven transformation, and accelerates development of invasive PDAC in mouse [61].

Another acinar-specific bHLH transcription factor Mist1 is required to maintain acinar cell identity. In the absence of Mist1, Kras^{G12D}-expressing mice exhibited severe exocrine pancreatic defects. The acinar cells with loss of Mist1 are predisposed to convert to a ductal phenotype and activate EGFR and Notch-signaling pathways, resulting in ADM *in vitro*. Transgenic mice with loss of Mist1 in exocrine pancreas show accelerated Kras^{G12D}-driven PanIN initiation [62].

NR5A2 is an orphan nuclear hormone receptor that regulates the development of the acinar lineage [63]. Although Nr5a2 is not essential for the development of the pancreatic acinar lineage, it is important for the maintenance of acinar identity. *Nr5a2* deletion (*Pdx-Cre^{late}; Nr5a2$^{c/c}$*) led to ADM and loss of regenerative capacity following acute pancreatitis; loss of Nr5a2 also dramatically accelerated the development of oncogenic Kras-driven ADM and PanINs [64]. Consistently, acute pancreatitis combined with the loss of one *Nr5a2* allele accelerated Kras^{G12V}-driven development of preneoplastic lesions in *Ptf1a-Cre; Kras$^{G12V+/–}$; Nr5a2$^{+/–}$* mice. Additionally, heterozygosity of *Nr5a2* impaired regeneration of pancreas after pancreatitis. These studies together demonstrate that Nr5a2 inhibits the ductal transformation induced by mutant Kras and thus serves as a tumor suppressor [65]. Transcriptomic analysis further revealed that heterozygous *Nr5a2* (*Nr5a2$^{+/–}$*) in murine acinar cells generated a pre-inflammatory state in the pancreas (conserved in histologically normal human pancreata with reduced *NR5A2* mRNA). In *Nr5a2$^{+/–}$* mice, Nr5a2 undergoes a dramatic transcriptional switch from differentiation-specific genes to inflammatory genes thereby promoting AP-1-dependent gene transcription [66].

Pancreatic and duodenal homeobox 1 (PDX1) is a transcription factor essential for pancreas development and differentiation of all pancreatic cell lineages [67]. In mature pancreas, Pdx1 expresses highly in β cells to maintain efficient insulin gene transcription [68], but expresses at lower levels in exocrine cells [69]. However, the role for Pdx1 in ADM has been suggested in an earlier study that *in vitro* culture of rat acinar cells formed ADM that was accompanied by the induction of Pdx1 expression. A recent study showed that the low expression levels of Pdx1 in acinar cells helps maintain acinar cell identity, as deletion of *Pdx1* in adult acinar cells impaired the re-differentiation of cerulein-induced ADM [70], indicating delicate regulations of some low-abundance transcription factors.

1.1.10 Ductal TFs mediate Kras-driven transformation of acinar cells

SRY-Box Transcription Factor 9 (Sox9) is required for pancreatogenesis and maintaining pancreatic ductal identity. Deletion of *Sox9* in Kras^{G12D}-expressing acinar cells dramatically reduced PanIN numbers in 8 to 12-month-old mice; on the other hand, overexpression of Sox9 accelerated the initiation of PanINs in as early as 3 to 4-week-old mice, indicating that Sox9 promotes Kras^{G12D}-mediated induction of PanINs. Ectopic Sox9 expression in acinar cells in the absence of oncogenic Kras did not change the morphology of acinar cells, but it suppressed the expression of acinar genes (*Amy* and *Mist1*) while promoted the expression of ductal gene *Krt19*. This indicates that Sox9 destabilizes the acinar cell state, but is not sufficient to induce complete ductal reprogramming [35].

Hepatic Nuclear Factor 6 (HNF6) was identified as the first transcriptional regulator of pancreatic duct development and controls a network of genes involved in cilium formation, including HNF1B, polyductin/fibrocystin and cystin [71]. Early and pancreas-wide *Hnf6* inactivation (Hnf6$^{\Delta panc}$) resulted in increased ductal cell proliferation and metaplasia, as well as characteristics of pancreatitis, which was most likely caused by defects in ductal primary cilia [72]. Expression of HNF6 was ectopically induced in acinar cells in human and murine ADM. HNF6 contributes to carcinogen (DMBA)-induced ADM by repression of acinar genes, modulation of ADM-associated changes in cell polarity, and by activation of ductal genes [73].

In summary, the transcription factors important for the maintenance of pancreatic acinar identity, differentiation, and homeostasis refrain Kras^{G12D}-induced reprograming of acinar cells into precursor lesions, while ductal specific genes are important mediators of the reprogramming.

1.2 Hepatocyte nuclear factor 1-beta (HNF1B) and PDAC

1.2.1 Molecular structure of the HNF1B

The hepatocyte nuclear factors (HNFs), including HNF1A/B, FOXA1/2/3 (also known as HNF3), HNF4A/G and ONECUT1/2 (also known as HNF6) are expressed in a variety of tissues and organs, including the liver, pancreas and kidney [74].

The HNF1 family comprises HNF1A and HNF1B. Both HNF1A and HNF1B proteins have three functional domains: the dimerization domain, the DNA-binding domain and the transactivation domain. The DNA-binding domain is characterized by a POU-specific domain and a POU-homeodomain. HNF1B is structurally similar to HNF1A and shares >90% sequence homology in the DNA-binding domain [75], which is known to bind to the consensus sequence GTTAATNATTANC [74]. The dimerization domain at the N-terminus allows HNF1A and HNF1B to form homodimers or heterodimers in nuclear extracts of kidney, liver and several cell lines [76] to regulate the transcription of target genes. Additionally, HNF1A and HNF1B genes each encode at least three isoforms (A, B and C), which variably express between different tissues and the same tissue of different species [77].

1.2.2 HNF1B is a key regulator for pancreatic organogenesis

In the mouse embryo, Hnf1b expression is firstly detected in the primitive endoderm on embryonic day (E)4.5, and subsequently detected in the foregut endoderm on E9, from which the liver and pancreas develop [74]. The sequential activation of Hnf1b, Hnf6 and Pdx1 directs the differentiation of endodermal cells into pancreatic progenitors [78]. Hnf1b expression later becomes confined to the progenitor cells in trunk compartment of the early branching pancreas, which gives rise to acinar, duct, and endocrine lineages [79]. In the postnatal or adult pancreas, Hnf1b is restricted to ductal epithelial cells.

In mice, heterozygous deletion of *Hnf1b* results in no obvious phenotype, while homozygous *Hnf1b*-deficient mouse embryos develop normally to the blastocyst stage, start implantation, but die soon afterwards, with poorly organized ectoderm and no discernible visceral or parietal endoderm [80]. When those *Hnf1b*-deficient mice were rescued by tetraploid aggregation, dorsal pancreas was severely reduced at E9.5 in *Hnf1b*-deficient mutants, whereas the ventral bud was undetectable; the pancreatic bud was extremely reduced at E12.5 and became absent at E13.5 [81]. In a recent study, constitutive inactivation of *Hnf1b* in Pdx1-expressing cells leads to a reduced pool of pancreatic multipotent progenitor cells (MPCs) due to decreased proliferation and increased apoptosis. Lack of Hnf1b resulted in cystic ducts with altered polarity and lack of primary cilia, as well as a loss and abnormal differentiation of acinar cells. Additionally, inactivation of Hnf1b at different time points results in the absence of Ngn3$^+$ endocrine precursors [82]. Thus, Hnf1b plays a crucial role in the regulatory networks that control pancreatic MPC expansion, acinar cell identity, duct morphogenesis and generation of endocrine precursors.

1.2.4 Diseases caused by *HNF1B* germline mutations

There were more than 50 different mutations identified in human *HNF1B* gene, which span the first eight (out of nine) exons of the gene (reviewed in [83]). In 1997, heterozygous mutations of this gene were first described in a Japanese family with maturity-onset diabetes of the young (MODY) [84], which is the most common form of monogenic diabetes and is characterized by onset typically before 25 years of age, β-cell dysfunction and also hyperinsulinemia [85]. This is likely to be a consequence of pancreatic hypoplasia [83].

Renal abnormalities (mainly cystic kidney) are another common clinical manifestation that was subsequently identified in patients with germline mutations of *HNF1B* [86]. HNF1β protein affects the pathogenesis of renal cysts at transcriptional and post-transcriptional levels. HNF1β directly regulates the expression of known polycystic kidney disease (PKD) genes, such as *PKHD1* and *PKD2*, as well as cAMP-dependent signaling, renal fibrosis, and Wnt signaling. In addition, HNF1B also regulates subsets of microRNAs and long noncoding RNAs [87].

Other phenotypes were less frequently observed, including pancreatic hypoplasia, biliary disorders, abnormal liver and intestine, urogenital tract abnormalities, hyperuricaemia, autism, early-onset gout and hypomagnesaemia [88], [89].

1.2.5 HNF1B in cancers

The status and expression level of HNF1B are also associated with the risk and progression of various cancers including hepatocellular carcinoma, pancreatic carcinoma, renal cancer.

Hepatocellular carcinoma (HCC)

An early study revealed that the levels of HNF1β protein showed no difference in well and poorly differentiated HCC, but higher than in the surrounding non-cancerous portions. In contrast, HNF1α protein was expressed at a higher level in well-differentiated HCC, but at lower levels in moderately and poorly differentiated HCC tissue [90]. This indicates HNF1B and HNF1A are differentially regulated in HCC and possibly regulate different subsets of genes.

Recent studies took closer examination of HNF1B in subtypes of HCC. It was shown that the expression of HNF1B was positively correlated with that of biliary/hepatic progenitor markers, and HCC with high level of HNF1B displayed biliary phenotype and tended to show poorer prognosis. Further, HNF1B expression was an independent prognostic factor for both overall survival and disease-free survival of HCC patients [91].

The *in vitro* studies shed some light on the functions of HNF1B in HCC cells. Overexpression of HNF1B in liver cancer cell lines upregulated liver progenitor cell markers, epithelial-mesenchymal transition (EMT)-associated genes, as well as stemness and invasion ability. This was partially mediated by activating the Notch pathway (indicated by NOTCH1 and HES1) [92].

Renal cancer

Renal cell carcinoma (RCC) consists of morphologically and genetically distinct subtypes, of which clear cell renal cell carcinoma (ccRCC), papillary RCC (pRCC) and

chromophobe RCC (chRCC) are the most prevalent, accounting for approximately 75%, 15% and 5% of all RCC, respectively [93].

HNF1B mRNA expression significantly decreased with RCC progression (normal renal tissue > primary tumor > metastasis; $P < 0.0001$), and high HNF-1B mRNA expression in primary tumor correlated with better prognosis ($P < 0.05$) [94]. According to TCGA data, HNF1B is downregulated in most of chRCC (accounting for ~5% of renal cancers) but not the other subtypes of renal cancers. In clinical specimens, combining *HNF1B* loss with *TP53* mutation produced an association with poor patient prognosis. In chRCC cells, combining *HNF1B* loss and *TP53* mutation increased cell proliferation and aneuploidy, by reducing the expression of the spindle checkpoint proteins MAD2L1 and BUB1B, and the cell-cycle checkpoint proteins RB1 and p27 [95]. This indicates that loss of *HNF1B* and malfunction of TP53 confer an aggressive phenotype in chRCC. In addition, loss of *HNF1B* induced p53/p21 pathway activation, cell death and cell senescence in MEFs and a human renal cell carcinoma cell line [95].

Pancreatic cancer

HNF1B is involved in the cancer risk, differentiation and gene expression regulation of PDAC, but its mechanisms are still unclear. A few large-scale genome-wide association studies (GWAS) identify associations of individual single-nucleotide polymorphisms (SNPs) of *HNF1B* with PDAC risk [96], [97]. Although susceptibility genes identified can be annotated into several pathways altered in PDAC, suggesting they may be biologically relevant for risk of PDAC, it is still elusive how these SNPs play a role in the regulation of gene expression.

The expression levels of HNF1B significantly decreased in pancreatic tumors and cells compared with normal tissue and cells [98], but the role of HNF1B in PDAC was elusive. Diaferia *et al.* examined the regulatory landscape (enhancers and promoters) of low- and high-grade human PDAC cell lines, and identified sets of transcription factors that are selectively expressed in low-grade PDAC, including IRF1, ELF3, FOXA1, KLF5 and HNF1B, as well as transcription factors selectively expressed in high-grade PDAC. They identified the repertoires of enhancers specific to low-and high-grade PDAC and

the cognate set of transcription factors acting to maintain their activity [99]. These indicate that the transcriptional phenotype associated with stage-specific programs could be largely explained by the activation of grade-specific enhancers. As an example of the candidate regulators of PDAC differentiation, KLF5 was selectively expressed in pre-neoplastic lesions and low-grade primary PDAC and cell lines, where it maintained the acetylation of grade-specific enhancers, the expression of epithelial genes such as keratins and mucins, and the ability to organize glandular epithelia in xenografts. Notably, in this paper HNF1B for the first time was found to be expressed in low-grade human PDAC but dramatically declined in high-grade PDAC [99]. Another study confirmed that gradual loss of nuclear HNF1B expression was detected in well differentiated towards poorly differentiated tumors compared to a non-neoplastic duct. In addition, regulatory network analysis predicted that HNF1A/HNF1B are the top-enriched master regulators of the genes expressed in the normal pancreatic tissue because within the 1325 down-regulated genes in PDAC, the most strongly enriched TF motifs were those for HNF1A/B [100]. These data suggested that HNF1B is not only a differentiation marker, but also might be a key player as a tumor suppressor in PDAC carcinogenesis and progression from duct cells.

A recent study published in 2019 showed that inactivation of *Hnf1b* in ductal cells on postnatal days 1, 2 and 3 led to loss of primary cilia of ducts, and more proliferative ductal cells. Besides, ductal deletion of *Hnf1b* led to enhanced signaling pathways that favor tumorigenesis, including upregulation of some components in Notch pathway, and significantly increase in *Egfr* and *Tgfb1* mRNAs. Altogether, these results show that Hnf1b plays a prominent role in the regulatory network maintaining the homeostasis of pancreatic ducts after birth. Strikingly, in their mouse strain *Sox9-CreER; Hnf1b$^{fl/fl}$; Elas-tTA; TetO-Flpase; FRT-Stop-FRT-Kras^{G12V}* that combined perinatal inactivation of Hnf1b in ducts and oncogenic activation of Kras^{G12V} in acinar cells, ductal deletion of *Hnf1b* dramatically promotes Kras-induced PanIN progression [101].

In summary, HNF1B is required for the homeostasis of ductal cell and is an important regulator of PDAC progression from ductal cells. However, the roles of HNF1B in acinar cells and acinar cell-originated PDAC is still unknown.

1.3 Aims of study

The primary aim was to elucidate the role of HNF1B in pancreatic carcinogenesis. Because $Kras^{G12D}$ activation reprograms acini into pancreatic cancer precursor lesions, and HNF1B is an important regulator of exocrine differentiation as well as a pancreatic cancer risk gene, we hypothesized that knockout of mouse *Hnf1b* gene in acinar cells may affect acinar dedifferentiation and thus neoplastic transformation. Therefore, mice with $Kras^{G12D}$ expression and wild-type, heterozygous, or homozygous *Hnf1b* deletion in mature acinar cells were generated (i.e., *ptf1aCreER; $Kras^{G12D}$* mice*, ptf1aCreER; $Kras^{G12D}$; $Hnf1b^{fl/wt}$* mice, and *ptf1aCreER; $Kras^{G12D}$; $Hnf1b^{fl/fl}$* mice), and the precancerous lesions (ADM and PanIN) were evaluated at indicated time points after tamoxifen induction with and without cerulein-induced pancreatitis.

To investigate whether Hnf1b is required for ADM, pancreatic acinar cells from *Hnf1b* knockout and *Hnf1b* wild-type mice were isolated, and subject to three-dimensional culture to mimic ADM. The effects of *Hnf1b* deletion on ADM formation and maintenance, as well as mRNA levels of acinar and ductal marker genes were evaluated.

The second aim was to investigate the effect of murine Hnf1b/human HNF1B expression on cellular behavior of murine and human PDAC cell lines, respectively. *Hnf1b/HNF1B* gene was knocked out in murine and human PDAC cell lines by lentivirus-mediated CRISPR-Cas9. The effects on cellular features such as cell proliferation, colony formation ability, and epithelial–mesenchymal transition (EMT) was determined. The molecular mechanisms of the effects mentioned above and downstream targets of HNF1B were identified.

2 Materials

2.1 Laboratory equipment

Equipment	Producer
Analytical balance ABS 220-4N	KERN & SOHN GmbH
Centrifuge 5424 R (refrigerated)	Eppendorf
CO2 incubator HERAcell®	Heraeus Holding GmbH
Electrophoresis power supply Power Pac 200	Bio-Rad Laboratories GmbH
Gel DocTM XR+ system	Bio-Rad Laboratories GmbH
Heated paraffin embedding module EG1150 H	Leica Microsystems GmbH
HERAsafe® biological safety cabinet	Thermo Fisher scientific, Inc.
Homogenizer SilentCrusher M with tool 6F	Heidolph Instruments GmbH & Co.
Microscope Axio Imager.A1	Carl Zeiss AG, Oberkochen
Microscope Axiovert 200M (Inverted)	Carl Zeiss AG, Oberkochen
Microtome Microm HM355S	ThermoFisher Scientific, Inc.
Microwave oven (90-900w)	Siemens
Multiskan™ FC Microplate Photometer	Thermo Fisher Scientific
Thermocycler T1	Biometra GmbH, Göttingen
Thermocycler TGradient	Biometra GmbH, Göttingen
Tissue processor ASP 300	Leica Mircosystems GmbH, Wetzlar
Vortex-Genie 2	Scientific Industries, Inc.
Western blot system SE 260 Mighty Small II	Hoefer, Inc., Holliston, MA, USA

2.2 Chemical reagents

Reagent	Catalog #	Producer
1 kb Plus DNA Ladder	N3200S	NEB
2-Mercaptoethanol, 98 %		Sigma-Aldrich Chemie
2-Propanol (isopropanol)		Carl Roth GmbH
3-(4,5-dimethylthiazol-2-yl)-2,5-diphenyl tetrazolium bromide (MTT)	4022.1	Carl Roth GmbH

Antigen Unmasking Solution, Citric Acid Based	H-3300	VectorLab
Agarose	840004	Biozym
Ammonium persulfate	9592.3	Roth
2-Mercaptoethanol	M3148-25ML	Sigma
Blasticidin S-HCL solution	sc-495389	Santa Cruz
Bovine serum albumin, fraction V (BSA)	A7030-100G	Sigma
FastDigest™ BbsI (BpiI)	ER1012	Thermofisher
BsmBI restriction enzyme	R0580L	NEB
Caerulein ammonium salt	H-3220.0001	Bachem
cOmplete™, Protease Inhibitor Cocktail	04693124001	Roche
Deoxynucleotide (dNTP) Mix 10mM	D7295	Sigma-Aldrich
Direct PCR-Tail Lysis reagent	102-T	VIAGEN
Glycine		Carl Roth GmbH
GoTaq® G2 Hot Start Green Master Mix	M7423	Promega
Immobilon Western HRP Substrate	WBKLS0100	Merck Millipore
Isoflurane	1214	CP-Pharma
NucleoBond Xtra Midi (10)	740410.1	Macherey-Nagel
NucleoSpin Gel and PCR Clean-up	740609.5	Macherey-Nagel
Oligo(dT)$_{15}$ Primer 20µg C110A	C1101	Promega
PageRuler Plus Prestained Protein Ladder	26619	Life Technologies
Paraformaldhyde Solution 4% in PBS	sc-281692	Santa Cruz
PhosStop^{TM} (Phosphatase Inhibitor)	04906837001	Roche
Proteinase K, recombinant, PCR grade	EO0491	Thermofisher
Puromycin dihydrochloride	P8833-10MG	Sigma-Aldrich
RA1 Buffer	740961.5	Macherey-Nagel
RNAlater Stabilization Reagent	AM7024	Thermofisher
Roti GelStain	3865.2	Roth
Skim Milk Powder	70166-500g	Sigma
SuperScript II Reverse Transcriptase	18064-014	Thermofisher
LightCycler 480 SYBR Green I Master	4707516001	Roche

T4 DNA Ligase (100.000 Untis)	MO202L	NEB		
Tamoxifen	T5648-1G	Sigma-Aldrich		
Tween-20	9127.1	Carl Roth GmbH		
Triton® X-100		Merck KGaA		
Tris Pufferan®		Carl Roth GmbH		

2.3 Antibodies

Table 2-1: Antibodies for Western blotting

Antibodies	Company	Catalog #	Species	Protein Size (kD)	Dilution
Akt	Cell Signalling	9272	rabbit	60	1:1000
β-actin (C4)	Santa Cruz	sc-47778	mouse	43	1:5000
GAPDH (14C10)	Cell Signalling	2118	rabbit	37	1:1000
HNF1B	Proteintech	12533-1-AP	rabbit	58-60	1:2000
HSP90	Cell Signalling	4874S	rabbit	90	1:1000
pAkt	Cell Signalling	4060	rabbit	60	1:2000
pCREB (87G3)	Cell Signalling	9198	rabbit	43	1:1000
pm-TOR	Cell Signalling	2974	rabbit	289	1:1000
CREB (48H2)	Cell Signalling	9197	rabbit	43	1:1000

Table 2-2: Primary antibodies for immunohistochemistry

Antibodies	Company	Catalog #	Species	Dilution	Unmasking
α-Amylase	Cell Signalling	3796	rabbit	1:1000	low pH
CD45	BDPharmigen	550539	mouse	1:20	20 µg/ml Proteinase K in 10 mM TrisHCl pH8 15 min at RT
CK19	Abcam	ab133496	rabbit	1:1000-1:5000	low pH
Cleaved Caspase 3	Cell Signalling	9661	rabbit	1:200-1:400	low pH
Clusterin-α	Santa Cruz	sc-6419	goat	1:200	low pH
CPA1	RD Systems	AF2765	goat	1:300	low pH
F4/80	Abcam	ab111101	rabbit	1:300	EDTA pH=8 boiled for 10 min
HNF1B	Proteintech	12533-1-AP	rabbit	1:3000	low pH
Ki67	BD Pharmingen	550609	mouse	1:400	low pH
MUC5AC	Cell Marque	292M-95	mouse	1:200	low pH

Table 2-3: Secondary antibodies for immunohistochemistry

Antibodies	Producer
Biotinylated anti-goat IgG (H+L)	Vector Laboratories, Inc., Burlingame, USA
Biotinylated anti-mouse IgG (H+L)	Vector Laboratories, Inc., Burlingame, USA
Biotinylated anti-rabbit IgG (H+L)	Vector Laboratories, Inc., Burlingame, USA
Biotinylated anti-rat IgG (H+L)	Vector Laboratories, Inc., Burlingame, USA

2.4 sgRNAs for CRISPR-Cas9

Table 2-4: sgRNA sequence for HNF1B

sgRNA Name	Sequence 5'-3'	Target Exon	Genebank ID	Comments
hCtrl-Guide_F	CACCGGTAGCGAACGTGTCCGGCGT		No target in human or mouse genome	Nature 509, 487–491
hCtrl-Guide_R	AAACACGCCGGACACGTTCGCTACC			
hHNF1B-Guide1_F	CACCGGCCGCTTGTCCGGCGACGA	1	6928	408-430
hHNF1B-Guide1_R	AAACTCGTCGCCGGACAAGCGGCC			
hHNF1B-Guide2_F	CACCGAGCCCTCGTCGCCGGACAAG			410-432
hHNF1B-Guide2_R	AAACCTTGTCCGGCGACGAGGGCTC			
hHNF1B-Guide3_F	CACCGCTGCAGGCGCTCAACACCG	1		476-498
hHNF1B-Guide3_R	AAACCGGTGTTGAGCGCCTGCAGC	1		
hHNF1B-Guide4_F	CACCGTTGCTGGAGCGACGTGAGCT	1		202-224
hHNF1B-Guide4_R	AAACAGCTCACGTCGCTCCAGCAAC	1		
mHnf1b sg1-F	CACCGACTGCCGTCCCCGAATTTCG	1	21410	279-298
mHnf1b sg1-R	AAACCGAAATTCGGGGACGGCAGTC	1		
mHnf1b sg2-F	CACCGTCTGACGTACCAAGTGTACA	2		683-702
mHnf1b sg2-R	AAACTGTACACTTGGTACGTCAGAC	2		

2.5 Primers for RT-PCR

Table 2-5: Primers for RT-PCR

Gene	Primer name	Sequence
Kras	RT_mKras_F	CAAGAGCGCCTTGACGATACA
	RT_mKras_R	CCAAGAGACAGGTTTCTCCATC
Bhlha15	RT_mMist_F	GCGCGTACGGCCTCG
	RT_mMist_R	GGGCCGGTTTTTGGTCTTCAT
Ptf1a	RT_mPtf1a_F	ACAAGCCGCTAATGTGCGAGA
	RT_mPtf1a_R	TTGGAGAGGCGCTTTTCGT
Sox9	RT_mSox9_F	CCACGTGTGGATGTCGAAG
	RT_mSox9_R	CTCAGCTGCTCCGTCTTGAT
Tnfa	RT_mTNFa_F	TGCCTATGTCTCAGCCTCTTC
	RT_mTNFa_R	GAGGCCATTTGGGAACTTCT
E2f8	mE2f8_R	TTTTCTGAGCCACATAAAAGGGG
	mE2f8_F	CTTCCTTGGGCTTGGTTGGT
Frnd4a	mFrmd4a_F	GAGGGCCGTCGATGTCAAG
	mFrmd4a_R	CCTTCAGGTTGAAATGAGAGGC
Nr5a2	mNr5a2_R	TCATGCTGCCCAAAGTGGAGA
	mNr5a2_F	TGGTTTTGGACAGTTCGCTT
Ins2	Ins2_F	GCTCTTCCTCTGGGAGTCCCAC
	Ins2_R	ATGCTGGTGCAGCACTGATC
Bmp4	mBmp4_F	TTCCTGGTAACCGAATGCTGA
	mBmp4_R	CCTGAATCTCGGCGACTTTTT
Jun	mJun_F	CCTTCTACGACGATGCCCTC
	mJun_R	GGTTCAAGGTCATGCTCTGTTT
Src	mSrc_F	GAACCCGAGAGGGACCTTC
	mSrc_R	GAGGCAGTAGGCACCTTTTGT
XS13	RT_mXS13_F	TGGGCAAGAACACCATGATG
	RT_mXS13_R	AGTTTCTCCAGAGCTGGGTTGT
E-cadherin	RT_hCDH1_F	CCCGGGACAACGTTTATTAC
	RT_hCDH1_R	GCTGGCTCAAGTCAAAGTCC

GAPDH	RT_hGAPDH_F	GCTCTCTGCTCCTCCTGTTC
	RT_hGAPDH_R	ACGACCAAATCCGTTGACTC
HNF1B	RT_hHNF1B_F	GACGGCGACGACTATGACAC
	RT_hHNF1B_R	GGGATGTTGTGTTGCTGCAT
ITGA1	hITGA1_F	CATCAGGTGGGGATGGTAAG
	hITGA1_R	TGGCTCAAAATTCATGGTCA
ITGB5	hITGB5_F	GGAAGTTCGGAAACAGAGGGT
	hITGB5_R	CTTTCGCCAGCCAATCTTCTC
N-Cadehrin	RT_hCDH2_F	TAAAGAACGCCAGGCCAAAC
	RT_hCDH2_R	CATTCGTCGGATTCCCACAG
PIK3R1	hPIK3R1_F	TGGACGGCGAAGTAAAGCATT
	hPIK3R1_R	AGTGTGACATTGAGGGAGTCG
PPP2R5C	hPPP2R5C_F	GTAATAAAGCGGGCAGCAGG
	hPPP2R5C_R	CAAAGTCAAAGAGGACGCAACA
SNAIL	RT_hSnail1_F	GCACATCCGAAGCCACAC
	RT_hSnail1_R	GGAGAAGGTCCGAGCACA
VIMENTIN	RT_hVim_F	TACAGGAAGCTGCTGGAAGG
	RT_hVim_R	ACCAGAGGGAGTGAATCCAG

2.6 Primers for ChIP-PCR

Table 2-6: Primers for ChIP-PCR

Gene	Primer name	Sequence
PPP1R12B	PPP1R12B intron_F	ACAAAAATACACCTGCACAATGA
	PPP1R12B intron_R	CAGTGCAGGGTCAAAGGTGA
PPP2R5C	PPP2R5C(intron4)_F	TGAATCGGAACCTTCCGTG
	PPP2R5C(intron4)_R	TGCAGCGAAATGGGGTGAA
ITGA1	ITGA1 intron_F	CACGCATGCAAAGCAGCTGGA
	ITGA1 intron_R	ACTGCTTTCCACAGTAATCGTCCCA

2.7 Primers for genotyping

Table 2-7: Primers and PCR product sizes for genotyping

Name	Primer forward (5´-3´)	Primer reverse (5´-3´)	Product (bp)
Cre(ER)	ACCAGCCAGCTATCAACTCG	TTACATTGGTCC AGC CACC	wildtype: 324 bp;
	CTA GGC CAC AGA ATT GAA AGA TCT	GTAGGTGGAAATTCTAGC ATCATC C	mutant: 199 bp
Kras^{G12D}	CAC CAG CTT CGG CTT CCT ATT	AGC TAA TGG CTC TCA AAG GAA TGT A	wildtype: 280 bp;
		CCA TGG CTT GAG TAA GTC TGC	mutant: 180 bp
Hnf1b$^{lox/lox}$	GTCCAAGCTCACGTCGC TCC	CCAGGTCTTTTGCAGAGA ACTGC	wildtype: 745 bp; mutant: 800 bp

2.8 Reagents for cell culture

Table 2-8: Reagents for cell culture

Reagents	Catalog Number	Vendor
Collagen Typ I Rat Tail 100mg	354236	Corning
Collagenase P 100mg, lyophilized, non-sterile	11213857001	Sigma-Aldrich
DMEM, high glucose	41965062	Thermofisher
DPBS no calcium, no magnesium 10x500 ml	14190169	Thermofisher
EGF 1 mg	AF-100-15	PeproTech
Fetal Bovine Serum, qualified	10270106	Thermofisher
FuGene HD Transfection Reagent 1ml	E2311	Promega
HBSS, no calcium, no magnesium, no phenol red	14175053	Thermofisher
Iscove's Modified Dulbecco's Medium	12440053	Thermofisher

(IMDM)

Matrigel (GFR) 10 ml	354230	Corning
Opti-MEM 500 ml	11058021	Thermofisher
Penicillin Streptomycin SOL 100ml	15140122	Life Technologies
RPMI 1640 Medium	21875091	Thermofisher
Trypsin 0.05% EDTA 100ml, phenol red	25300054	Life Technologies
Trypsin inhibitor (soybean) powder 1g	17075029	Thermofischer
Waymouth's Medium	31220023	Thermofisher

2.9 Home-made solutions

Ampicillin stock solution (100 mg/ml):

1 g sodium ampicillin dissolved in 10 ml injection water. Aliquoted and stored at -20 °C. The stock solution is stable within 6 mon at -20°C.

Agar plate:

5 g LB Broth, 3 g Agar, 200 ml dH$_2$O. Autoclaved at 121°C for 15 min.

Autoclave with program 8. Cool down to ~50 °C. Add 200 µl of Ampicillin stock. Mix and pour into petri dish (10-20 ml/dish).

Dexamethasoned stock solution:

The powder was dissolved in DMSO at 10 mg/ml, aliquoted and stored at -20°C.

Puromycin stock solution:

The powder was dissolved in sterile water at 4 mg/ml, aliquoted, and stored at -20 °C. The stock solution is stable for at least three years at -20°C.

Radioimmunoprecipitation assay buffer (RIPA buffer)

50 mM Tris-HCl, pH 8.0	1 ml of 1M Tris-HCl
150 mM NaCl	3 ml of 1M NaCl
0.1% Triton X-100	25 µl of 80% Triton
0.1% SDS	200 µl of 10%SDS
cOmplete™ protease inhibitors	2 tablets
PhosSTOP™ phosphatase inhibitors	2 tablets

dH$_2$O	15.8 ml
Total volume	20 ml

5x Laemmli buffer:

10% SDS, 25% 2-mercaptoethanol, 50% glycerol, 0.01% bromophenol blue, 0.3125 M Tris-HCl.

Running buffer for SDS-PAGE:

25 mM Tris, 190 mM glycine, 0.1% SDS.

10× Transfer buffer:

15.14 g Tris, 71.25 g Glycine, dissolved in <u>500 ml</u> dH$_2$O

Transfer buffer:

100 ml 10× Transfer buffer, 800 ml dH$_2$O, 100 ml methanol.

Tris-buffered saline with Tween 20 (TBST) buffer:

20 mM Tris, pH 7.5, 150 mM NaCl, 0.1% Tween 20. (2.42g Tris, 8.76g NaCl, 800 ml dH$_2$O, 1.0 to 1.5 ml of 37%HCl to adjust pH, bring to <u>1L</u> with dH$_2$O)

Blocking buffer for WB:

5% bovine serum albumin (BSA) in TBST.

Mild Stripping buffer (recipe from Abcam)**:**

15 g glycine,1 g SDS, 10 ml Tween20. Adjust pH to 2.2 with HCl and bring the volume up to <u>1 L</u> with dH$_2$O.

2.10 Kits and disposables

Reagents	Catlaog No.	Provider
ABC-Kit HRP Vectastain	PK-6100	Vector Labs
Avidin/Biotin Blocking Kit	SP-2001	Vector Labs
Biocoat Matrigel Invasion Chambers	354480	Corning
Counting Chamber Slides 50 slides	C10228	Thermofisher
CL-Xposure Film, 7 x 9,5 in (18 x 24 cm) 100 stk	34089	Thermofisher
DAB Peroxidase Substrat Kit	SK-4100	Vector Labs
Falcon 15 ml conical tubes	9180323	Greiner
Falcon 50 ml conical tubes	9178579	Greiner
ImmEdge Hydrophobe Barrier Pen	H-4000	Vector Labs
Filter 0,45 µm, Nalgene 25 mm Syringe Filter	723-2545	Thermofisher
LightCycler® 480 Multiwell Plate 96, white	4729692001	Roche
Maxwell® 16 LEV SimplyRNA Tissue Kit, 48 preps	1000420005	Promega
One Shot™ Stbl3™ Chemically Competent E. coli	C737303	Life Technologies
Pierce™ BCA Protein Assay Kit	23227	Life Technologies
CL-Xposure Film 18x24cm (100 sheets)	34089	Thermofisher
Immobilon-FL 26,5cm x 3,75m PVDF 0,45µm	IPFL00010	Merck Millipore
SimpleChip Enzymatic ChIP	9003s	Cell Signaling Technology

3 Methods

3.1 Mouse experiments

3.1.1 Mouse breeding and housing

All of the mice related procedures were evaluated and reviewed by the Zentrum für Präklinische Forschung of the Technische Universität München, which follows the federal German guidelines for ethical animal treatment (Regierung von Oberbayern). Mice were kept under specific pathogen free (SPF) conditions. The mice were maintained at 22-25 °C and subject to 12 h light/12 h dark cycle. The mice were anesthetized with isoflurane and sacrificed by cervical dislocation at the end of the experiment.

The mouse strains used for breeding include:

Hnf1b$^{flox/flox}$ (Hnf1b^{tm3Mya}): loxP sites flanking the promoter region, the transcription initiation site, and exon 1 of *Hnf1b* [102].

Ptf1a$^{Cre-ERTM}$ (Ptf1a$^{tm2(cre/ESR1)Cvw}$): fusion of *Cre* recombinase gene and mouse estrogen receptor gene *Esr1* (CreERTM) replacing the exon 1 and 2 of *Ptf1a* gene [103].

LSL-Kras^{G12D} (*Kras ^{tm4Tyj}*): the *Kras2* locus was targeted with a cassette containing an oncogenic DNA sequence encoding the Kras2 protein in which the glycine (G) at position 12 had been substituted with an aspartic acid (D). A loxP flanked stop codon was inserted upstream of *Kras2* sequence to avoid the expression of the mutant transcript until Cre-mediated recombination [104].

The mice with acinar-specific ablation of *Hnf1b* (*Ptf1aCre$^{ERT2+/-}$, LSL-Kras$^{G12D+/-}$; Hnf1b$^{fl/fl}$*) were derived from the breeding of *Ptf1aCre$^{ERT2+/-}$, LSL-Kras$^{G12D+/-}$* and *Hnf1b$^{fl/fl}$* mice. Each breeding pair contains only one heterozygous *ptf1aCre^{ERT2}* locus, and one heterozygous *LSL-Kras^{G12D}* locus.

All mice used had a mixed genetic background (*ptf1aCreER$^{+/-}$, LSL-Kras$^{G12D+/-}$* were derived from C57BL/6 mice while the genetic background of *Hnf1b$^{fl/fl}$* mice were unclear).

3.1.2 Tamoxifen gavage

Tamoxifen (Sigma-Aldrich) was dissolved in rapeseed oil and ethanol (9:1, v/v) at a concentration of 30 mg/ml by shaking at 60°C for about 30 min. Tamoxifen was protected from light during preparation and storage (in aluminium foil wrapped tubes). The tamoxifen was administrated to mice aged at 5-9 weeks old, using a 1-ml syringe and a 22-gauge feeding needle. Each mouse received 6 mg/gavage, and was gavaged every other day for 3 times.

The mouse was captured at its neck and back, tightly enough to keep its head immobilized (important!!!) but also to allow proper breathing. The feeding needle was introduced in the mouth behind the tongue to a maximum depth of approximately 1.5 cm, and 0.2 ml of solution was delivered quickly.

3.1.3 Cerulein-induced pancreatitis

One week after last tamoxifen gavage, acute pancreatitis was induced by cerulein. The mice were fed with a standard diet but fasted overnight before induction of pancreatitis. The mice were injected intraperitoneally with eight injections of cerulein administered at a dose of 100 μg/kg (in 0.1 ml PBS) at a 1 h interval.

To accelerate the $Kras^{G12D}$-induced carcinogenesis, the mice were injected with cerulein for one day, and sacrificed on day 21 after the injections for analysis; to evaluate the role of Hnf1b in pancreatitis and regeneration, the mice were injected for two days (eight injections each day), and sacrificed on day 2 and 7 after the last injection.

3.2 Cell culture

3.2.1 Isolation of pancreatic acinar cells

24-well tissue culture plates were coated with 250 μl/well collagen (1 mg/ml) ~1 h before acini isolation. The collagen mixture was made by adding the following reagents in A-D order:

A. 10×PBS = Final volume/10

D. Rat-tail collagen type 1 = $\underline{\text{final volume} \times \text{final collagen concentration*}}$

$\qquad$ Collagen conc. in bottle**

B. 1M NaOH = volume of collagen (see results from D) × 0.023

C. H_2O = final volume – volume collagen – volume 10× PBS

The whole pancreas from a 6- to 9-week-old mouse was dissected, rinsed with ice-cold HBSS, and transferred to a 1.5-ml microcentrifuge tube containing 200 μl of HBSS. The pancreas was minced with sharp spring scissors in 1.5-ml tube until the tissue pieces became approximately 1 mm^3 in size. The minced pancreas was washed with cold HBSS and centrifuged at 1000 rpm, 4 °C for 2 min. The supernatant was discarded. The minced pancreas was resuspended in 5 ml HBSS containing 0.4 mg/ml of collagenase P, and 0.1 mg/ml of soybin trypsin inhibitor at 37°C incubator for 10 min in a 50-ml centrifuge tube, with gently shaking every 3 to 5 min. The digestion was stopped by adding 10 ml HBSS containing 5% FBS. The suspension was centrifuged at 800 rpm, 4 °C for 2 min. The supernatant was discarded. The cell pellet was washed with 10 ml HBSS containing 5% FBS, spinned down at 600 rpm for 2 min. The supernatant was discarded. The pellet was resuspended *gently* (important!) in 10 ml HBSS containing 5% FBS, and passed through a 100-μm nylon filter into 50 ml conical tube. The strainer was washed with another 10 ml HBSS containing 5% FBS. The cell suspension was centrifuged at 300 rpm, 4 °C for 5 min. The acinar cell pellets were resuspended in culture media to adjust the cell density, and mix with matrigel at 1:1. 500 μL of cell suspension was plated in each well embedded with collagen. The cell density should be around 30% confluent under a microscope. The plate was incubated in 5% CO_2 incubator at 37°C for at least 1 h to allow the matrigel to solidify. 500 μL of pre-warmed acinar culture media (supplemented with EGF final conc. 50 ng/ml if the cells did not express Kras^{G12D}) were added to each well thereafter. The cells should survive for at least 4 to 7 days in gel culture.

3.2.2 Three-dimensional culture and sample collection

The media on top of Matrigel was supplemented with fresh media on day 3 after seeding. The media on top were removed, and then 0.5 ml of pre-warmed collagenase P (0.4 mg/ml in HBSS) was added to each well digest Matrigel and collagen at 37°C for 20 min. The mixture of gel and cells from duplicate wells was collected in a 15-ml tube and 1 ml pre-warmed collagenase P was added to the tube. The mixture of gel and cells was incubated at 37°C for another 20 to 30 min. The 15-ml tubes were centrifuged at 3000 rcf for 5 min. The supernatant was carefully removed, but with ~0.5 ml left. The cell pellets were resuspended with 1 ml of HBSS in 1.5-ml microcentrifuge tubes, and then centrifuged at 5000 rpm for 5 min at 4°C. The supernatant was removed, and 250 μl of RNA lysis buffer (RA buffer:2-mercaptoethanol=100:1) was added. The cells were lysed by pipetting for 10 times, and lysates were store at -80 °C until RNA extraction.

3.2.3 Culture of cancer cell lines

Human PDAC cell lines were maintained in RPMI1640 (Corning) supplemented with 10% FBS (Hyclone) and 1% penicillin/streptomycin (Corning). CFPAC-1 was cultured in IMDM supplemented with 10% FBS, and penicillin/streptomycin. Murine PDAC cell lines and HEK293T were grown in DMEM supplemented with 10% FBS, and 1% penicillin/streptomycin.

3.2.4 Cell viability assay

The cells (1×10^3 cells/well) were seeded in 96-well culture plates (Corning). Then, 20 μl of MTT reagent (5 mg/ml prepared in PBS) was added immediately, or at indicated time points. After 4-h incubation at 37°C, 100 μl of acidified SDS (10% SDS:37% HCl = 1000:1, v/v), and the plates were incubated at 37°C overnight. The spectrometric absorbance was measured at 590 nm with a microplate reader (MulitSkan).

3.2.5 Colony formation assay

The cells were seeded in 12-well plates with a density of 500 cells per well and cultured for 10 to 14 days. The cells were washed with PBS, stained with 0.1% crystal violet for 20 min at room temperature, and washed with tap water. Finally, the area of the colonies was calculated with ImageJ to evaluate cell proliferation.

3.2.6 Lentivirus infection and selection

The optimal concentrations of antibiotics (e.g., puromycin for lentiGuide, blasticidin for lentiCas9) for selection were titrated before infection. The optimal concentration refers to the minimum concentration of antibiotics resulting in (nearly) complete cell death after 3 to 7 days of selection with antibiotics. The optimal concentration of puromycin for human PDAC cell lines (except Panc-1) was 1 to 2 μg/ml, and blasticidin was 5 μg/ml.

The cells to be infected in 6-well plates were seeded one day before infection (~30% confluence under a microscope after seeding).

The cells were infected with different amount of virus suspension (50 μl, 100 μl and 200 μl). A non-infected well (the same cell line without viral infection) was kept as control well.

Two days after infection, the medium was refreshed with fresh medium containing antibiotics at optimal concentration. When the cells became confluent, the cells were split and selected with antibiotics again. The selection was stopped when the cells in non-infected well had completely died. The infected well which showed ~10 to 50% of cell death (e.g., the well infected with 100 μl of viral suspension) was kept for subsequent assays.

3.3 Molecular experiments

3.3.1 Genotyping PCR

Each tail cut or ear punch was lysed in 100 μl of DirectPCR Lysis Reagent (Tail) (Viagen) and 10 μl Proteinase K for 2 h or overnight at 55 °C and inactivated at 95 °C for 15 min. 0.5 μl of the supernatant was mixed with 5 μl 2x GoTaq Green Master Mix (Promega), 5 μl of nuclease-free water and the respective combination of primers for the different genotyping-PCRs in a final volume of 12.5 μl. The primers for genotyping PCR are listed in **Table 2-7**.

Table 3-1: The PCR conditions for genotyping

Step	Temperature	Time
Initial Denaturation	95°C	3 min

	95°C	30 sec
36 Cycles	58°C	30 sec
	72°C	1 min
Final Extension 72°C		5 min
Hold	4 or 12°C	

3.3.2 Reverse transcription polymerase chain reaction (RT-PCR)

A small piece of tissue (~2 mm × 2 mm × 2 mm) was sampled from the tail of the pancreas, immersed in RNAlater solution (Invitrogen) and stored at 4°C overnight and then -20°C. The tissue was resuspended in 250 µl of homogenization buffer (Promega) in a 2-ml tube, and homogenized with TissueLyser LT (Qiagen) at 50 rpm for 2 min.

The RNA was extracted automatically with Maxwell RSC instrument and a Maxwell® 16 LEV simplyRNA Purification Kit (Promega). The concentrations of RNA were determined using a NanoDrop™ 2000 spectrophotometer (ThermoFisher). Equal amount of RNA (300 ng to 1000 ng, depending on the RNA concentrations each batch) was used for first-strand cDNA synthesis.

The following components were added to a nuclease-free PCR tube:

Oligo(dT)12-18 (500 µg/ml)   1 µl
300 ng to 1 µg total RNA   x µl
dNTP Mix (10 mM each)   1 µl
Nuclease-free water   to 12 µl

The mixture was heated at 65°C for 5 min and quick chilled on ice. The tube was briefly centrifuged and added with:

5X First-Strand Buffer   4 µl
0.1 M DTT   2 µl
Nuclease-free water   1 µl

All the contents were mixed by pipetting, and incubated at 42°C for 2 min. 1 µl (200 units) of SuperScript™ II RT was added and the contents were mixed by pipetting

gently up and down. The tubes were incubated at 42°C for 50 min and then 70°C for 15 min to inactivate the reaction.

The following reagents were added to each well on a white PCR plate:

SYBR Green Master Mix	5 µl
Forward+ Reverse primer (10 µM)	1 µl
cDNA from first-strand reaction (1:10)	4 µl

The plate was sealed with an adhesive sealing film and centrifuged at 1000 rpm for 2 min. The plate was loaded to the LightCycler 480 Instrument II (Roche), using the following conditions for amplification: 3 min at 95°C (initialization), followed by 40 cycles of: 20 seconds at 95°C (denaturation), 20 seconds at 60°C (annealing), and 20 seconds at 72°C (extension).

The primers for RT-PCR are listed in **Table 2-5**.

3.3.3 ChIP-PCR

HNF1b binding in the PPP2R5C, PPP1R12B and ITGA1 genes were examined by a Chromatin immunoprecipitations (CHIP) assay using the SimpleChIP® Plus Enzymatic Chromatin IP Kit (Cell Signaling Technology) according to the manufacturer's protocols. The cells were cross-linked using formaldehyde (1%) at room temperature. Then, the cross-linking was stopped by adding 100 µl of 10×Glycine per 1-ml PBS + PIC and mix for 5 min at room temperature. 0.5 µl of Micrococcal Nuclease was incubated with the cell lysate complex for 20 min at 37°C with frequent mixing to digest DNA to a length of approximately 150–900 bp (!), checked in a 1.5% agarose gel. The digested cell lysates were further sheared by sonication (30% input, 30 sec for 5 to 6 cycles. The protein-DNA was immunoprecipitated using antibody against HNF1B (3 µg/IP), or anti-IgG (1 µg/IP). To elute the chromatin and reverse the crosslinks, 150 µl of the 1×ChIP Elution Buffer was added to the 2% input sample tube, or each IP sample. The chromatin was eluted by incubating for 30 min at 65°C with vortexing (1000 rpm). The beads were pelleted and the eluted chromatin was carefully transferred to a new tube. To all tubes, including the 2% input sample, 6 µl of 5 M NaCl and 2 µl of Proteinase K were added, and incubated for 2 h at 65°C. DNA was purified using Spin Columns (provided in this kit, not the ones for plasmid purification). Five volumes of DNA Binding

Buffer (750 µl) was added to each DNA sample and vortexed briefly. Each sample was transferred to a DNA spin column in collection tube, and centrifuged at 18,500 g for 30 sec. The column was washed with750 µl of DNA Wash Buffer, and centrifuged at 18,500g for 30 sec. The liquid was discarded, and the spin column was centrifuged again at 18,500g for 30 sec to remove the remnant liquid. 50 µl of DNA Elution Buffer was added to each spin column and the column was placed into a clean 1.5 ml microcentrifuge tube. The column was centrifuged again at 18,500g for 30 sec to elute DNA.

Quantification of DNA by quantitative PCR. 1 µl of 2% input chromatin DNA was included to determine the efficiency of IP; 2 µl of the DNA sample from anti-IgG or anti-HNF1B was used as template for real-time PCR. Amplification was performed on LightCycler 480 with the following PCR program:

a. Initial Denaturation 95°C 3 min

b. Denature   95°C 20 sec

c. Anneal   60°C 20 sec

d   Extension: 72°C 20 sec

      Repeat steps b to d for 40 cycles.

IP efficiency was evaluated with the equation shown below:

Percent Input = 2% x $2^{(C[T]\ 2\%Input\ Sample\ -\ C[T]\ IP\ Sample)}$

The primers used to amplify target sequences are listed in **Table 2-6**.

3.3.4 Western blot

The cells were digested with 0.05% Trypsin-EDTA (ThermoFisher), centrifuged at 2000 rpm for 2 min, washed once with PBS, and then lysed with radioimmunoprecipitation assay buffer (RIPA buffer) on ice for at least 10 min. The cell lysates were sonicated with lowest power (10% input) and the samples were centrifuged at 13000rpm for 10 min at 4 °C. The protein concentration was assessed by BCA Protein Assay (Pierce) according to the manufacturer's instructions. Lysates were diluted with 5x laemmli buffer and heated at 95 °C for 5 min. The samples were separated by reducing SDS-PAGE and transferred on PVDF membranes (Merck-Millipore). After blocking with 5 % milk powder or BCA (Sigma) in 1xTBS/0.1 % Tween-20 (TBST) for 1 h at room temperature, membranes were incubated in primary antibody (listed in **Table 2-1**)

diluted in the blocking buffer overnight at 4 °C. After three washes with TBST, membranes were incubated in blocking buffer with secondary antibody (1:2000 or 1:5000) for 1 h at room temperature followed by three washes with TBST. The blots were incubated with Immobilon Western Chemiluminescent HRP Substrate (Millipore) for 2 to 5 min, and then detected using Gel Doc XR+ System (Bio-Rad).

3.3.5 Cloning of CRISPR -Cas9 plasmids

sgRNA design

The first exon(s) in coding sequences (CDS) shared between all the mRNA isoforms was input for sgRNA design using CCTop [105].

The sgRNAs with the lest off targets and highest efficiency were selected. Two partially complementary oligos with 4 nt overhangs compatible for cloning into B*sm*BI site (the same as B*bs*I site) in pLentiGuide-Puro were synthesized.

5' –**CACC**GNNNNNNNNNNNNNNNNNNNN –3'

3' –CNNNNNNNNNNNNNNNNNNNN**CAAA** –5'

Each pair of oligos were annealed in a PCR tube containing: 1 µl of oligo 1 (100 µM), 1 µl of oligo 2 (100 µM), 1 µl of T4 ligase buffer and 7 µl of nuclease-free H_2O. The tube was incubated in a thermocycler at 95°C for 5 min and then ramped down *slowly* to 25°C within ~40 min. The annealed oligos were diluted at 1: 50 with nuclease-free H_2O.

Digestion & ligation system was prepared in a PCR tube as follows:

pLentiGuide.   100 ng

T4 ligase buffer   2 µl

T4 ligase (400 U/µl, NEB)   1 µl

*BsmB*I (10 U/µl, NEB)   1 µl

Annealed oligos (the diluted)   1 µl

nuclease-free H_2O to total volume of 20 µl.

The PCR tube was incubated on thermal cycler for 9 or 10 cycles of {37°C for 5 min+16°C for 10 min}, then 55°C for 5 min, 80°C for 5 min and store at 4°C or used for transformation immediately. Two controls should be included at the same time:

Control 1: 100 ng of pLentiGuide diluted in 20 µl of nuclease-free H_2O;

Control 2: 100 ng of pLentiGuide after digestion (the same system as above except

"Annealed oligos").

Transformation

Three Amp⁺ agar plates were prewarmed in a 37 °C incubator. 10 µl of the final product from digestion&ligation step, 10 µl of Control 1 or 10 µl of Control 2 each was mixed with 50 µl of ice-cold competent stbl3 cells, respectively. The mixture was smeared immediately and evenly on Amp⁺ agar plates (work closely to a flame to keep sterile). The plates were dried at room temperature on the bench and then incubated at 30°C(!) overnight. Typical results: several to dozens of colonies will be seen the next morning. 10 µl of Control1 will give rise to hundreds or thousands of colonies while Control 2 will show no colony.

Colonies identification

Two to three colonies (usually sufficient to get at least 1 positive clone) were marked with a mark pen on the back of agar plate. Each colony was picked with a 200-µl tip, boiled for 5 min in 10 µl of PCR-grade water in a PCR tube. The tube was centrifuge briefly, and 1 µl of supernatant was taken as template for colony PCR, using U6 sequencing primer **(**U6_Fwd**)** and sg-reverse as primers. The PCR product would be ~270 bp if a positive colony was picked. The verified colony was inoculated into LB medium (containing 100 µg/ml Amp) for amplification. The plasmids were extracted according to the manufacture's instruction (NucleoSpin Plasmid, Mini kit for plasmid DNA). The plasmid was further verified by DNA electrophoresis and sequencing. DNA electrophoresis is helpful to check whether the plasmid size is still correct. The concentrations and volumes of sequencing primer (U6_Fwd) and plasmids were adjusted according to the requirements of Eurofins as follows. The premixed samples should consist of 2 µl of primer at a concentration of 10 µM and 15 µl purified DNA (50–100 ng/µl).

The correct colonies from agar plate were inoculated directly to 150–200 ml liquid LB (containing 100 µg/ml Amp) in a 500-ml Erlenmeyer flask and shaken at 200–250 rpm, 30 °C until the medium becomes cloudy (12–20 h). Alternatively, the colonies were inoculated into 5 ml LB (starter culture) at first, and then 0.5 ml of the starter culture of log phase (~8h after inoculation) were added into 150 to 200 ml liquid LB (containing

100 µg/ml Amp) and shaken overnight. The plasmids for transfection or lentivirus package were isolated using NucleoBond™ Xtra Midi kit (Macherey-Nagel).

3.3.6 Lentivirus package

HEK293T cells were seeded at a density of 1.0–1.5 million cells per 10-cm dish in 10 ml medium (DMEM + 10% FBS + 1% P/S) one day before transfection. The medium was replaced with DMEM + 10% FBS w/o P/S half an hour before transfection. The transfection mix was prepared as follows for one 10-cm plate, and a master mix could be made accordingly.

Table 3-2: The reagents for transfection

Reagents	amount (µg)	volume (µL)
psPAX	1.25	
pMD2.G	0.75	
lenti. Vector	2	
O-MEM or RPMI w/o FBS	-	270

The reagents were mixed by pipetting for 10 times. The FugeneHD vial was vortexed before use, and 11 µl of FugeneHD was added. The mixture was mixed thoroughly by pipetting for 10 times, and incubated for 10-15 min at RT. The mixture was added dropwise to HEK293T cells, and the dish was returned to 37°C overnight.

The medium of the transfected cells was replaced with 4 ml of DMEM containing 30% FBS. Two days after transfection, the viral supernatant was collected in 15-ml Falcon tubes and stored at 4°C. 4 ml of DMEM containing 30% FBS was added to the dish again. The supernatant was collected again and pooled with the supernatant collected one day before. The virus suspension was centrifuged at 3000 rpm for 5 min, filtered through a 0.45-µm filter (green) with syringe, and aliquoted in cryotubes. The viral supernatant was snap frozen with liquid nitrogen and store at -80 °C.

3.4. Histology analysis

3.4.1 Formalin-Fixed Paraffin-Embedded (FFPE) tissue sections

The dissected pancreas tissue was fixed overnight in 4% paraformaldehyde solution in PBS (Santa Cruz), and then transferred to 70% ethanol. The tissues were dehydrated using an Enclosed Tissue Processor (Leica ASP300S), and embedded in paraffin. The paraffin blocks were then stored at -20 °C overnight before cutting. For staining analysis, series of 1.5-µm sections were cut using a microtome (HM355S, Thermofisher).

3.4.2 Haematoxylin and eosin (H&E) staining

The FFPE sections were deparaffinized with Xylene, rehydrated with ethanol, stained with hematoxylin, blued with diluted ammonia, differentiated with diluted HCl, stained with eosin, and dehydrated as follows. Finally, the slide was mounted with mounting media (Pertex) and sealed with a coverslip (VVR).

Table 3-3: The procedure for H&E staining

Steps	Reagents	Time × repeats	Note
1	Xylene	5 min × 2	
2	100% EtOH	1 min × 3	
3	dH$_2$O (in a tank)	10 dips × 2	
4	Hämalaun	3 min	
5	dH$_2$O (in a tank)	10 dips × 4	
6	Diluted ammonia	3 sec (5 dips)	25% ammonia: dH$_2$O = 1:12.5 (v/v)
7	dH$_2$O (in a tank)	10 dips × 2	
8	Diluted HCl	3 sec (5 dips)	37% HCl: dH$_2$O = 1:100 (v/v)
9	Diluted ammonia	3 sec (5 dips)	the same as step 6
10	dH$_2$O (in a tank)	10 dips × 2	
11	70% EtOH	3 sec (5 dips)	
12	Eosin	1 min	0.2% in ethanol
13	100% EtOH	1 min × 3	
14	Xylene	3 min ×2	
15	Cover-slipping		

3.4.3 Immunohistochemistry (IHC)

The tissue sections were deparaffinized and rehydrated as follows: ROTI Histol (Xylene substitutes; Roth) for 5 min and 3 min; 100% Ethanol for 2 min ×2; 96% Ethanol for 2 min ×2; 70% Ethanol for 2 min ×2; rinsed with deionized H_2O (dH_2O) from the tap. Antigen unmasking was used to improve detection of antigens in paraffin embedded tissue sections when used in combination with heat-mediated pre-treatment protocols. A plastic box was filled with 220 ml of dH_2O and 2 ml of low-pH unmasking solution (H-3300; Vector Labs).

The slides were put on the rack in the box and the unmasking solution was boiled with a microwave oven on highest power (900W) for 5 min and then lowest power (90W) for 15 min. The samples and solution were cooled down for 30 min at room temperature. The slides were washed in dH_2O briefly. The tissue sections were circled with an ImmEdge hydrophobic barrier pen (Vector Labs), incubated with 3% H_2O_2 (dilute the 30% H_2O_2 solution at 1:10 with dH_2O) for 10 min in dark, rinsed briefly in dH_2O and incubated with 1×PBS containing 0.3% Triton X-100 for 3 min if nuclear antigen is to be detected.

The slides were rinsed with 1×PBS for 5 min. A wet chamber was made with wet paper in a tissue section box. The tissue sections were blocked with 50–100 µl of 5%–10% FBS in 1×PBS for 1 h at room temperature. 50–100 µl of primary antibody diluted in recommended diluent (i.e. 5% FBS in 1×PBS) was incubated with the sections over night at 4°C.

The slides were washed with 1×PBS for 5 min×3, and then incubated with 50-100 µl of biotinylated secondary antibody (diluted 1:1000 in recommended diluent) for 1 h at room temperature. The VECTASTAIN Elite ABC reagents were prepared as follows: 10 µl of reagents A, 10 µl of B, and 1 ml of 1×PBS. The ABC solution was incubated for at least 30 min at 4°C. The slides were washed with 1×PBS for 5 min ×3. 50-100 µl of ABC complex was added to each section and incubated for 20 min at RT. The slides were washed with 1×PBS for 5 min ×3. The DAB solution was prepared as follows:
1 ml 1×PBS + 20 µl of DAB + 16 µl of H_2O_2, and then vortexed briefly. 50 µl of DAB solution was added to each section and the development of staining was monitored

closely under a microscope. When the specific staining developed, the slides were immersed in H_2O to stop the development. The slides were rinsed in dH_2O. The sections were then counterstained with hematoxylin for ~5 sec. The slides were washed with dH_2O 4 to 5 times. The sections were dehydrated: 70% ethanol for 2 min × 2, 96% ethanol for 2 min × 2, 100% ethanol for 2 min × 2, and Xylene for 5 min × 2. The slides were applied with Pertex and sealed with coverslips.

3.5 RNA-sequencing and data analysis

RNA samples from acinar cells were extracted using Maxwell® 16 LEV simplyRNA Purification Kit (Promega). The concentrations of total RNA were normalized to 20 ng/µl and sent to the facility in TUM (Institute of Molecular Oncology and Functional Genomics) for cDNA library construction and RNA-seq.

Reads were mapped to mouse genome (GRCm38/mm10) and the expression level of each gene was normalized to rlog with DESeq2. A gene was regarded as a differentially expressed gene (DE gene) if the adjusted p-value was < 0.05 and the absolute log2-scaled fold of change >1.

3.6 Statistical analysis

Statistical analysis was performed using the GraphPad Prism software (Version 6.0; GraphPad Software, Inc., San Diego, CA). All quantitative data are presented as mean ± standard deviation (SD) if not specified. Statistical differences were analyzed using the two-tailed unpaired Student's t-test, the Mann-Whitney U test, or one-way ANOVA. Statistical significance is displayed as *$p < 0.05$, **$p < 0.01$ or ***$p < 0.001$.

4 Results

4.1 Hnf1b expression pattern in mouse pancreas

To investigate the expression pattern of Hnf1b in different conditions, the expression of Hnf1b in the pancreata of wild-type mice was checked by immunohistochemistry (IHC) staining. It was reported that Hnf1b expression was restricted to ductal cells in postnatal mice [79], and Hnf1b is recognized as a marker for ductal lineage. Consistently, our IHC staining showed that Hnf1b strongly expressed in pancreatic ductal cells and centroacinar cells in the pancreata of adult mice, while no expression in acinar cells (**Figure 4-1A**).

Since Hnf1b is a ductal marker, it was hypothesized that Hnf1b would be up-regulated during acinar-to-ductal metaplasia (ADM). To test this, the expression of Hnf1b in the pancreata of wild-type mice was determined on day 2 and day 4 after cerulein injection, since cerulein-induced acute pancreatitis is accompanied with intensive ADM. RT-PCR results showed that the mRNA level of *Hnf1b* was significantly up-regulated after cerulein injection (**Figure 4-1B**). IHC staining with anti-Hnf1b antibody also demonstrated that the Hnf1b protein level was up-regulated in acinar cells undergoing ADM (**Figure 4-1A**). These data suggested that Hnf1b may play a role in ADM, and thus might be involved in carcinogenesis.

A more important aim of this project is to understand the role Hnf1b in pre-cancerous lesions. Because *ptf1a-Cre; LSL-Kras^{G12D}* (CK) and *ptf1a-Cre; LSL-Kras^{G12D}; p53$^{fl/fl}$* (CKP) mice are commonly used mouse models to study pancreatic carcinogenesis, the histological sections of CK and CKP mice harvested at different time points were stained with anti-Hnf1b. It was shown that Hnf1b expression levels were elevated in ADM (**Figure 4-1C**), which is consistent with what was found in cerulein-induced acute pancreatitis (**Figure 4-1B**). However, Hnf1b protein was lost in most of low-grade PanINs, but started to express again in high-grade PanINs and well-differentiated cancerous ducts (**Figure 4-1C**). Thus, it was hypothesized that Hnf1b may be also required for Kras^{G12D}-induced carcinogenesis.
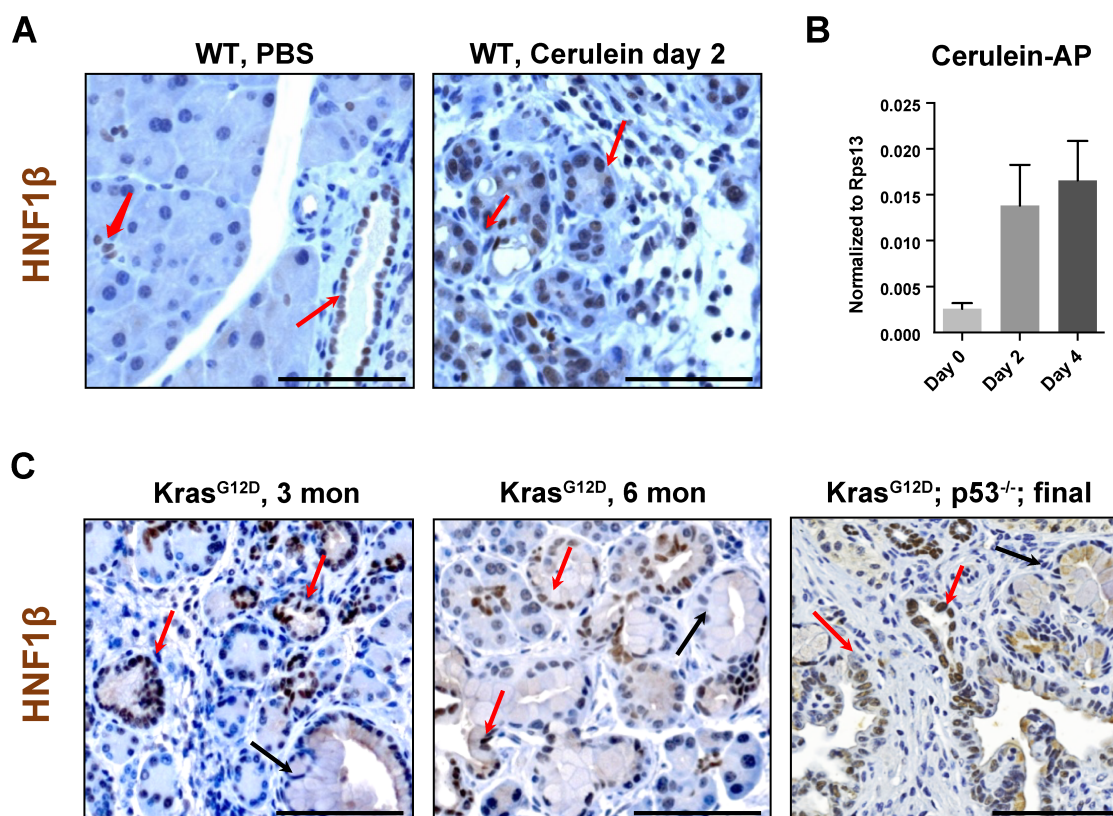
Figure 4-1: Expression of Hnf1b in pancreas under different conditions.
(A) Immunostaining for Hnf1b in normal pancreas and pancreas undergoing pancreatitis. Red arrows indicate positive staining, while black arrows show the negative expression of Hnf1b in low-grade PanINs. Scale bar=100 μm. (B) Quantitative RT-PCR data of Hnf1b expression, showing the levels of Hnf1b mRNA were elevated in wild-type (WT) mice during pancreatitis at indicated time points (n = 4 for each group). p = 0.0009 by one-way ANOVA analysis. (C) Expression of Hnf1b during tumor development. Red arrows indicate positive staining of Hnf1b, while black arrows indicate negative staining in some PanINs. Scale bar = 100 μm.

4.2 Verification of the conditional Hnf1b knockout mouse model

Since Hnf1b deficiency in pancreatic progenitor cells led to severe pancreatic hypoplasia and perinatal lethality [82], in this thesis *Hnf1b* was knocked out in the pancreas of postnatal mouse in an inducible manner. In addition, based on genetically engineered mouse models, identical oncogenic drivers could trigger PDAC in both ductal and acinar cells but with distinct pathophysiology [106], and ductal deletion of Hnf1b facilitated tumorigenesis [101]. Therefore, the specific interest of this project is to understand whether and how Hnf1b can affect the carcinogenesis originating from adult acinar cells.

To obtain the deletion of *Hnf1b* in adult acinar cells with expression of mutant Kras, *ptf1a-Cre^{ER};LSL-Kras^{G12D}* mice were crossbred with *Hnf1b$^{fl/fl}$* or wild-type mice to get *ptf1a-Cre^{ER};LSL-Kras^{G12D}* (*iCK*), *ptf1a-Cre^{ER};LSL-Kras^{G12D};Hnf1b$^{fl/wt}$* (*iCKH$^{+/-}$*) and *ptf1a-Cre^{ER};LSL-Kras^{G12D};Hnf1b$^{fl/fl}$* (*iCKH$^{\Delta}$*) mice (**Figure 4-2A**), and then the mice were gavaged with tamoxifen when they were 6 to 8 weeks old.

To validate whether *Hnf1b* gene expression was ablated in the pancreas of the novel mouse model after gavage, the recombination of *Hnf1b* locus, and expression level of *Hnf1b* mRNA were detected by recombination PCR, and RT-PCR, respectively.
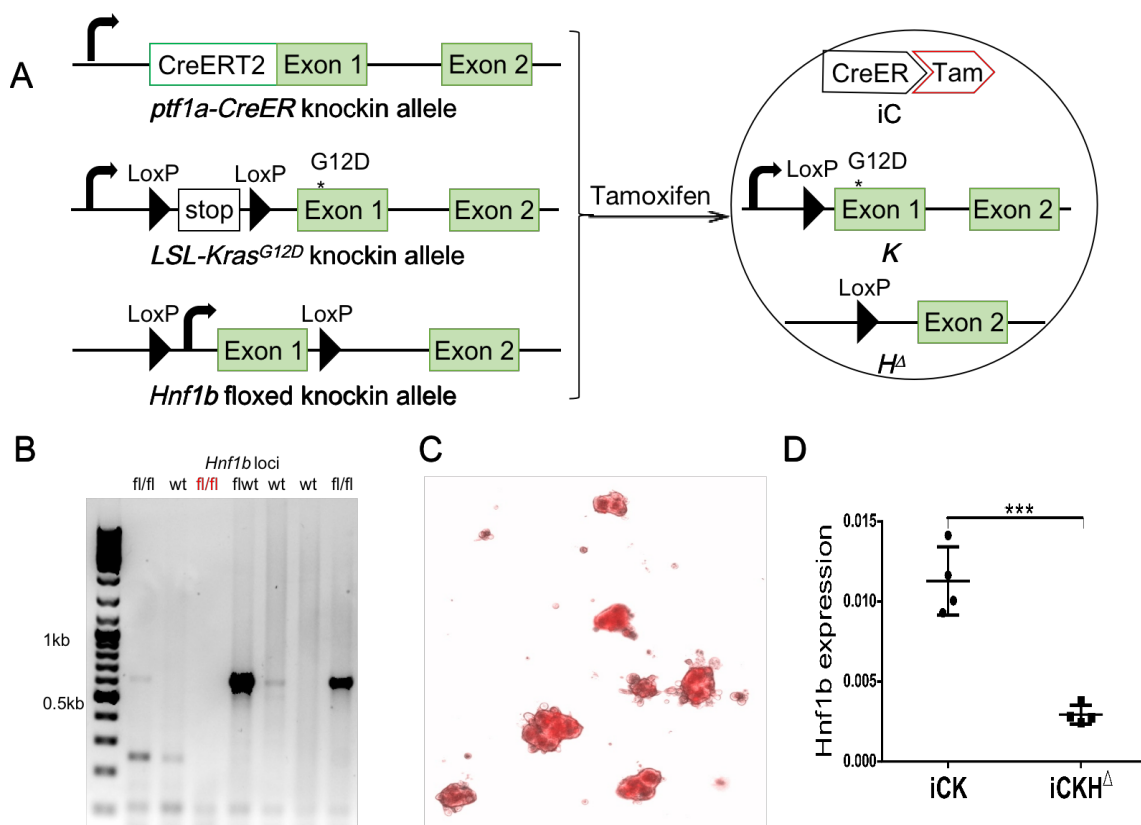
Figure 4-2: Verification of mouse model.
(A) Schematic of the alleles in *ptf1a-Cre^ER; LSL-Kras^G12D; Hnf1b^flox/flox* (acinar iCKH^Δ) mouse model. Once tamoxifen binds to the fusion protein Cre^ERT2, the latter translocates from the cytoplasm to the nucleus and excises genomic sequences between loxP sites. Therefore, tamoxifen gavage induces Cre-mediated DNA recombination and results in the expression of oncogenic Kras^G12D and inactivation of Hnf1b expression. (B) Mice with different genotypes of *Hnf1b* (wt, flox/wt and flox/flox) were gavaged with tamoxifen. The pancreatic DNA was extracted, and genomic PCR was used to detect the presence of the *Hnf1b* deletion (expected size ≈ 650 bp). (C) The acinar cells isolated from a *Ptf1aCreER/+; Rosa26-LSL-tdTomato* mouse one week after tamoxifen gavage. Most of the cells show red fluorescence, indicating a Cre-mediated recombination. (D) The expression of *Hnf1b* mRNA in the primary acinar cells isolated from mice after tamoxifen gavage (n = 4 for each genotype). Data are expressed as mean±SD. *** $p < 0.001$.

After tamoxifen gavage, there was a specific deletion band detected in pancreatic genome of mice harboring *Hnf1b* loxP loci (except the third mouse died before pancreas harvest) (**Figure 4-2B**), indicating Cre-mediated recombination had occurred. In addition, *ptf1a-Cre^ER; Rosa26-tdTomato* mice (reporter mice) were used to monitor the efficiency of tamoxifen induction. The acinar cells were isolated and cultured in gel, and most the acinar cells demonstrated red fluorescence (**Figure 4-2C**), indicating a high induction efficiency with our gavage protocol. Moreover, when primary acinar cells were isolated, *Hnf1b* mRNA also significantly declined in iCKH^Δ acinar cells (**Figure 4-2D**). Taken together, these data showed that the Hnf1b expression was specifically and efficiently inactivated in acinar cells after tamoxifen induction in iCKH^Δ mice.

4.3 Knockout of Hnf1b inhibited pancreatitis-accelerated carcinogenesis

Although Hnf1b expression was up-regulated in ADM, it is unknown whether its expression affects the formation of ADM and PanINs. To investigate the role of Hnf1b in carcinogenesis quickly, the precursor lesions were evaluated in pancreatitis-accelerated model (**Figure 4-3A**), as cerulein-induced inflammation accelerates the $Kras^{G12D}$ driven carcinogenesis process [107], [108]. Firstly, among different genotypes there was no difference in pancreas to body weight ratio (**Figure 4-3B**), which is a parameter for acute inflammation or tumor burden [109]. Secondly, histological analysis of the pancreata showed that compared to PBS, cerulein injections led to much more discernible lesions in iCK mice on day 21 after last cerulein injection (**Figure 4-4A**). Compared to those of iCK mice, there were much less lesion areas (remodeled area including ADM and PanINs) in the pancreata of iCKH$^\Delta$ mice (**Figure 4-4B**), but no statistical difference in PanIN numbers (total number in whole section normalized to area) (**Figure 4-4C**).
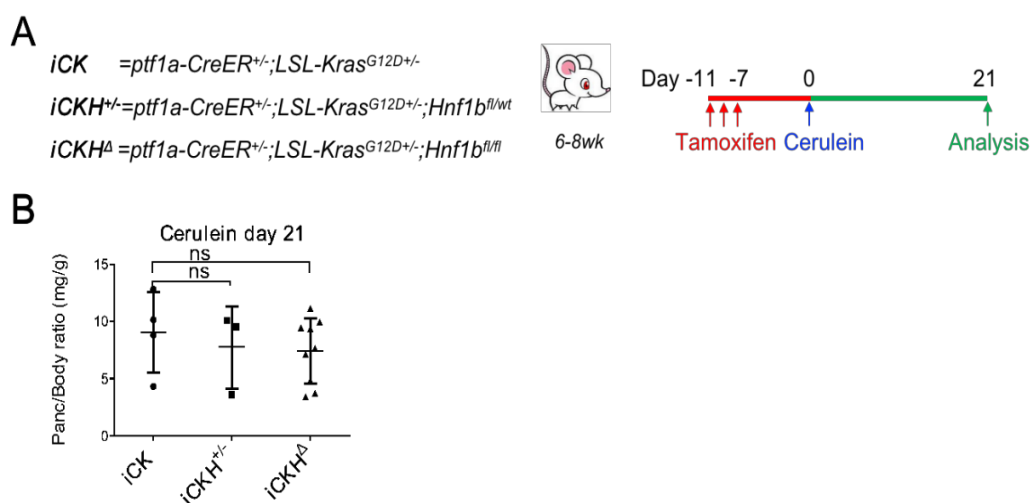

Figure 4-3: Cerulein-induced acute pancreatitis accelerated Kras^{G12D}-induced carcinogenesis model.
(A) schematic of pancreatitis accelerated carcinogenesis. (B) The ratios of pancreas weight to body weight when the mice were sacrificed. Data are shown as means ± SD. ns: not significant for two-tailed t-test.
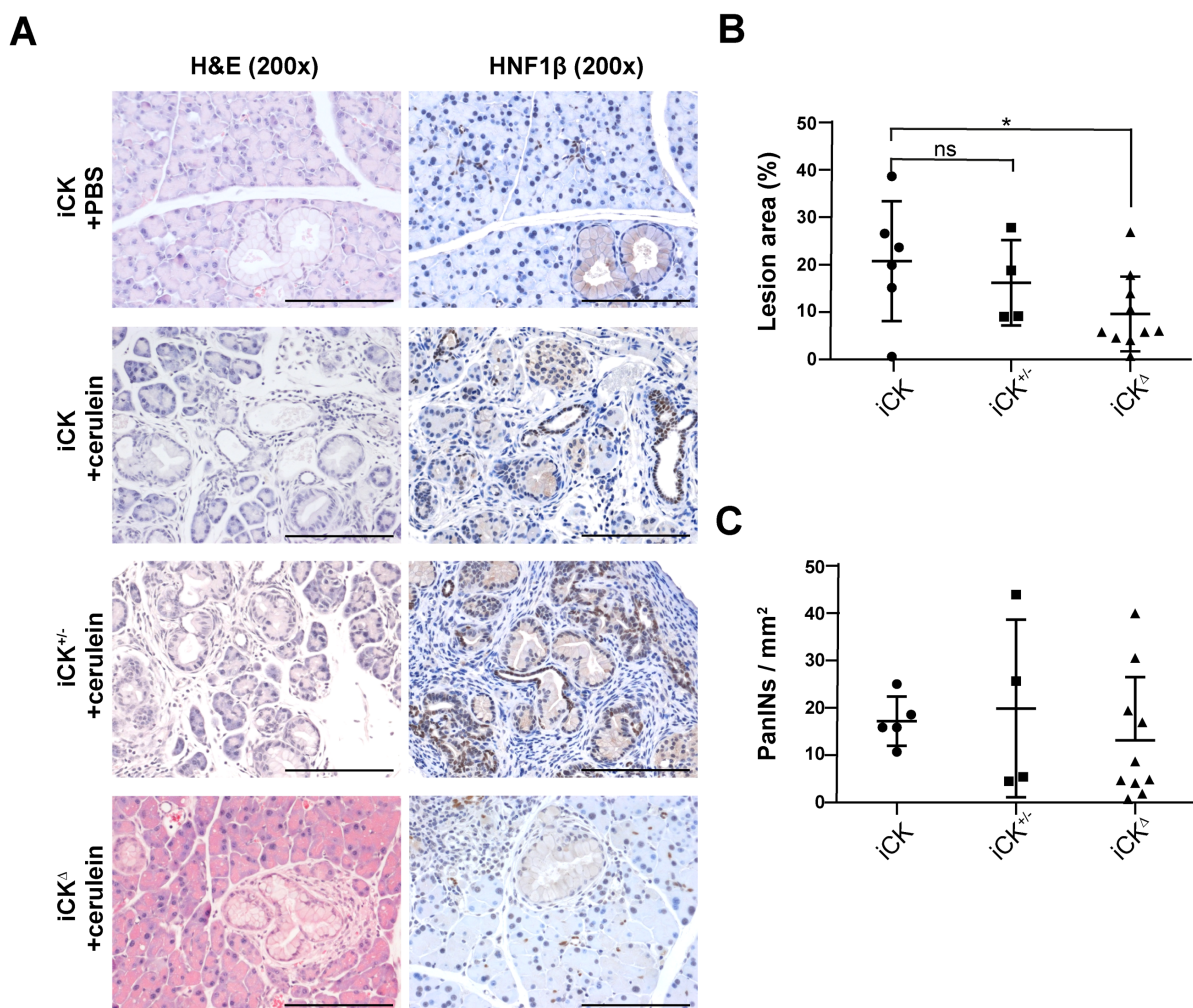
Figure 4-4: Knockout of Hnf1b in acinar cells inhibits lesions caused by inflammation and Kras^{G12D}.
(A) Representative figures of Hematoxylin and eosin (H&E) staining showing the histological features of precursor lesions in indicated experimental groups (magnifications: 200×). Hnf1b protein expression was detected by immunohistochemical staining (IHC). Scale bar = 100 µm. (B) Percentage of lesion areas in different genotypes. (C) PanIN number normalized to area. Data are shown as means ± SD. *$p < 0.05$.

Taken together, the data in pancreatitis-accelerated carcinogenesis model indicated that Hnf1b is an important mediator for inflammation and Kras^{G12D}-induced early stage of cancer progression.

4.4 *Hnf1b* ablation in acinar cells inhibited Kras^{G12D}-induced carcinogenesis

The combination of cerulein-induced inflammation potentiates Kras^{G12D}-induced carcinogenesis and enables us to observe early precancerous lesions quickly; on the other hand, inflammation also complicates the scenario of carcinogenesis. To determine the relationship between Hnf1b and mutant Kras during the initiation of pancreatic cancer, the effects of Hnf1b on Kras^{G12D}-induced carcinogenesis without cerulein injection were further checked.

Three months after tamoxifen induction of Kras^{G12D} expression and Hnf1b deletion in adult acinar cells, there were significantly fewer PanINs in iCKH$^{\Delta}$ mice compared to iCK mice, indicated by histological examination and CK19 staining (**Figure 4-5B and D**). Similarly, there were also fewer lesions in iCKH$^{+/-}$ and iCKH$^{\Delta}$ mice (**Figure 4-5B and C**). These data indicate that Hnf1b is required for Kras^{G12D}-induced precursor lesions *in vivo*.

A

iCK $= ptf1a\text{-}CreER^{+/-};LSL\text{-}Kras^{G12D+/-}$

$iCKH^{+/-}= ptf1a\text{-}CreER^{+/-};LSL\text{-}Kras^{G12D+/-};Hnf1b^{fl/wt}$

$iCKH^{\Delta} = ptf1a\text{-}CreER^{+/-};LSL\text{-}Kras^{G12D+/-};Hnf1b^{fl/fl}$
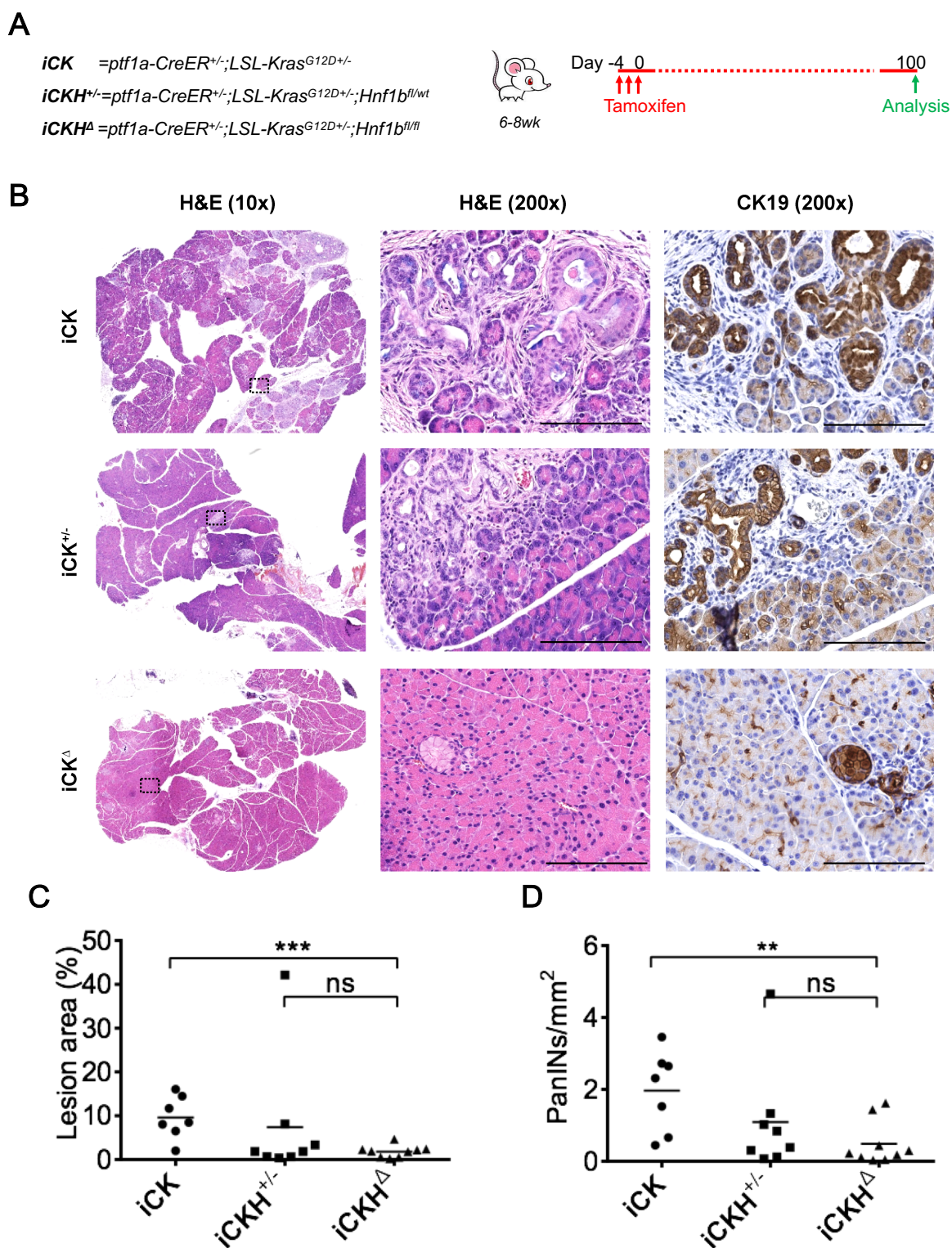

B

C

D

Figure 4-5: Knockout of Hnf1b in acinar cells inhibits Kras^{G12D}-induced carcinogenesis.
(A) Schematic of experiment procedure. (B) H&E staining and CK19 protein (ductal marker) expression in Kras^{G12D}-expressing pancreata with different *Hnf1b* genotypes. Scale bar = 100 μm. (C) Percentage of lesion areas in different groups. (D) PanIN number normalized to area. The bar shows the mean of each group. **p < 0.01, ***p < 0.001, ns: not significant.

4.5 Hnf1b upregulation is not essential for ADM

The above data showed that Hnf1b was required for Kras^{G12D}-driven carcinogenesis. However, there were still sparse lesions in iCKH$^{\Delta}$ pancreata at 3 months. We wondered whether these lesions derived from recombined or unrecombined acinar cells. To address this question, the expression of Hnf1b protein was evaluated with IHC staining. The results showed that in iCK pancreata, the ADM units usually associated with strong Hnf1b staining in nuclei, while in iCKH$^{\Delta}$ pancreata the staining was just as weak as the background staining in normal acinar cells (**Figure 4-6**), indicating no expression of Hnf1b in these ADM structures. Furthermore, the ADM units in iCK pancreata with strong Hnf1b staining were in late stage, indicating that Hnf1b upregulation may be a late-stage event in ADM. Taken together, Hnf1b upregulation is dispensable for early formation of ADM.
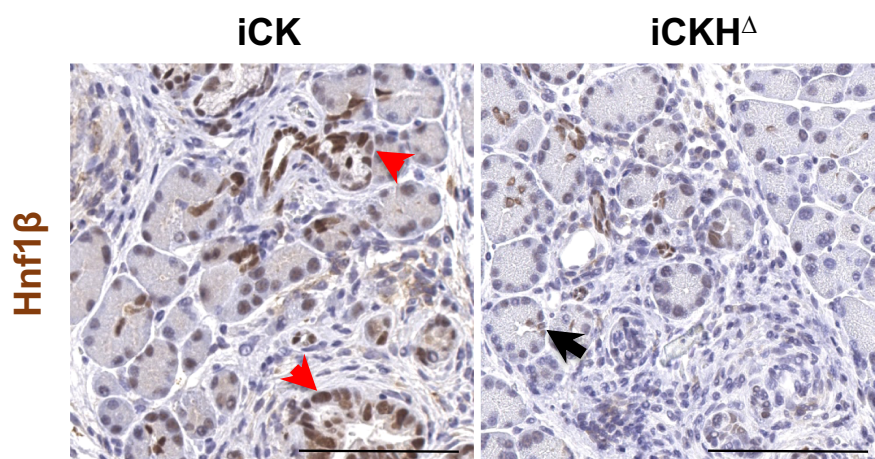
Figure 4-6: ADM formation without Hnf1b upregulation in *Hnf1b* knockout mice.
The Hnf1b IHC staining was performed with the sections from mice of indicated genotypes 3 months after Tamoxifen induction. The red arrows indicate the ADM with upregulation of Hnf1b protein, while the black arrow shows the ADM without upregulation of Hnf1b, compared to the neighboring acinar cells. Scale bar = 100 μm.

4.6 Establishment of *in vitro* culture of acinar cells

Acinar-to-ductal metaplasia (ADM) is a transdifferentiating process occurring during pancreatitis or pancreatic carcinogenesis, and considered as the main origin of pancreatic pre-neoplastic lesions when oncogenic signaling has activated [40], [110]. Therefore, knockout of *Hnf1b* in acinar cells was hypothesized to inhibit ADM and thus delay PanIN formation.

In vitro 3D culture of acini facilitates the observation of ADM and provides advantages to investigate the initial mechanisms regulating ADM and even carcinogenesis [111],[112].

To establish the *in vitro* culture for acinar cells, acinar cells were isolated from the pancreata of iCK mice and cultured in Matrigel for 5 days. It is shown that on day 3, there were already duct-like cystic structures (**Figure 4-7A**), which are considered as an indication for ADM. RT-PCR results further revealed that during the *in vitro* culture, acinar cell marker gene *Ptf1a* decline though not significantly (p = 0.123 for day 0 vs day3) due to the sample size, while the ductal marker gene *Krt19* upregulated (p = 0.002 for day 0 vs day3). In addition, the *Hnf1b* mRNA tended to increase (p = 0.268 for day 0 vs day3). Moreover, there was increase in *Kras* mRNA (p = 0.008 for day 0 vs day3) (**Figure 4-7B**). Altogether, these changes indicate that ADM occurred during the gel culture.
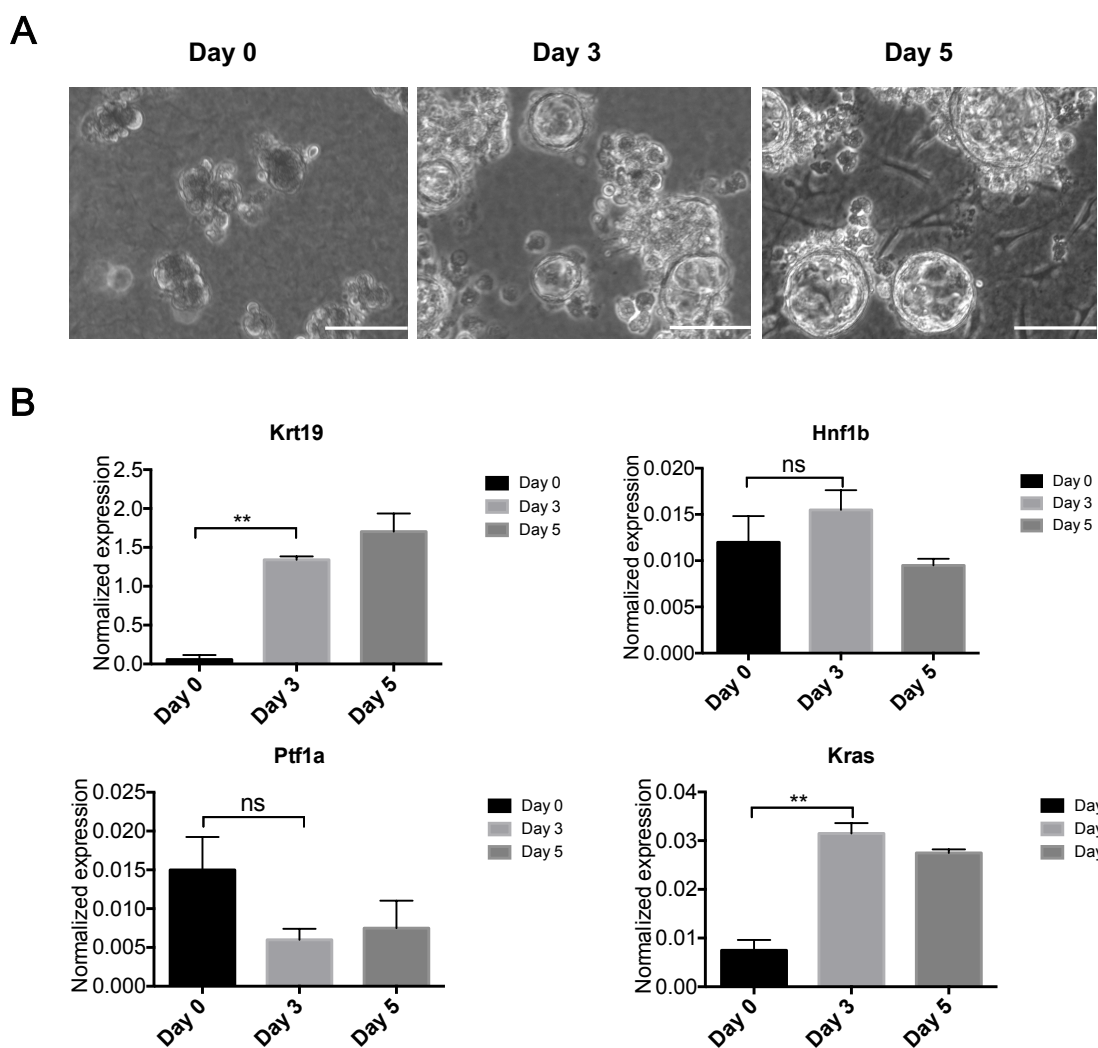
Figure 4-7: Establishment of 3D culture of acinar cells.
(A) The morphology of acinar cells during 3D culture at indicated time. Magnification: 100× and scale bar=100 μm. qRT-PCR data of selected genes at indicated time point (n=2 for each genotype). **p < 0.01, ns: not significant.

4.7 RNA-sequencing of acinar cells and metaplasia cells

To profile the gene expression pattern during ADM, the acinar cells from iCK and iCKH$^\Delta$ mice were harvested on day 0 (immediately collected after isolation) and day 3, and the RNA was extracted for RNA-sequencing.

To evaluate the correlation between samples, the Pearson correlation analysis was performed. The results demonstrated that the samples on the same time point (day 0 and day 3) resembled each other. In contrast, the correlation is low between the samples of day 0 and the samples of day 3 (**Figure 4-8**), indicating ADM occurred between day 0 and day 3.
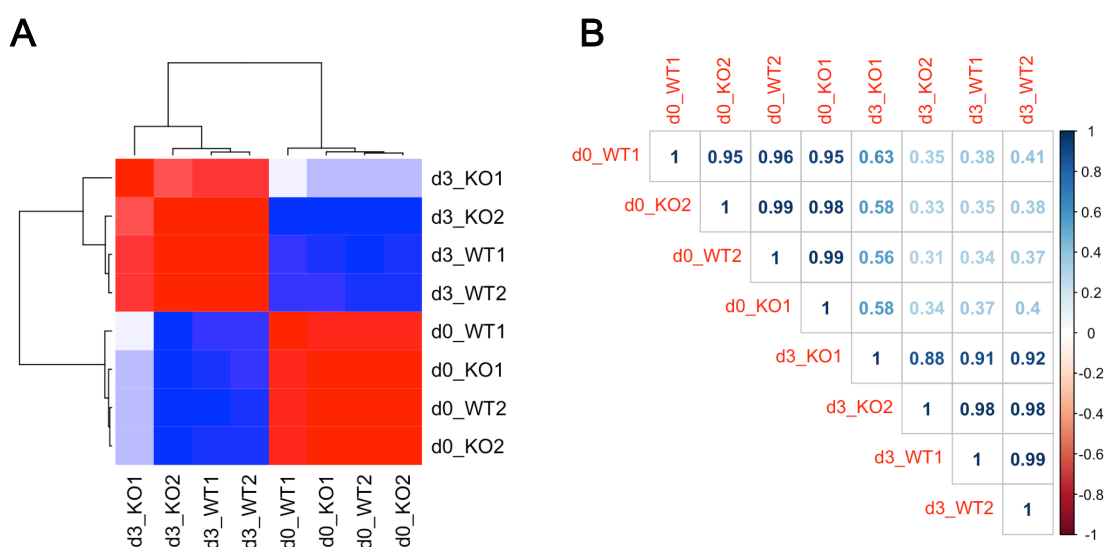
Figure 4-8: Pairwise comparisons of the correlation between samples.
The acinar cells were collected on day 0 (immediately after isolation) and day 3 from Matrigel culture. (A) Heatmap of the correlation. The correlation matrix is reordered according to the correlation coefficient using "hclust" method. The coefficients ranged from low to high, indicated by color blue to red respectively. WT, cells from iCK mice; KO, cells from iCKH$^\Delta$ mice. (B) Pearson correlation analysis between all biological RNA-samples. The Pearson correlation coefficients between each two samples are indicated in each plot. The value denotes the correlation coefficient and the color of the value from the light blue to dark blue indicates the correlation coefficient from low to high. n = 2 for each group at each time point.

Results of the hierarchical clustering showed that the time point more largely determine the expression profile. All samples at day 0 are very similar and very distinct from the samples on day 3. On day 3, the iCK are very similar while the two iCKH$^\Delta$ samples showed a slight difference possibly due to the heterogeneity of the individuals.

On day 0, there were 358 differentially expressed (DE) genes between iCK and iCKH$^\Delta$ cells, with 207 upregulated genes in iCKH$^\Delta$ cells and 151 downregulated (**Figure 4-9A**). On day 3, there were fewer DE genes according to the identification criteria

(log2Fold change >1 and p-value < 0.05), i.e. 28 genes upregulated in iCKH$^\Delta$ cells and 18 downregulated (**Figure 4-9B**). Some DE genes were verified with RT-PCR using the same samples sent for RNA-sequencing. RNA-seq results showed that on day 3, *E2f8* is a downregulated DE gene, and *Ins2* was upregulated in iCKH$^\Delta$ cells, while *Ins1* and *Hnf1b* are not DE genes. *E2F8* encodes a transcription factor which is involved in cell proliferation and cancers. For example, E2F8 suppresses the proliferation of mouse embryonic fibroblasts [113], but also contributes to human hepatocellular carcinoma by upregulating cyclin D1 [114]. *Ins1* and *Ins2* encode preproinsulins (precursor to insulin); in high fat diet-fed mice expressing the *Kras* oncogene (*Ptf1a^{CreER}; LSL-Kra^{G12D}; Ins1$^{+/-}$; Ins2$^{-/-}$*), reduction in endogenous insulin production led to a reduction in PanIN lesions and pancreatic fibrosis [115]. Therefore, these genes of interest were detected by RT-PCR. The RT-PCR results of *Ins2* (0.01652 vs 0.08163, p = 0.006) agreed to the RNA-seq data, while *E2f8* decreased in iCKH$^\Delta$ cells but failed to be significant (0.00035 vs 0.00011, p = 0.197). The non-DE gene *Ins1* was also significantly declined in iCKH$^\Delta$ cells (**Figure 4-9C**). This can be due to the difference in the methodology and the small sample size.
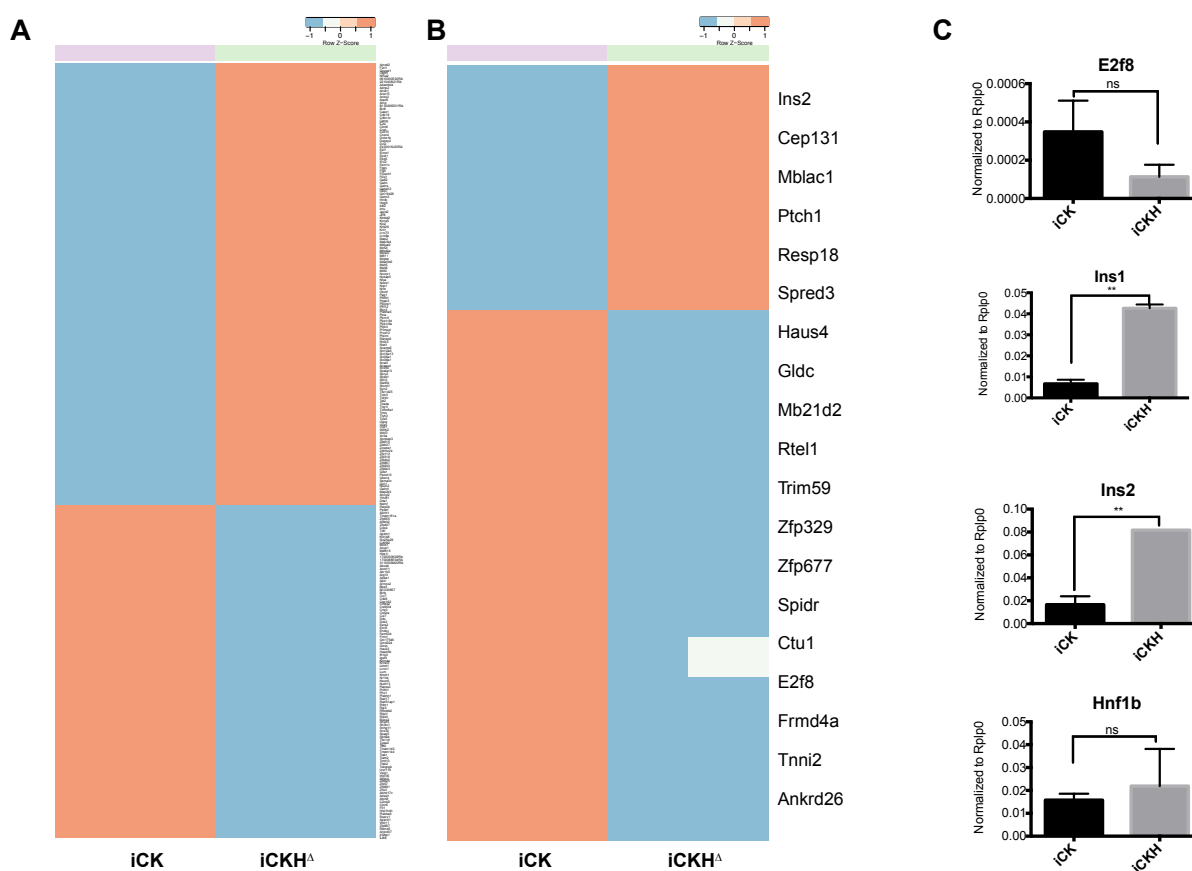

Figure 4-9: Differentially expressed (DE) genes between the iCK and iCKH$^\Delta$ acinar cells at

different time points.
The acinar cells were collected immediately (day 0) (A) and from the 3D culture on day 3 (B) (n=2 for each genotype at each time point). The DE genes referred to the gene with log2 (fold change)>1 and p < 0.05. (C) RT-PCR of expression levels of selected genes with the same day-3 samples. **p < 0.01, ns: not significant according to t-test.

However, it is noticeable that the mRNA levels of some ductal genes tended to be lower and acinar genes were higher in iCKH$^\Delta$ cells on day 3. In addition, some genes involved in proliferation/cell cycle were lower (e.g. *Ccnd1* and *Mki67*) in iCKH$^\Delta$ cells than that in iCK cells (**Figure 4-10**). Although the difference was not statistically significant, it still provides clues for the further experiments to identify whether the expression status of Hnf1b affects the cell identity during ADM.
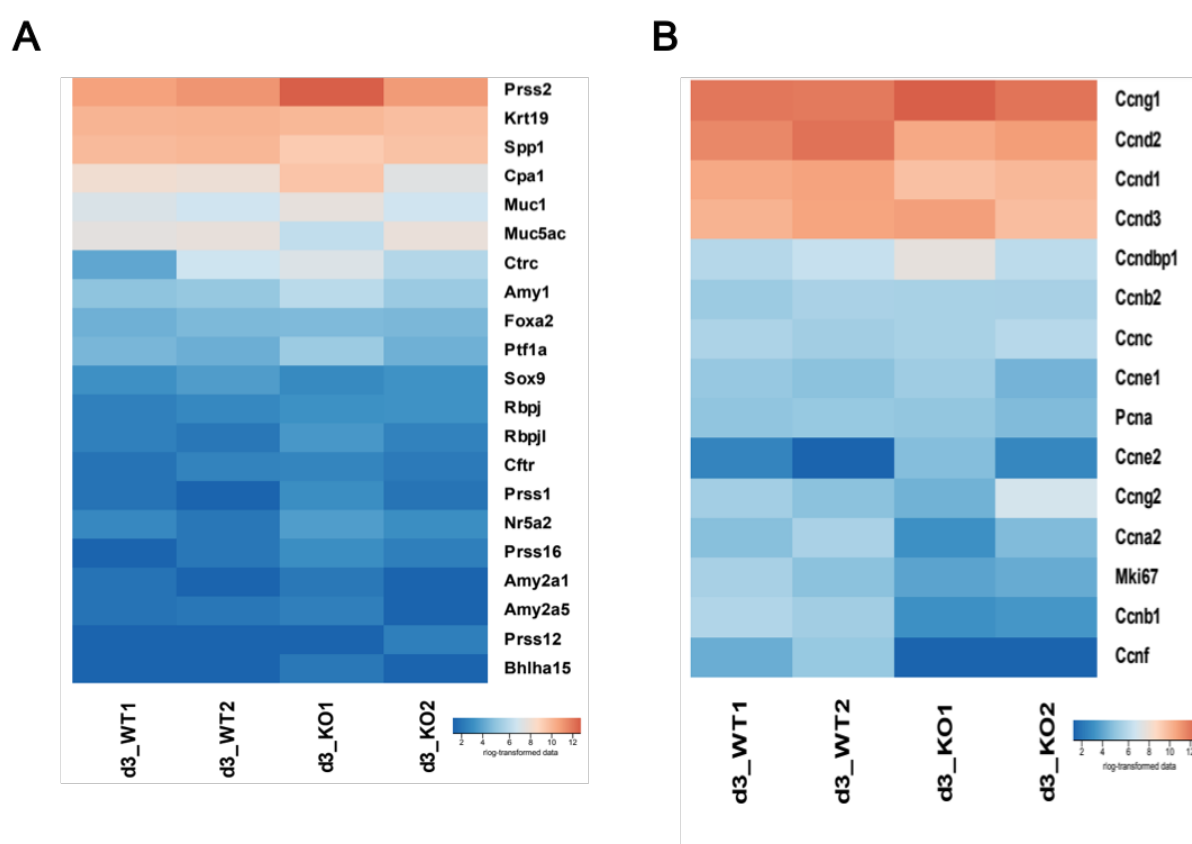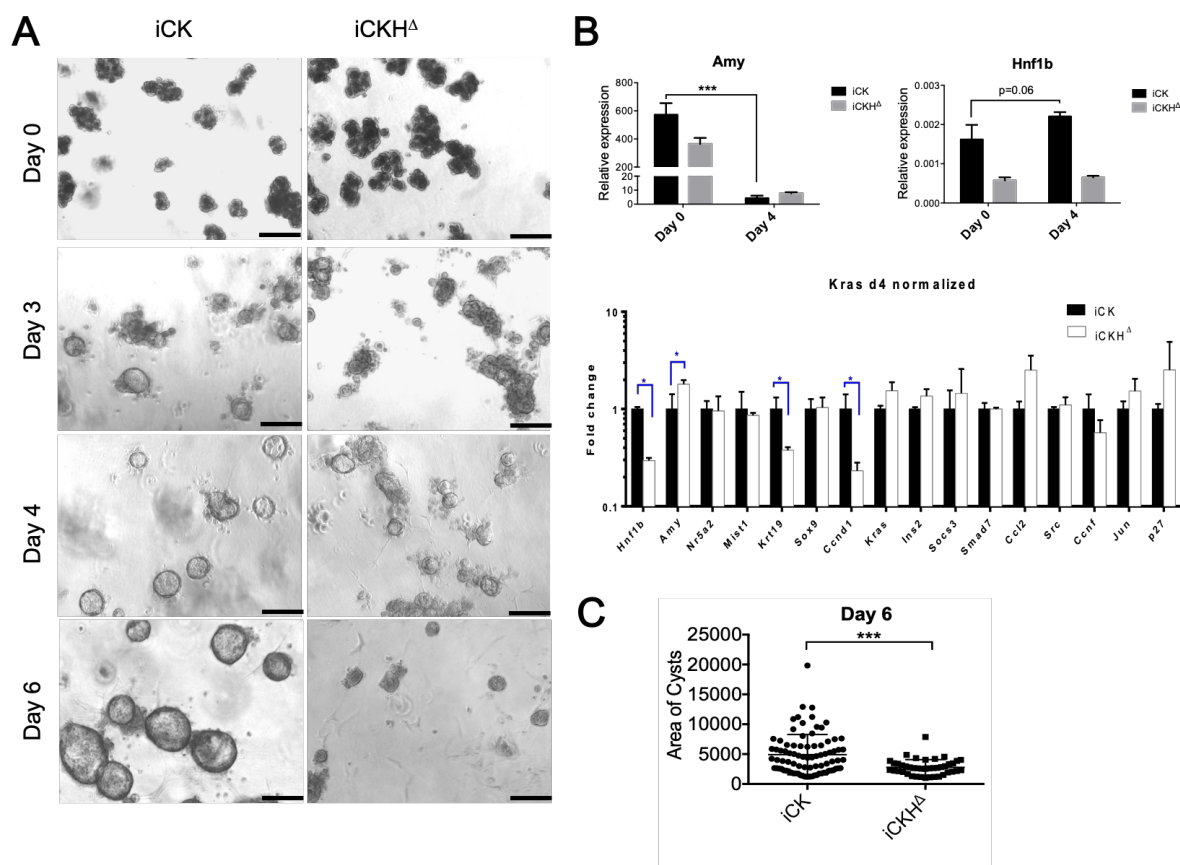

Figure 4-10: Heatmaps of selected genes expressed in the iCK and iCKH$^\Delta$ acinar cells on day 3.
(A) Expression profiles of some acinar maker genes and ductal marker genes. (B) Selected cell cycle-related genes. The acinar cells were collected from the 3D culture on day 3 (n = 2 for each genotype).

4.8 Hnf1b ablation inhibited ADM in the presence of Kras^{G12D} *in vitro*

To analyze how Hnf1b affects ADM in the presence of Kras^{G12D}, acinar cells were also isolated from iCK and iCKH$^\Delta$ mice and cultured in Matrigel for 7 days. On day 3 after isolation, cyst structures started to form in both iCK and iCKH$^\Delta$ groups. On day 4, most of the acini became cysts and continued to grow, but the cysts in iCKH$^\Delta$ group seemed defective and smaller. On day 6, the cysts in iCK group grew larger while the cysts in iCKH$^\Delta$ group appeared not growing (**Figure 4-11A**). Accordingly, the area of the iCK cysts was bigger than that of the iCKH$^\Delta$ cysts on day 6 (**Figure 4-11C**). These findings demonstrate that Hnf1b is dispensable for ADM occurrence, but is required for Kras^{G12D}-mediated cell proliferation.

To explore the mechanisms of how Hnf1b affects ADM and regulates cell proliferation, some genes were selected and detected by RT-PCR using the iCK and iCKH$^\Delta$ cultures on day 4. In iCKH$^\Delta$ group, Hnf1b was efficiently inhibited, the mRNA level of an acinar marker *Amy1* was elevated, while a ductal marker gene *Krt19* was down-regulated. Consistently with the cellular phenotype, there was a lower level of *Ccnd1* in iCKH$^\Delta$ group ($p < 0.05$) (**Figure 4-11B**).

In addition, the levels of *Cdkn1b* (encoding p27^{kip1} protein) and *Jun* (encoding c-Jun) were higher in iCKH$^\Delta$ group than those in iCK group, indicating there were more senescent cells in iCKH$^\Delta$. To reveal the cell senescence, the acinar cells were stained with senescence associated β-galactosidase (SA-β-gal) staining solution on day 4 and incubated overnight. It was observed that the β-gal$^+$ cells (in blue) were attached to but not included in the cyst structure, indicating that the senescent cells and the proliferative cells are independent cell subpopulation (data not shown).

Figure 4-11: Hnf1b is dispensable for Kras^{G12D}-induced ADM but affects ADM proliferation.
(A) Pancreatic acini were isolated from mice after tamoxifen gavage (n=3 for each genotype), seeded in Matrigel for 3D culture. Scale bar=100 µm.(B) qRT-PCR of acinar, ductal and carcinogenesis-related genes in cyst structures at indicated time point (day 4, n=3 for each genotype). (C) Quantification of the area of cysts in iCK and iCKH$^\Delta$ on day 6 in Matrigel culture with ImageJ. *: p < 0.05, ***: p < 0.001.

4.9 *Hnf1b* ablation inhibited ADM without Kras^{G12D} *in vitro*

Murine acinar cells are highly plastic and ADM can be induced by different stimuli besides endogenous Kras^{G12D}. To validate the role of Hnf1b during metaplasia in other conditions, primary acinar cells from iC (*ptf1a-Cre^{ER}*) and iCH$^{\Delta}$ (*ptf1a-Cre^{ER}; Hnf1b$^{flox/flox}$*) mice were isolated and stimulated with cerulein or EGF for transdifferentiation. On day 3 after stimulation, there were already ADM (cyst structures in gel) formed in both iC and iCH$^{\Delta}$ groups (Figure 4-12), which indicates that Hnf1b is not essential for ADM formation. Similar to the acinar cell culture of acinar cells with oncogenic Kras mutation, the cysts continued to grow on day 4, but the size of cysts in iCH$^{\Delta}$ group was smaller, indicating lower cell proliferation level in acinar cells when Hnf1b is ablated. Therefore, Hnf1b is not essential for the occurrence of ADM, but Hnf1b may still regulate the maintenance and/or proliferation of ADM.
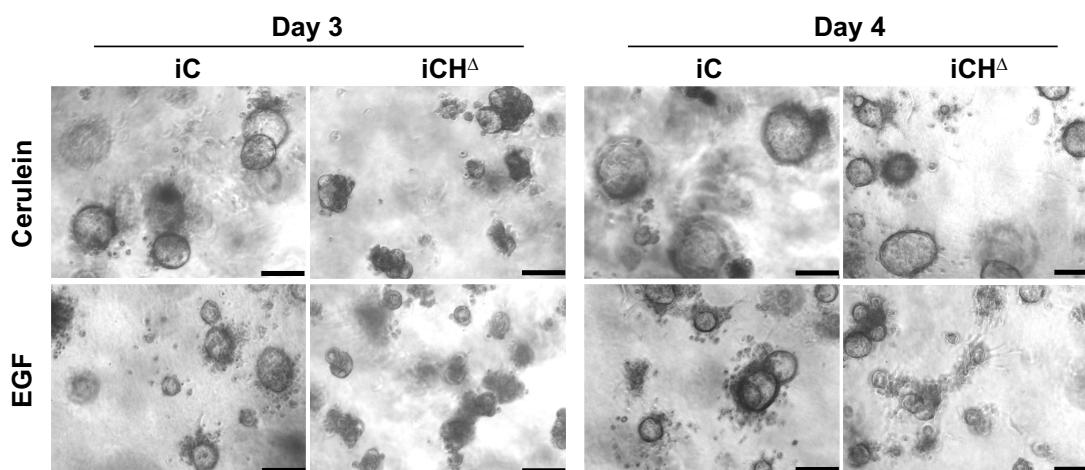
Figure 4-12: Hnf1b is dispensable for ADM formation.
Pancreatic acini were isolated from mice after tamoxifen gavage (n=3 for each genotype), seeded in Matrigel for 3D culture, and transdifferentiation was induced with cerulein (2 ng /ml) or EGF (50 ng/ml). Ducts formed were photographed (magnification: 50×). Scale bar=100 µm.

To investigate how Hnf1b resulted in the cellular difference that was observed under a microscope, RT-PCR was performed to detect acinar and ductal marker genes, as wells as genes involved in cell growth, and carcinogenesis. In the presence of cerulein, knockout of Hnf1b retained higher expression of acinar marker genes such as *Nr5a2*, while inhibited the up-regulation of ductal marker gene *Krt19* (encoding Ck19) ($p < 0.05$ for both). Notably, *Ccnd1* (Cyclin D1) level was lower in *Hnf1b*-knockout cells ($p < 0.05$), indicating that the cells were less proliferative, which is consistent with that smaller cyst structures were observed under a microscope.

Similarly, when acini were stimulated with EGF for 4 days, there was a lower expression level of *Ccnd1* in *Hnf1b*-knockout cells. However, there was no statistical difference in the expression levels of acinar marker genes or ductal marker genes between iC and iCH^Δ cells at this time point (Figure 4-13). Taken together, Hnf1b is dispensable for the occurrence of metaplasia, but regulates the cell proliferation.
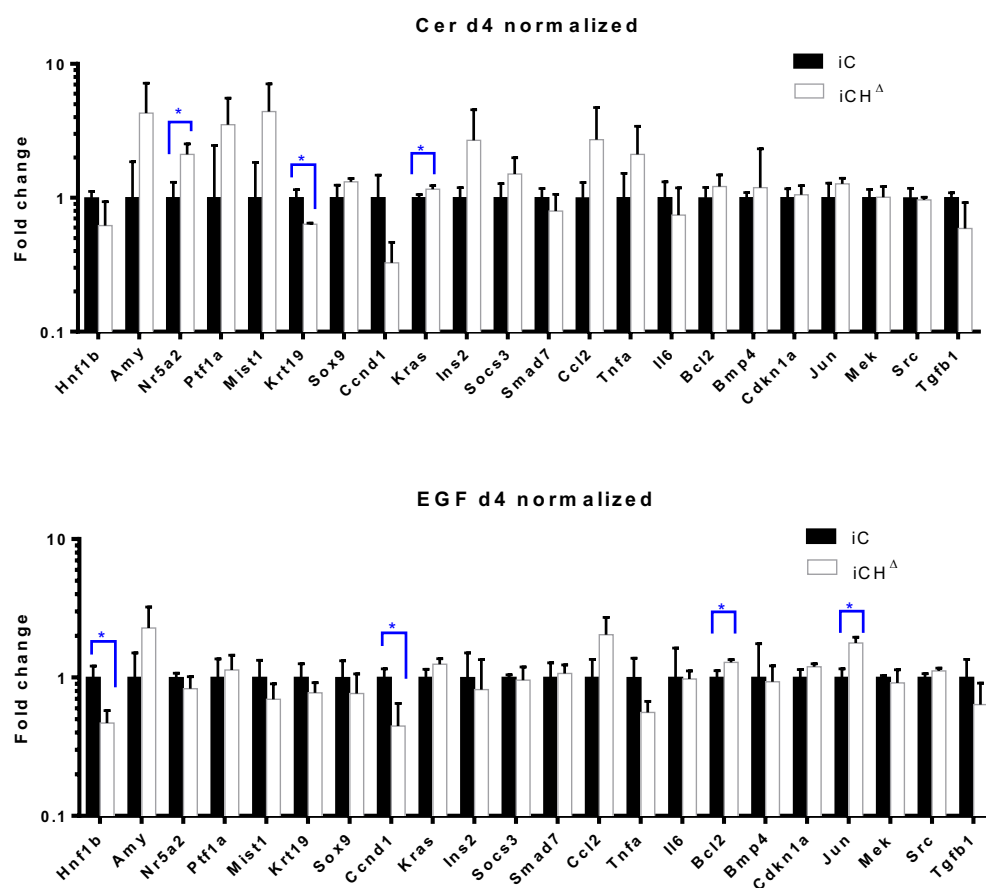

Figure 4-13: Hnf1b positively regulates ADM proliferation.
The acinar cells from the pancreata of iC and iCH^Δ mice and stimulated with cerulein (2 ng/ ml) or EGF (20 ng/ ml) for 4 days and the RNA was extracted for qRT-PCR. The mRNA expression of acinar, ductal and carcinogenesis-related genes in cyst structures at indicated time point (n = 3 for each genotype). *p < 0.05.

Taken together, Hnf1b is not essential for ADM in response to different stimuli *in vitro*, but it is required for the proliferation of metaplastic cells in the absence and presence of Kras^G12D expression.

4.10 Ablation of *Hnf1b* impairs the proliferation of metaplastic cells

To verify whether Hnf1b is also required for the proliferation of metaplastic cells *in vivo*, the iCK and iCKH$^\Delta$ mice were injected with cerulein and the pancreata were collected on day 2 and day 7 after cerulein injection. It is shown that when Hnf1b was ablated, there were less proliferative cells (indicated by Ki67$^+$ staining) in ADM structures, although the severity of lesions seemed similar between the iCK and iCKH$^\Delta$ pancreata (**Figure 4-14**).
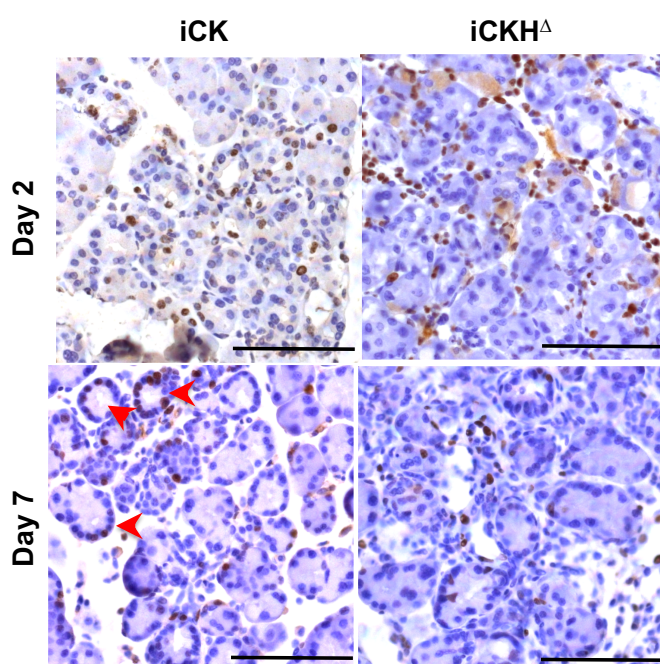
Figure 4-14: Knockout of Hnf1b represses proliferation of metaplastic cells.
Ki67 staining was performed to reveal the cell proliferation of iCK and iCKH$^\Delta$ mice after cerulein induced acute pancreatitis at indicated time points. The red arrows indicate the proliferative cells within ADM. Magnification: 200×. Scale bar = 100 μm.

4.11 Hnf1b is not required for recruitment of macrophages during acute pancreatitis

The initial hypothesis how Hnf1b inhibited $Kras^{G12D}$-induced PanIN formation had been that up-regulation of Hnf1b in acinar cells is required for ADM, and therefore knockout of Hnf1b inhibits ADM formation and thus delays PanIN formation. Based on the *in vitro* acinar culture data it is conceivable that Hnf1b affects PanIN formation through cell autonomous regulation, i.e. the regulation of cell proliferation.

On the other hand, PanIN formation also depends on non-autonomous regulations, i.e. the microenvironment of exocrine pancreas, such as recruitment of immune cells, activation of pancreatic stellate cells, etc. It has been reported that macrophages infiltrating the pancreas drive the ADM [116], a key early event in pancreas carcinogenesis. Therefore, the effect of Hnf1b on macrophage recruitment in cerulein-induced acute pancreatitis was checked.

There was no difference in ADM number between iC and iCH$^\Delta$ mice on day 2 after cerulein injection, and high percentage of cells undergoing ADM showed no expression of Hnf1b (**Figure 4-15A and B**), which confirmed that Hnf1b is dispensable for ADM formation. In addition, there was also no statistical difference in macrophage number (**Figure 4-15C**), although iCH$^\Delta$ group showed less macrophage infiltration based on F4/80 staining.
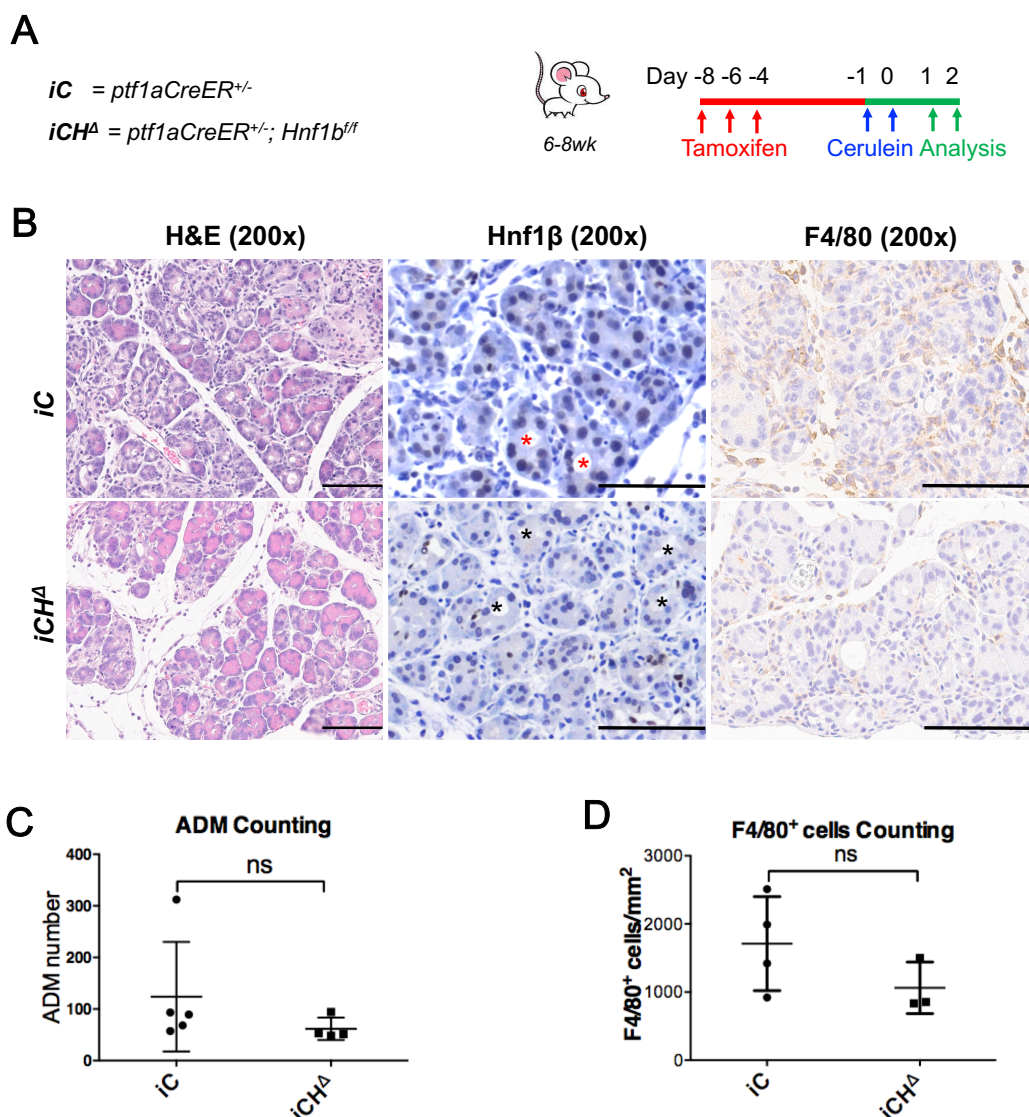
Figure 4-15: Knockout of Hnf1b alleviates acute pancreatitis induced by cerulein.
(A) Schematic representation of the experimental procedure. (B) H&E staining, as well as IHC staining with anti-Hnf1b and anti-F4/80 antibodies in iC and iCH$^\Delta$ mice (n = 4 and 3, respectively) on day 2 after cerulein injections. Red stars indicate the up-regulation of Hnf1b protein in ADM, and black stars indicate the ADM without Hnf1b expression. Scale bar = 100 μm. (C) ADM number was quantitated in each section. (D) F4/80 positive cells were counted in 8 random fields (200×) in each section and normalized to area.

On molecular level, the mRNA levels of Hnf1b and another ductal marker gene *Krt19* tended to be lower in iCH$^\Delta$ pancreata than those of the iC group. On the other hand, the mRNA levels of acinar marker genes including *Amy*, *Ptf1a* and *Bhlha15* was higher in iCH$^\Delta$ pancreata (**Figure 4-16**). The findings above indicate that deletion of *Hnf1b* in mature acinar cells to some extent protects acinar cells from inflammation-induced ADM.
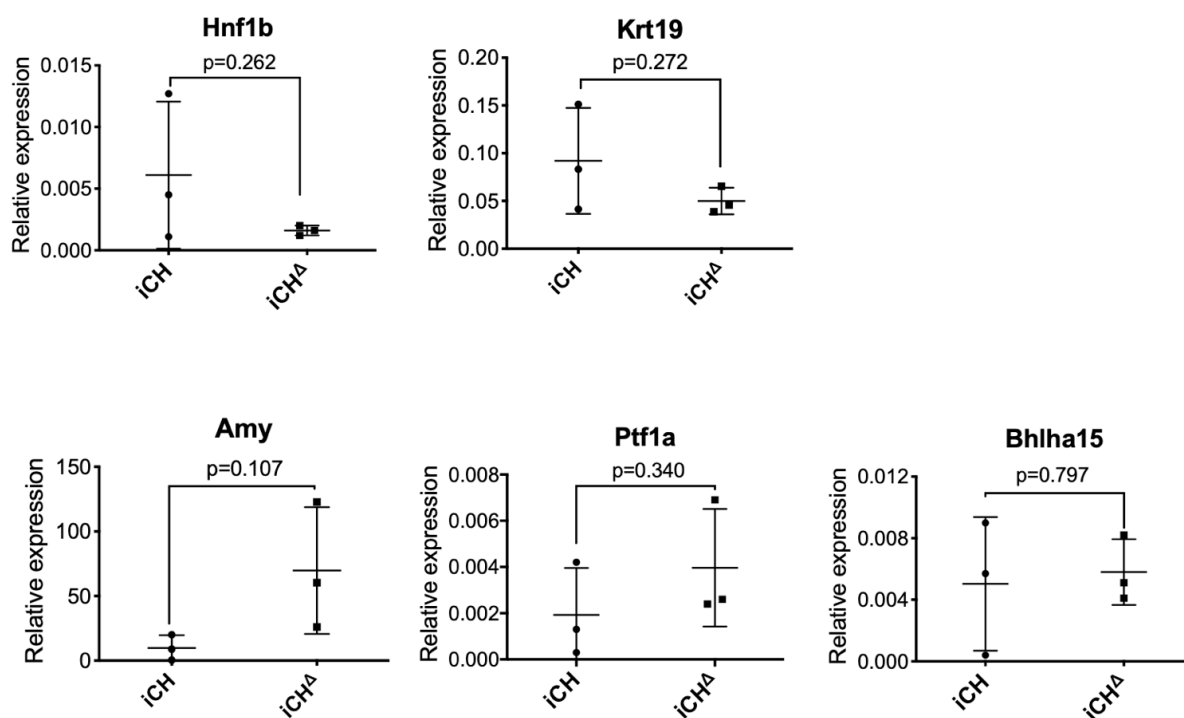
Figure 4-16: Expression of acinar marker and ductal marker genes in response to acute pancreatitis.
The pancreas tissue was collected from the mice of the indicated genotypes on day 2 after cerulein injections. RNA expression levels of ductal marker genes (Hnf1b, Krt19) and acinar marker genes (Amy, Ptf1a, and Bhlha15) evaluated with RT-PCR. Data are presented as mean ± SD.

4.12 Hnf1b may be functional in acinar cells

A recent study in pancreatic ductal cells demonstrated that early ductal deletion of Hnf1b (on postnatal days 1 to 3) led to loss of primary cilia, increased ductal cell proliferation, and alteration of ductal cell polarity. Moreover, ductal deletion of Hnf1b also inhibited acinar cell proliferation whereas significantly increased acinar cell apoptosis [101]. Therefore, Hnf1b may be also important for specific cellular process in mature acinar cell homeostasis.

To address this question, we induced the ablation of the *Hnf1b* gene in mice without Kras^{G12D} expression. Six months after tamoxifen gavage, H&E staining did not show appreciable lesions, inflammation, changes in acini structure or polarity. In addition, Amylase expression in the control and Hnf1b knockout mice appeared to be the same (**Figure 4-17**), indicating no effect of Hnf1b ablation on acinar functions.

The RNA-sequencing data of the freshly isolated acinar cells revealed that there were hundreds of differentially expressed genes between the iCK and iCKH$^{\Delta}$ group (**Figure 4-18A**). A further question was whether Hnf1b also plays a role as transcription factor regulating its target genes in normal acinar cells. To address this, Chromatin immunoprecipitation (ChIP) was performed using acinar cells without Kras^{G12D} expression. The ChIP-PCR results showed that the binding sequences of three well-identified Hnf1b target genes *Pkhd1* and *Cys1* and *Egfr4,* while in acinar cells Hnf1b only enriched in *Pkhd1* and *Cys1* (**Figure 4-18B**). This indicated that Hnf1b binds to a cohort of genes in acinar cells, which are different from those in cancer cells. Altogether, these findings indicate that Hnf1b is still functional in adult acinar cells.
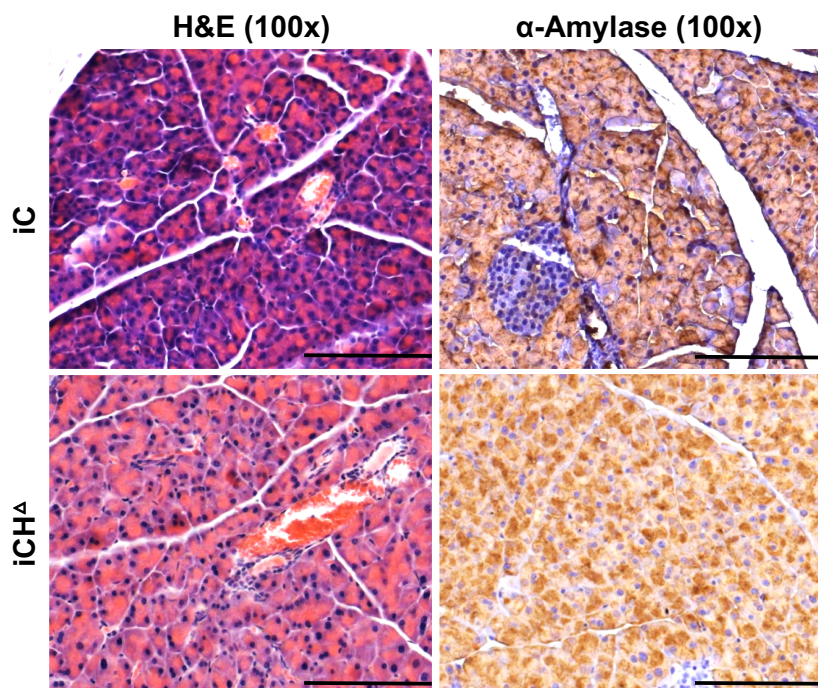
Figure 4-17: Ablation of Hnf1b did not affect acinar cells.
Six months after tamoxifen gavage, H&E staining and IHC staining for amylase was performed with pancreatic sections of control mice (iC) and *Hnf1b* knockout mice (iCH$^\Delta$). n = 2 for each genotype. Ablation of Hnf1b in mature acinar cells did not lead to obvious morphological changes. Amylase expression extent and intensity seemed the same between different genotypes. Scale bar = 200 μm.
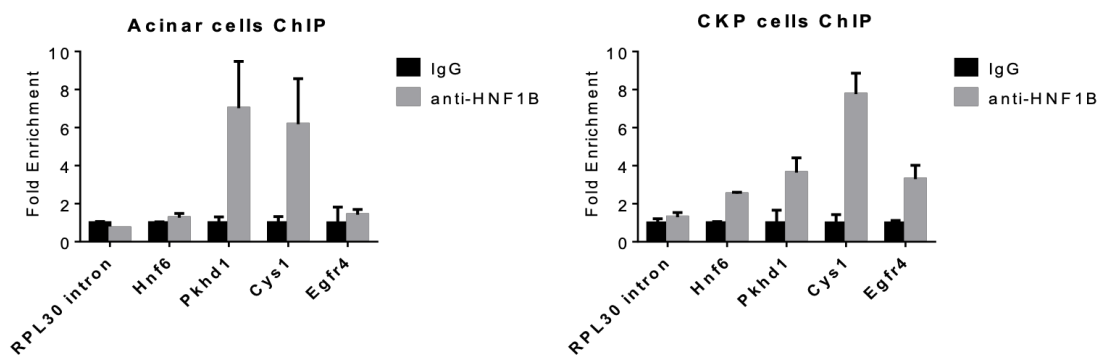
A

B
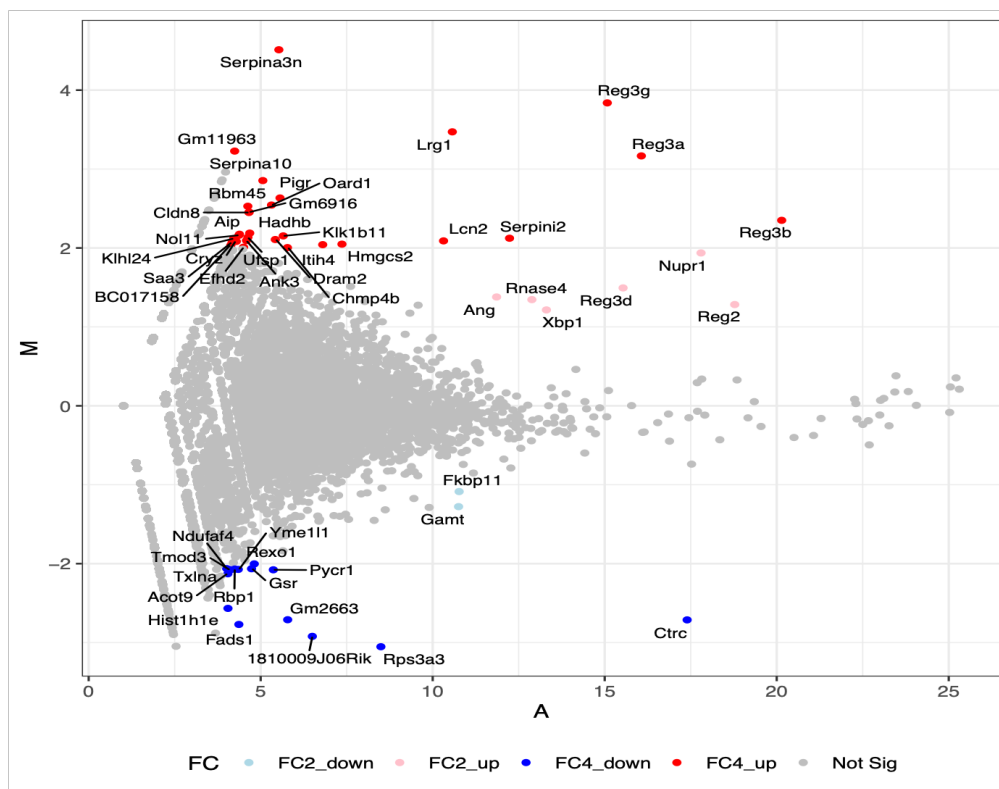
Figure 4-18: Hnf11b may be functional in mature acinar cells.
(A) MA plot of DE genes of freshly isolated (day 0) iCK and iCKH$^\Delta$ acinar cells. Each dot denotes a gene. DE genes upregulated (red and pink) and downregulated (blue and light blue) in iCK cells are highlighted on the plot. DE genes with |FC|≥4 are in darker colors, while DE genes with 4>|FC|≥2 are in lighter colors. (B) ChIP-PCR with murine PDAC cells (CKP cells) (which have high-levels of Hnf1b mRNA) and acinar cells (which have lower levels of Hnf1b).

4.13 HNF1B in human PDAC cell lines

HNF1B was reported to express in well-differentiated human PDAC specimens and cancer cell lines [99]. It is also suggested that HNF1B regulated a cohort of genes specifically expressed in well-differentiated PDAC [117]. However, the role of HNF1B in PDAC cells has not been investigated yet. This part aims to evaluate the effects of HNF1B on biological characteristics of PDAC cells *in vitro* and clarify the related mechanisms.

4.13.1 HNF1B is dispensable for epithelial–mesenchymal transition (EMT)

The expression levels of HNF1B in human PDAC cell lines were evaluated by using RT-PCR and Western blot. As shown in **Figure 4-19A**, mRNA levels of HNF1B were high in well-differentiated cancer cell lines (Paca3, Colo357, and Capan-1) [118], but no expression was detected in poorly-differentiated cell lines such as MIA PaCa-2 and PANC-1. Consistently, HNF1B protein levels were detected in Paca3, Colo357, Capan-1 and Su8686 (**Figure 4-19B**), suggesting that HNF1B is a marker for differentiation of PDAC cells.
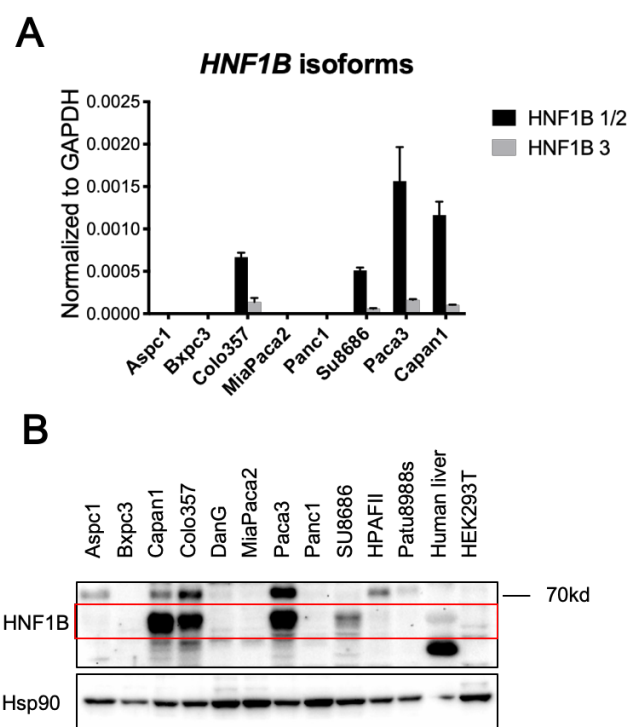

Figure 4-19: Expression of HNF1B in human PDAC cell lines.
(A) HNF1B mRNA levels in human PDAC cell lines. Primers specific to mRNA isoform 1/2, and 3 were used for quantitative PCR. (B) HNF1B protein expression detected by Western blot. Each lane was loaded with 20 µg of protein. The bands within the red frame are HNF1B proteins (61 kDa). Hsp90 was used as loading control.

To explore the role of HNF1B in the differentiation of PDAC cells, TGF-β was used to induce EMT and the expression level of HNF1B was assessed. It is shown that two days after induction, Colo357 cells extended in morphology while no change was observed in CPFAC-1 cells (**Figure 4-20A**). In addition, the mRNA levels of *CDH1* (encoding the epithelial marker E-cadherin) significantly declined, while *CDH2* (encoding the mesenchymal marker N-cadherin) decreased in Colo357 cells ($p < 0.05$), indicating EMT may be induced. Intriguingly, the mRNA level of HNF1B significantly upregulated in Colo357 but downregulated in CFPAC-1 cells in response to TGF-β (**Figure 4-20B**).
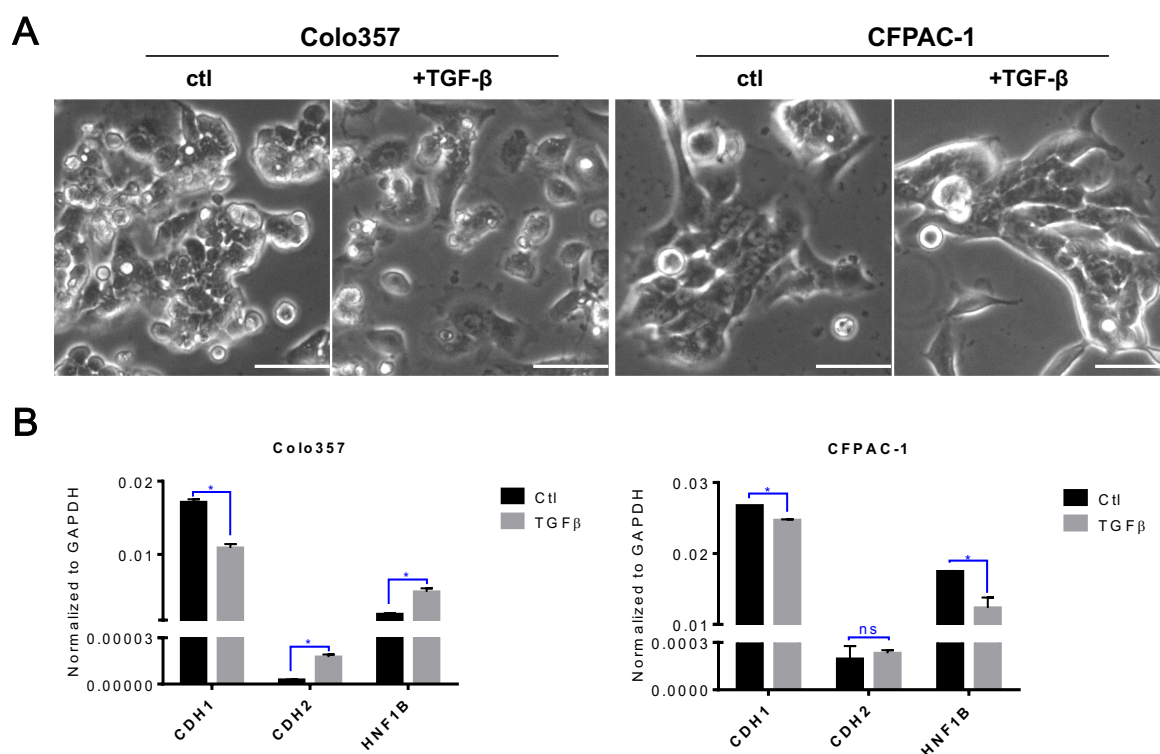

Figure 4-20: TGF-β induced EMT.
(A) Morphology of PDAC cells after TGF-β stimulation. Colo357 and CFPAC-1 cells were seeded at 2×10^5 cells/well in 12-well plates. Human recombinant TGF-β was added (final conc. = 20 μg/ml) and cultured for 2 days to induce EMT. The cells were observed under a microscope and pictures were taken. Scale bar = 50 μm. (B) Expression of *HNF1B* and EMT markers evaluated with RT-PCR.

To further determine whether HNF1B is responsible for EMT, HNF1B was knocked out in HNF1B-expressing cell lines using CRISPR-Cas9. However, ablation of HNF1B in Paca3, Colo357 and CFPAC-1 did not lead to any change in the expression of epithelial marker (E-Cadherin) or mesenchymal marker (Vimentin) (**Figure 4-21A**). Accordingly, no change in morphology was observed (**Figure 4-21B**). These results suggested that HNF1B correlates with but does not determine PDAC differentiation *in vitro* (at least in
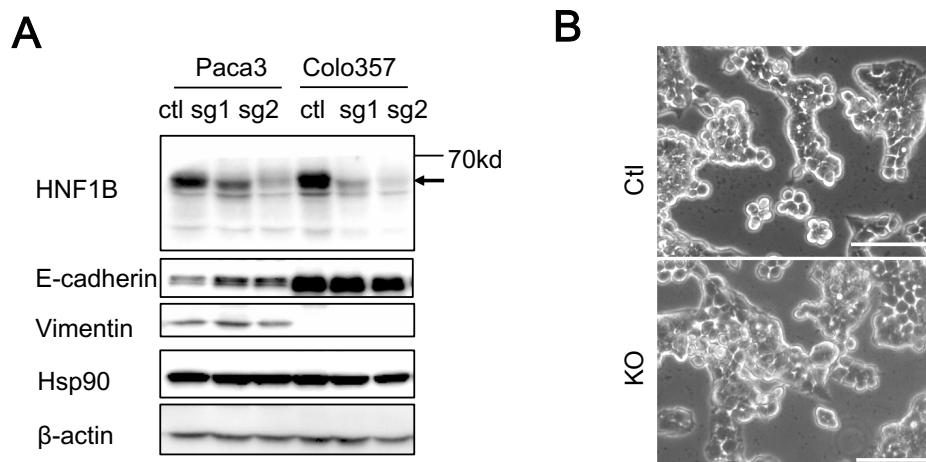
the cell lines tested above).

Figure 4-21: Knockout of HNF1B does not affect EMT of human PDAC cell lines.
(A) Knockout of HNF1B by CRISPR-Cas9 does not affect the expression of EMT markers. (D) Morphology of Colo357 cells under a microscope, showing no change between ctl and HNF1B-knockout (KO) cells. Scale bar = 100 μm.

4.13.2 HNF1B regulates the proliferation of PDAC cells *in vitro*

To examine the role of HNF1B in human PDAC cell growth, HNF1B was inactivated CRISPR-Cas9 with different sgRNAs mediated by lentivirus in three cell lines. MTT assay showed that HNF1B inactivation in Paca3, Colo357 and Capan1 cells did not significantly affect cell viability (**Figure 4-22A**, showing Colo357 as representative). Colony formation assays illustrated no difference between lenti-ctlsg with lenti-sgHNF1B (**Figure 4-22B**). However, in CFPAC-1 cells (which has highest mRNA level of HNF1B according to EMBL-EBI Expression Atlas), knockout of HNF1B significantly inhibited cell proliferation as well as colony formation (**Figure 4-22A**). Therefore, HNF1B is required for cell proliferation of some PDAC cells with high-level HNF1B.
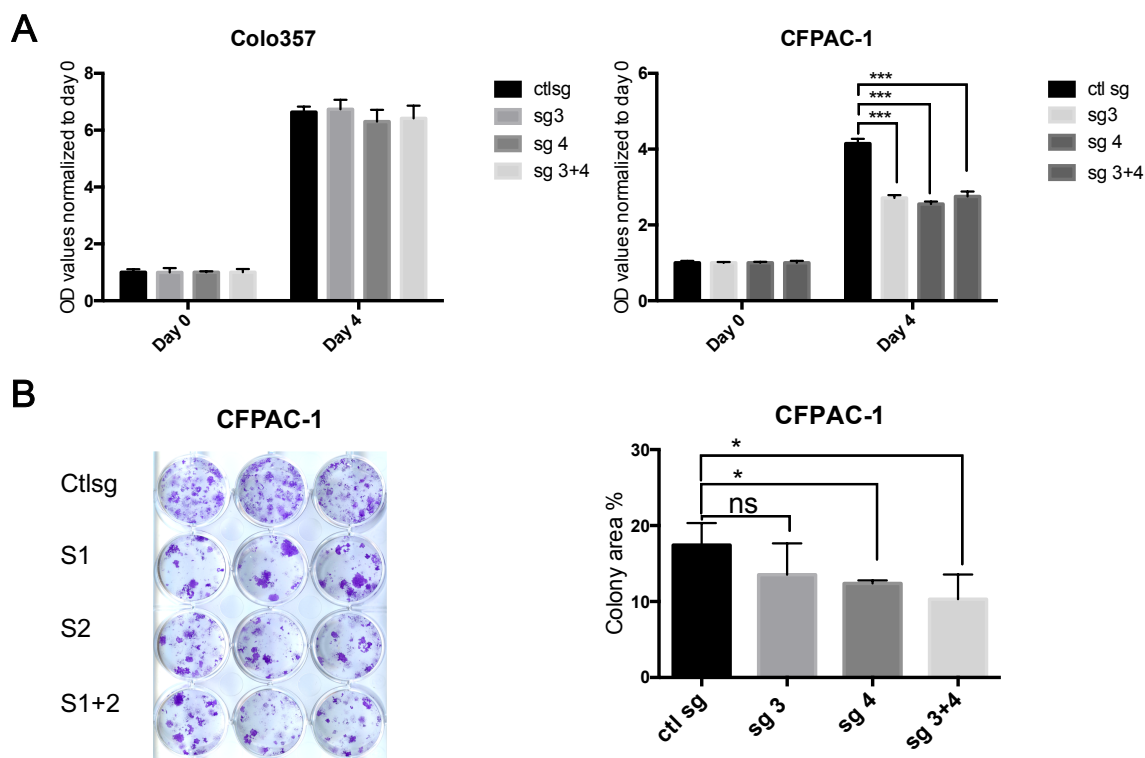
Figure 4-22: Knockout of Hnf1b inhibits the proliferation and colony formation of CFPAC-1 cells.
(A) Cell viability assay for Colo357 and CFPAC-1 cells. The cells were seeded at 1000/well in 96-well plate, MTT was added on the day of seeding and day4 after seeding to evaluate cell proliferation. Each stable cell strain was seeded in 5 duplicate wells.
(B) CFPAC-1 cells were seed in a 12-well plate at 500 cells/well (n=3 wells for each cell line), and cultured for 14 days. The cells were stained with crystal violet, the plate was scanned and the area was quantified with ColonyArea plugin of ImageJ.

4.13.3 HNF1B positively regulates proliferation of CFPAC-1 via PI3K/Akt pathway

It was reported that HNF1B positively regulate phosphorylation of Akt (Ser473) under different conditions in liver [119], [120]. The PI3K/Akt pathway mediates multiple cellular processes, such as stimulation of cell proliferation, inhibition of apoptosis and regulation of glucose metabolism, and it has been estimated to be deregulated in approximately 50% of all cancer types including PDAC [121].

To check the effects of HNF1B on Akt phosphorylation, Western blot was performed and the results showed that phosphorylation of Akt (Ser-473) dramatically decreased in CFPAC-1 cells when HNF1B was efficiently ablated. In contrast, p-Akt was not affected when HNF1B was knocked out in Paca3 cells (**Figure 4-23**). In addition, the p-CREB and p-mTOR showed no changes. These findings highlight that HNF1B maintain the activation of Akt pathway in CFPAC-1 cells.
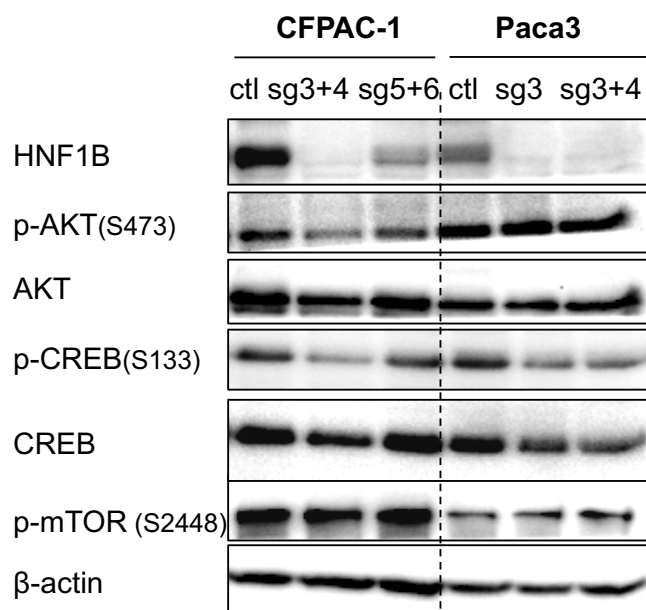
Figure 4-23: HNF1B regulates proliferation of CFPAC-1 via PI3K/Akt pathway.
CFPAC-1 and Paca-3 cells were infected with lentiviral vectors carrying control sgRNA or sgRNAs against HNF1B as indicated. The cell lysates were immunoblotted with anti-HNF1B, as well as other antibodies against phosphorylated proteins and total proteins involved in Akt pathway. β-actin was used as a loading control.

To identify how HNF1B affects Akt phosphorylation from transcriptional level, the ChIP-sequencing data for HNF1B in the ChIP-Atlas database [122] was browsed for potential target genes. The predicted target genes bound by HNF1B in CFPAC-1 cells were input into DAVID analysis (https://david.ncifcrf.gov/). The genes enriched in PI3K/Akt pathway included *ITGA1*, *PIK3R1*, *PPP2R5C*, as well as genes involved in phosphatases PP1 and PP2A were screened with RT-PCR (**Figure 4-24A**). RT-PCR results showed the mRNA levels of two activators for Akt pathway, *ITGA1* and *PIK3R1* decreased when HNF1B had been knocked out, while a negative regulator for Akt phosphorylation [123], *PPP2R5C* increased (**Figure 4-24B**). In contrast, the expression levels of *PPP2R5C* gene was not affected by knockout of HNF1B in Colo 357 cells; *ITGA1* mRNA level decreased (p = 0.0016), but the basal mRNA level was much lower than those in CFPAC-1 cells ($5×10^{-5}$ vs $1×10^{-3}$) (**Figure 4-24C**). Taken together, HNF1B affect phosphorylation of Akt by regulating these target genes in a context-dependent manner.
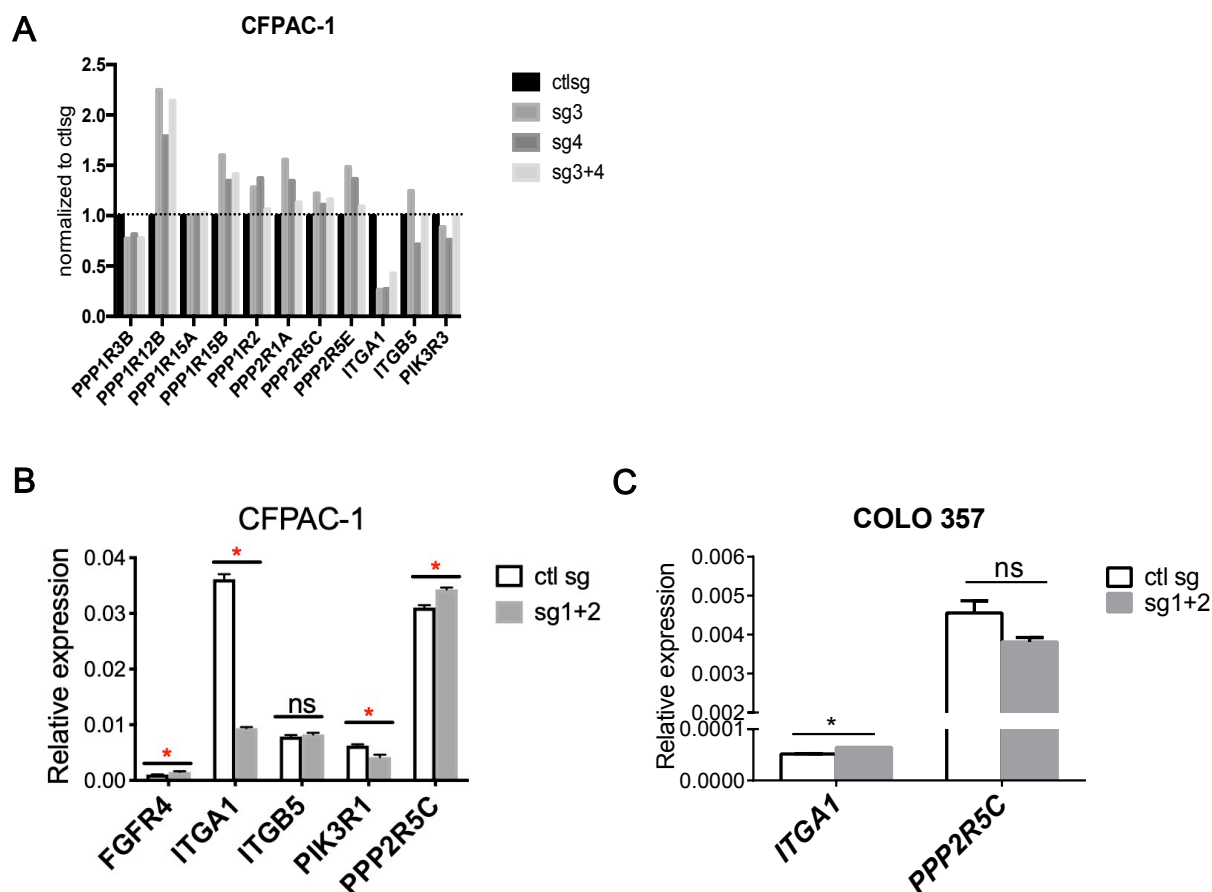
Figure 4-24: Detection of potential target genes of HNF1B by quantitative RT-PCR.
(A) Primary screening of the expression levels of the genes involved in PP1A, PP2A and PI3K/Akt pathway. All the genes were picked according to the ChIP-seq data in CFPAC-1 cells, which are deposited in ChIP Atlas website.
(B) qRT-PCR data in CFPAC-1 in another independent experiment. (C) qRT-PCR data in COLO 357. n = 2 for each sample.

Furthermore, ChIP-PCR was performed to analyze whether HNF1B binds to the predicted loci of *ITGA1* and *PPP2R5C* (102276118 to 102276792 on chromosome 14 according to human genome assembly GRCh37.p13. Firstly, the conditions of ChIP were titrated in murine PDAC cell lines expressing high level of Hnf1b. Some known target genes of Hnf1b in mouse embryonic pancreas [82] were used to test whether ChIP was successful. Since the DNA fragments of target genes (e.g. *Pkhd1* and *Cys1*) were significantly enriched in anti-Hnf1b IP (**Figure 4-25A**), the antibody and the conditions were suitable for ChIP. After that, CPFAC-1 cells were used for ChIP to detect the predicted target genes. It was shown that the predicted HNF1B binding sequences of *PPP2R5C* and *ITGA1* were enriched in anti-HNF1B IP but not that in IgG group (**Figure 4-25B**). This indicates that HNF1B binds to these genes in CFPAC-1 cells. Furthermore, the protein expression of PPP2R5C was detected when HNF1B

expression was knockout or over-expressed. The Western blot results showed that knockout of **HNF1B** enhanced the expression of *PPP2R5C*, while over-expression of HNF1B inhibited the expression of PPP2R5C in CFPAC-1 cells (**Figure 4-26**). The RT-PCR, ChIP-PCR and Western blot results suggested that HNF1B negatively regulates the expression of PPP2R5C from transcription level, while PPP2R5C as a subunit of phosphatase PP2A which decreases the phosphorylation of Akt. Therefore, HNF1B positively regulates AKT and therefore affect the proliferation of CFPAC-1 cells.
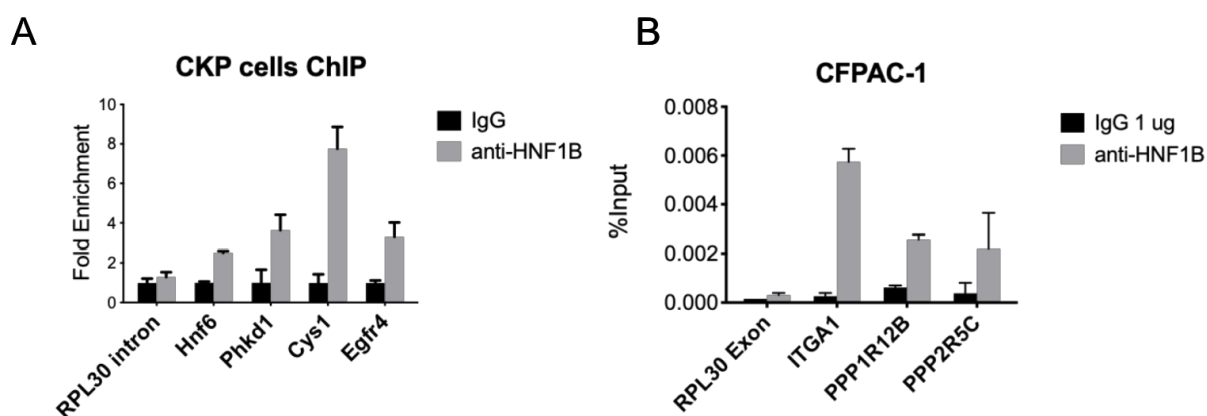

Figure 4-25: ChIP-PCR to validate target genes in CFPAC-1 cells.
(A) ChIP in murine PDAC cells with a high level of Hnf1b. Quantitative PCR assays detected the enrichment of DNA fragments in anti-HNF1B antibody (3 µg incubated with about 10 µg of genomic DNA) immunoprecipitated samples, and in the anti-IgG (1 µg) negative control samples. RPL30 intronic fragment was use as the control. This is the same as Figure 4-18B. (B) ChIP-PCR in CFPAC-1 cells with the same conditions.
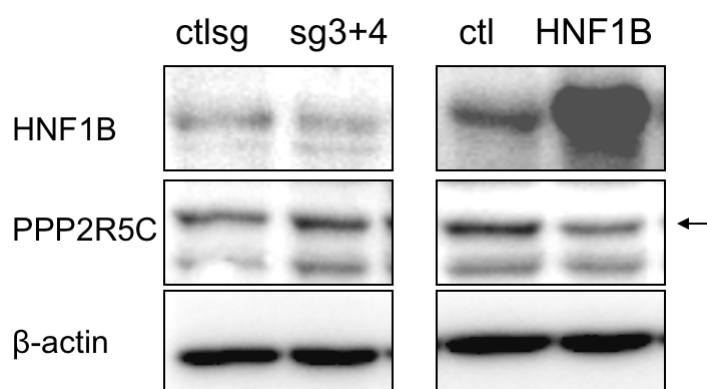

Figure 4-26: HNF1B regulates PPP2R5C in CFPAC-1.
CFPAC-1 cells were infected with lenti-ctlsg (lane ctlsg), lent-sg3+lenti-sg4 against HNF1B (lane sg3+4), lenti-Cas9-Blast (lane ctl) and lenti-HNF1B-Blast (lane HNF1B, to overexpress HNF1B). PPP2R5C protein expression detected by Western blot. Each lane was loaded with 20 µg of protein. The arrow indicates the specific band of PPP2R5C.

4.14 The role of Hnf1b in murine PDAC cell lines

To analyze if Hnf1b plays a similar role in murine PDAC cells to regulate cellular processes including cell proliferation, a cohort of murine PDAC cell lines established from Kras^{G12D} tumor mice was examined. It is shown that *Hnf1b* mRNA levels in epithelial PDAC cells were higher than those in mesenchymal PDAC cells (**Figure 4-27A**). However, knockout of *Hnf1b* did not lead to a dramatic change in the morphology of the epithelial cells (**Figure 4-27B**). Western blot results revealed that knockout of *Hnf1b* resulted in hyper-phosphorylation of Akt on Ser473, which is opposite to what was observed in human CFPAC-1 cells (**Figure 4-27C**).
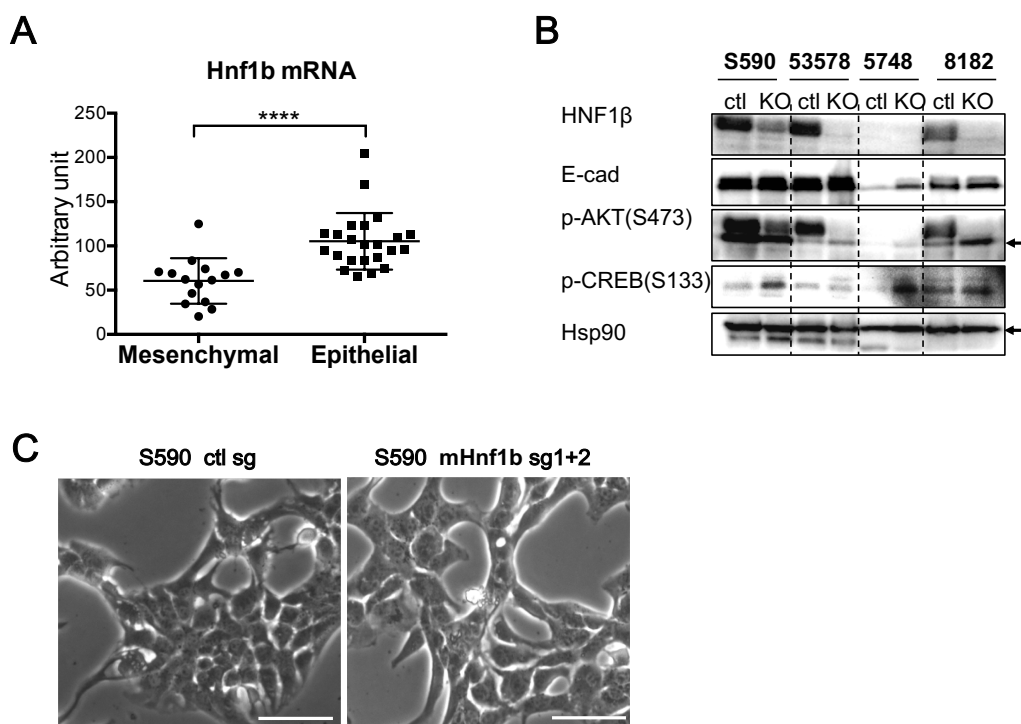

Figure 4-27: *Hnf1b* expression in murine PDAC cell lines.
(A) Relative expression of Hnf1b in mesenchymal and epithelial murine PDAC cell lines. The results were based on RNA-sequencing data. **** $p < 0.0001$. (B) Detection of E-cadherin, p-Akt (Ser473), and p-CREB (Ser133) in murine PDAC cell lines by Western blot. Ctl: the stable cell lines infected with lenti-ctlsg; KO: the stable cell line infected with lenti-sg against *Hnf1b*. Hsp90 was used as loading control. The arrows indicate the specific bands. (C) Morphology of cancer cells infected with lenti-ctl sg or lenti-sg against Hnf1b. No apparent difference was observed. Scale bar = 50 μm.

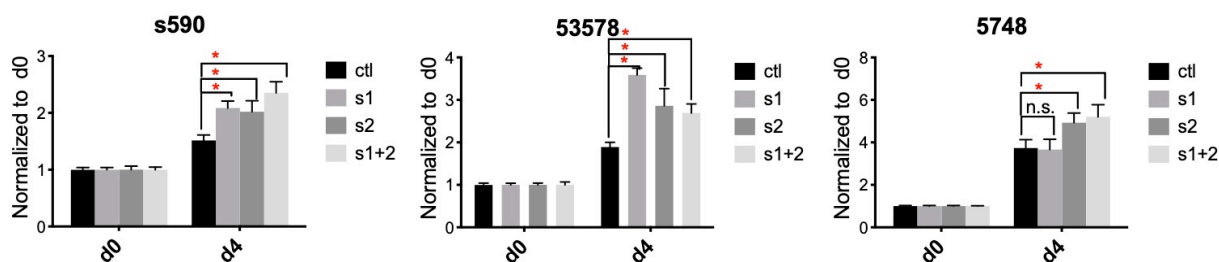Accordingly, knockout of *Hnf1b* promoted cell proliferation (**Figure 4-28**) and colony formation (**Figure 4-29**).

Figure 4-28: Knockout of Hnf1b promotes proliferation of murine epithelial pancreatic cancer cells.
The proliferation of three murine PDAC cell lines infected with lenti-ctl sg or lenti-sgs for Hnf1b was analyzed by MTT assay for 4 days. The absorbance values were normalized to those on day 0 (the day of seeding). *: $p < 0.05$, ns: not significant.
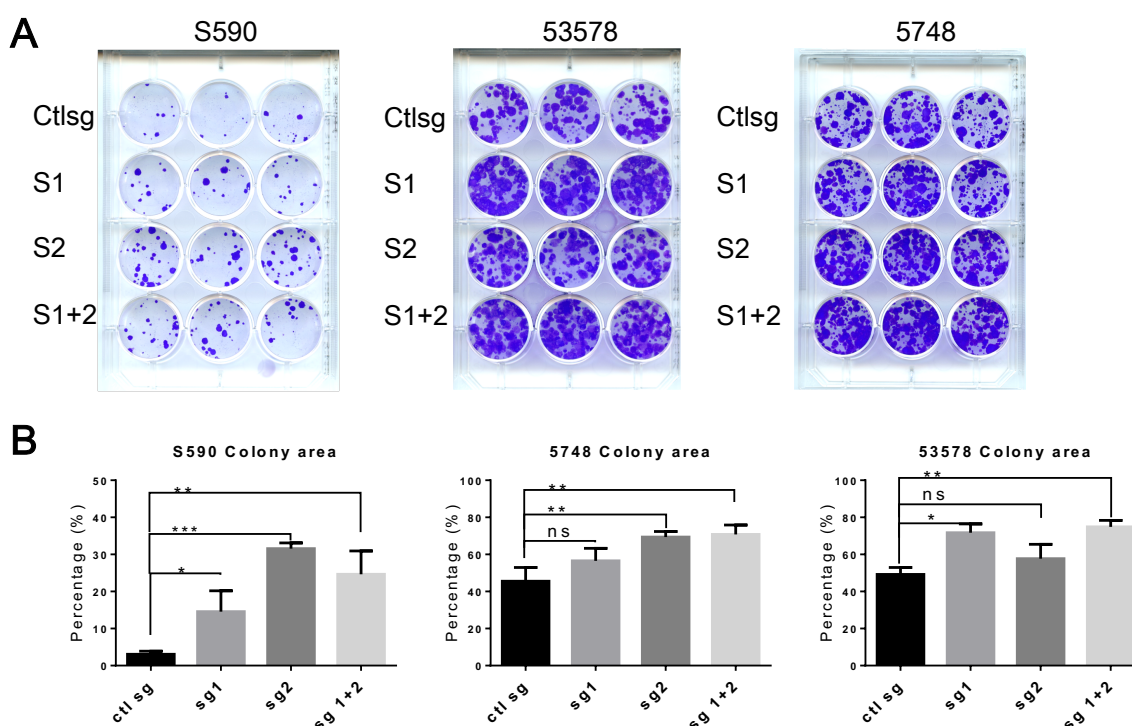

Figure 4-29: Hnf1b KO promotes colony formation of murine epithelial pancreatic cancer cells.
(A) Colony formation assay of different murine PDAC cell lines in 12-well plates. Every treatment of one PDAC cell line was seeded in triplicate (1.0×10^3 cells/well), cultured for 10 days, and then stained with crystal violet. (B) Areas of colonies formed were calculated. The data are represented as mean ± SEM (n=3), *: $p < 0.05$, ns: not significant.

To explore how Hnf1b regulate the Akt pathway in murine PDAC cells, the expression levels of the murine genes which are homologous to the HNF1B target genes in human CFPAC-1 cells. RT-PCR data showed that *Ppp2r5c* mRNA level was not affected by knockout of *Hnf1b*; although the other genes had different changes in different cells (**Figure 4-30**), the fold change between Hnf1b-expressing and Hnf1b deficient cells was limited and inconsistent in different cells. Therefore, knockout of Hnf1b did not

have a universal effect on the transcription of these genes in Akt pathway in murine cancer cells. This indicates that Hnf1b regulates Akt pathway in a distinct manner in murine PDAC cells.

In sum, these data suggested that Hnf1b inhibits cell proliferation via negative regulation of p-Akt in murine PDAC cells, but the mechanisms may be different from those in CFPAC-1 cells.
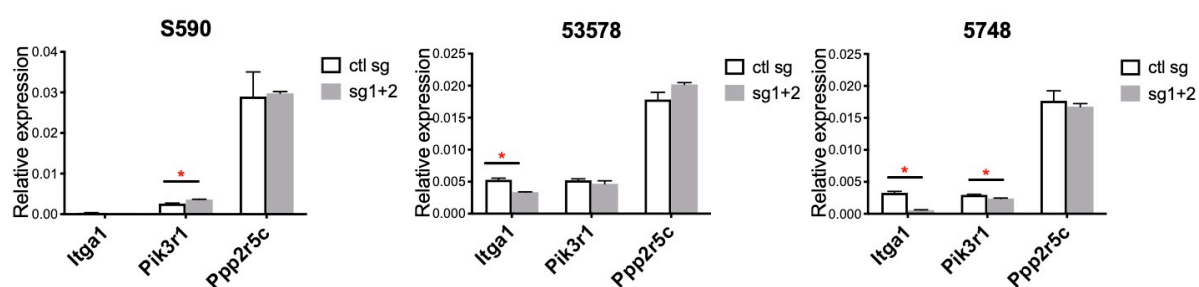

Figure 4-30: Validation of candidate target genes in murine PDAC cell lines.
Real-time PCR analysis of potential target genes in three mouse PDAC cell lines. The mRNA levels were normalized to the mRNA level of *Xs13* gene. The data represent the mean± SD. Statistics were calculated between the same cell line infected with lenti-ctrlsg and lenti-sg1+2 (*Hnf1b* knockout). *p < 0.05.

5 Discussion

This study for the first time evaluates the role of Hnf1b in mature acinar cells in Kras^{G12D}-induced pancreatic carcinogenesis, as well as the effects of HNF1B on PDAC cells *in vitro*. It is demonstrated that Hnf1b up-regulates during ADM in the presence of Kras^{G12D} and/or pancreatitis, and that deletion of *Hnf1b* in acinar cells prevents Kras^{G12D}-induced PanIN formation. Surprisingly, Hnf1b is dispensable for the formation of ADM *in vitro*, but required for the proliferation of ADM. In addition, deletion of human *HNF1B* in CFPAC-1 cell line impaired the cell growth due to inhibited phospho-AKT, whereas knockout of *Hnf1b* in murine PDAC cell lines promoted proliferation via increasing phospho-AKT. Taken together, our results illustrate that Hnf1b mediates Kras^{G12D}-induced transformation of mature acinar cell and highlight context-dependent functions of Hnf1b in PDAC cells.

5.1 Hnf1b expression does not affect the initiation of ADM

During *in vitro* 3D culture, isolated acini rapidly undergo metaplasia which has dramatic changes in both cellular morphology and gene expression profiles. In our culture conditions, isolated acini became condensed one day after culture, and cystic structures appeared 2 days after culture and became hollow later. In contrast, the mRNA levels of *Hnf1b* increased but rose rather gently (the fold change in expression on day 4 relative to day 0 was <2) (**Figure 4-11B**). Additionally, in the absence of Kras^{G12D}, cerulein and EGF were used to induce ADM, but no dramatic elevation of Hnf1b expression was detected either. This modest upregulation of Hnf1b level may explain why Hnf1b did not determine the *initiation* of ADM.

5.2 Cell proliferation is important for carcinogenesis

The *in vitro* three-dimensional culture of acinar cells (**Figure 4-11** and **4-12**) and *in vivo* data (**Figure 4-6** and **4-15B**) revealed that Hnf1b is dispensable for the initiation of ADM, but is required for the cell proliferation.

ADM and proliferation can be separative processes. On the molecular level, there are also molecules/pathways that play differential roles in these two processes. For example, during cerulein-induced pancreatitis, p21$^{WAF1/Cip1}$(encoded by *Cdkn1a*), a key regulator of cell cycle and cell differentiation was up-regulated in acinar cells, but not in ADM. ADM was enhanced in the absence of p21, but the pancreatic cell proliferation

(indicated by Ki67 staining) did not increase [124]. It was reported that activated Akt1 inhibited ADM during pancreatitis, but supported cell proliferation [125]. These provide a molecular basis for the uncoupling of ADM and proliferation. Here, a high percentage of ADM cells *without* Ki67 expression in cerulein-induced AP was observed (**Figure 4-14** and **15**). Hnf1b was dispensable for ADM, but was required for the proliferation of the metaplastic cells where Hnf1b expression level had elevated. However, whether Hnf1b regulates the proliferation of metaplasia cells through Akt pathways remains to be elucidated.

It is suggested that cell proliferation is an early event required for the transition from ADM to PanIN. Firstly, in Kras^{G12D} mouse, ADMs are more proliferative than early PanIN, and as metaplastic structures grew in size, the percentage of Ki67-positive cells also increased [126]. Additionally, we observed that PanINs are usually bigger than a single acinus. These indicate that PanIN formation requires cell proliferation. Secondly, telomere shortening as the earliest event in pancreatic carcinogenesis[127] can be a result of a cell proliferation during ADM. In human pancreatectomy specimens for either adenocarcinoma or chronic pancreatitis, telomere length was strikingly reduced in most of PanINs compared to adjacent normal structures. Notably, even PanIN-1A, the earliest putative precursor lesion, demonstrated a dramatic reduction of telomere length in 21 of 23 (91%) foci examined [127]. Furthermore, telomere shortening was also observed in ADMs associated with PanIN but not in isolated ADMs [128]. This indicates that there are different fates of ADM based on their proliferation ability. Based on these observations above, I speculate that the proliferative ADMs give rise to PanIN. Hnf1b positively regulates the proliferation of ADM, and therefore promotes Kras^{G12D}-induced PanIN formation. This may explain why fewer lesions were observed in iCKH$^{+/-}$ and iCKH$^{\Delta}$ group (**Figure 4-5**).

In addition, the expression patterns of Hnf1b in acinar cells are parallel to the proliferation indices of the cells during carcinogenesis induced by Kras^{G12D}. There were ~20% of proliferative cells (indicated by Ki67 and PCNA staining) in ADM structures in *Pdx1-Cre; LSL-Kras^{G12D}* and *Nestin-Cre;LSL-Kras^{G12D}* mice [98], which is consistent with that the ductal cells within ADM units are highly proliferative in *Ptf1a-Cre; LSL-Kras^{G12D}* mice [126]. However, the percentage of proliferative cells in mPanIN-1A

dramatically declined (to 2.9% and 1.5% for *Pdx1-Cre; LSL-Kras*^{G12D} and *Nestin-Cre;LSL-Kras*, respectively). And then, in advanced mPanIN-2/3 and cancer cells in *Pdx1-Cre;LSL-Kras*^{G12D};*Ink4a/Arf*$^{lox/lox}$ pancreata, proliferative cells increased to 19.9% and 46.7%, respectively [129].

Interestingly, in this study Hnf1b expression levels (both mRNA and protein) elevated in ADM *in vitro* and *in vivo* (**Figure 4-1** and **4-11**), then declined or lost in most of mPanIN-1 *in vivo*, and then upregulated again in advanced mPanINs and cancerous ducts (**Figure 4-1** and **4-4A**). These results indicate that Hnf1b may be an important player in the proliferation and transition from ADM to PanIN.

5.3 Hnf1b regulates cell proliferation

The transcription factor HNF1A, which is homologous to HNF1B, provides clues to understanding the role of HNF1B. HNF1A works as a heterodimer with HNF1B in kidney extract and liver [76]. In normal pancreas, HNF1A expresses in acinar and endocrine cells, but not in duct cells [130]. A recent publication showed that Hnf1a deficiency in pancreas (*Pdx1Cre; Hnf1a*$^{fl/fl}$ mouse) did not affect pancreas organogenesis, but did promote Kras^{G12D}-induced oncogenesis [131]. Hnf1a recruits a H3K27 demethylase, Kdm6a. Hnf1a and Kdm6a regulate shared target genes did not affect the expression level of Kdm6a but is required for Kdm6a's binding to its target genes. Kdm6a activates acinar differentiation, suppresses acinar cell growth, and is required for Kras^{G12D}-induced oncogenesis.

According to our RNA-sequencing data, it was shown that the freshly isolated iCKH$^\Delta$ cells have elevated *Kdm6a* and *Kdm3b*, while on day 3 after culture, the mRNA levels of *Kdm6a* and *Kdm3b* were lower that iCK cells (Data not shown). This can partially explain why Hnf1b deficiency inhibit Kras^{G12D}-induced proliferation.

Hnf1b regulates cell proliferation through context-dependent pathways. The most relevant study is the deletion of Hnf1b in murine pancreatic duct cells. They observed an increased proliferation of *Hnf1b*-deleted ductal cells and an up-regulation of the YAP pathway [101], suggesting a link between them. Although YAP pathway contributes to proliferation, it was not identified that difference in the mRNA levels of YAP and its

target genes between the acinar cells with and without Hnf1b.

5.5 The role of Hnf1b in PanINs

In this study, it was observed that Hnf1b expression is lost in PanIN1 and then re-expresses in high-grade PanINs and cancerous ducts (**Figure 4-1**). This expression pattern is similar to that of Hnf6, but different to that of Sox9 or Klf5 (which elevates in ADM, and continuously expresses in PanIN 1, 2, 3, and cancer cells) [35], [132]. This indicates there are different sub-cohorts of genes that play different roles during the progression from low-grade PanINs to high-grade PanINs. It is unknown whether the downregulation of Hnf1b in PanIN1 is required for the further cancerous progression. We found that in spontaneous carcinogenesis model Hnf1b haplodeficiency already inhibited Kras^{G12D}-induced precursor lesions (**Figure 4-5**). On the one hand, transformation depends on oncogenic Kras activity but is counteracted by the factors involved in maintenance the acinar cell homeostasis. Although prenatal expression of oncogenic Kras in pancreas usually results in precursor lesions and invasive carcinoma, mature acinar cells are quite resistant to oncogenic Kras-induced transformation unless Kras comes to a high activity to reprogram acinar cells [46]. On the other hand, Hnf1b may be involved in the maintenance of homeostasis of acinar cells. It is possible that Hnf1b expression level in acinar cell is kept under a threshold to keep the cell identity and resist to oncogenic Kras-induced transformation.

5.6 HNF1B and cancer

Hnf1b is a tumor suppressor in murine PDAC cells. In human PDAC tissue, HNF1B expresses in cancerous duct structures, and then decreases in metastatic cancer cells [98, 114]. In murine PDAC tissue, we observed the similar expression pattern of Hnf1b (**Figure 4-1**). However, in murine PDAC cells, Hnf1b preferentially expresses in epithelial cells but gets lost in mesenchymal cells (**Figure 4-27**). In addition, knockout of *Hnf1b* in three murine PDAC cell lines also led to higher proliferation (**Figure 4-28**). These findings suggest that Hnf1b is a suppressor for murine tumor growth.

In contrast, human HNF1B acts as an oncogene in PDAC. According to TCGA data (analyzed by Human Protein Atlas, https://www.proteinatlas.org/ENSG00000275410-HNF1B/pathology/pancreatic+cancer), the PDAC patients with higher mRNA level of

HNF1B associated with worse prognosis (p = 0.017). In human PDAC cell lines, I ablated the expression of HNF1B in three well-differentiated PDAC cells, but only CFPAC-1 showed inhibition of proliferation (**Figure 4-22**). This is likely because that the difference in transcriptome/proteome profiles between these cell lines. For example, according to Collisson's molecular subtyping, CFPAC-1 is ascribed as classic PDAC, while Colo 357 is recognized as quasi-mesenchymal PDAC cell [133], highlighting the heterogeneity on molecular level. Nevertheless, the clinical data of Human Protein Atlas and our *in vitro* data suggest that human HNF1B is an oncogene in PDAC.

Epithelial-mesenchymal transition (EMT) is a process in which epithelial cells lose cell–cell adhesion and apical-basal polarity, but acquire mesenchymal features such as spindle-shaped morphology and higher motility [134]. In cancer, EMT contributes to metastasis and therapy resistance [135]. Several studies have indicated HNF1B is involved EMT but few of them provide evidence for that. In prostate cancer cell lines, HNF1B expression was suppressed directly by enhancer of zeste homolog 2 (EZH2), while overexpression of HNF1B significantly suppresses EZH2-mediated EMT [136]. In human liver cancer cell lines, overexpression of HNF1B significantly elevated the invasion ability and EMT-associated genes [92]. In human PDAC, HNF1B and HNF1A correlate with the differentiation of human PDAC [137]. In this study, however, knockout of *HNF1B* in human and murine PDAC cells *in vitro* did not affect EMT (Figure 4-21 and 27). Considering the difference between *in vitro* culture and pathophysiological conditions [138], it would require a novel mouse model (e.g. *Ptf1aCre^{ER}; Kras^{G12D}; TP53^{R172H}; Hnf1b$^{fl/fl}$*) to analyse whether *Hnf1b* deletion affects cancer survival, EMT or metastasis *in vivo*.

Recently, it was reported that FOXA2 interacts with HNF1B and AP-1 to regulate the differentiation of well-differentiated PDAC cells [139]. In their study, when HNF1B gene was knocked out in CFPAC-1 cells, there was lower circularity index and weaker adhesion, but no EMT-related gene was examined. In this thesis, when HNF1B was knocked out by CRISPR-Cas9, there was no effect on EMT, but reduced proliferation was observed (**Figure 4-21** and **4-22**). This may be due to the difference in methodology. Or otherwise, the role of HNF1B is compensated by other factors. Moreover, ChIP with acinar cells and murine PDAC cells showed that Hnf1b bound to

the regulating sequences in *Pkhd1* and *Cys1* genes in acinar cells, but in cancer cells it preferred to bind to *Pkhd1*, *Cys1, Hnf6* and *Egfr4* (**Figure 4-18**). It is likely that the Hnf1b binding pattern in the genome shifts in different biological contexts. Also, the specific partners with Hnf1b under different conditions require further identification.

6 Conclusion

This project primarily aimed to reveal the role a ductal and progenitor-specific transcription factor Hnf1b in carcinogenesis *in vivo*. Therefore, the expression pattern of Hnf1b in different stages of murine PDAC were investigated. In an inducible mouse model for PDAC carcinogenesis, the role of Hnf1b was evaluated, showing Hnf1b is required for $Kras^{G12D}$-driven carcinogenesis. Furthermore, in $Kras^{G12D}$-expressing pancreas and pancreatic acinar cells, Hnf1b is not essential for the initiation of ADM, but is required for the proliferation of metaplasia cells. This can explain why ablation of Hnf1b in mature acinar cells inhibited PanIN formation. In sum, Hnf1b is a mediator for $Kras^{G12D}$-driven carcinogenesis.

The second aim of this project is to check the effects of HNF1B on cancer cells *in vitro*. Our *in vitro* data showed that HNF1B has different roles in cancer cell proliferation. In murine PDAC cells, Hnf1b expressed in epithelial PDAC cell lines but lost in mesenchymal cells. Ablation of Hnf1b in epithelial PDAC cells resulted in elevated phospho-Akt and accelerated cell proliferation, suggesting that Hnf1b is a tumor suppressor in murine PDAC cells. In contrast, in human PDAC cell lines, HNF1B is a marker for the differentiation of cancer cells, and positively regulates cell proliferation via Akt pathway in specific cell line, which suggests that HNF1B is oncogenic in human PDAC cells.

In summary, our study has investigated the expression patterns and the role of Hnf1b in different stages of PDAC, and contributes to a better understanding of this pancreatic transcription factor in different contexts of pancreatic cancer.

7 Abbreviations

ABC	avidin-biotin complex
ADM	Acinar-to-ductal metaplasia
α-SMA	Alpha-smooth muscle actin
AP	Acute pancreatitis
APS	Ammonium persulfate
BSA	Bovine Serum Albumin
ChIP	Chromatin immunoprecipitation
DAB	3,3'-diaminobenzidine
dH$_2$O	deionized water
DMSO	Dimethyl sulfoxide
EMT	Epithelial mesenchymal transition
FBS	Fetal bovine serum
iC	ptf1a-Cre^{ER}
iCH$^\Delta$	ptf1a-Cre^{ER};Hnf1b$^{fl/fl}$
iCK	ptf1a-Cre^{ER};LSL-Kras^{G12D}
iCKH$^{+/-}$	ptf1a-Cre^{ER};LSL-Kras^{G12D};Hnf1b$^{fl/wt}$
iCKH$^\Delta$	ptf1a-Cre^{ER};LSL-Kras^{G12D};Hnf1b$^{fl/fl}$
IHC	Immunohistochemistry
kDa	kilodalton
Kras	Kirsten rat sarcoma viral oncogene homolog
Krt19	Cytokeratin 19
PanIN	Pancreatic intraepithelial neoplasia
PBS	Phosphate buffered saline
PCR	Polymerase chain reaction
PDAC	Pancreatic ductal adenocarcinoma
PVDF	Polyvinylidene fluoride
P/S	Penicillin and Steptomycin
PSC	Pancreatic stellate cells
PTF1α	Pancreas transcription factor 1 subunit alpha

(q)RT-PCR	(quantitative) Reverse Transcription Polymerase Chain Reaction
rcf	Relative centrifugal force
rpm	revolutions per minute
SDS	Sodium dodecyl sulfate
TCGA	The Cancer Genome Atlas
TGFβ	Transforming growth factor beta
WT	Wild type
µM	micromolar

8 References

1   Da Silva Xavier G. The Cells of the Islets of Langerhans. *J Clin Med* 2018; 7: 54.

2   Pandol SJ. Normal Pancreatic Function. *Pancreapedia* 2015.

3   Tsuji K, Yang M, Jiang P, *et al.* Common bile duct injection as a novel method for establishing red fluorescent protein (RFP)-expressing human pancreatic cancer in nude mice. *J Pancreas* 2006; 7: 193-199.

4   Riskin A, Agostoni C, Shamir R. Physiology of the gastrointestinal tract. In: *Neonatology: A Practical Approach to Neonatal Diseases*. 2012.

5   Reinus JF, Simon D. *Gastrointestinal anatomy and physiology: The essentials*. 2014.

6   Cleveland MH, Sawyer JM, Afelik S, *et al.* Exocrine ontogenies: On the development of pancreatic acinar, ductal and centroacinar cells. *Semin Cell Dev Biol* 2012; 23: 713-719.

7   Inada A, Nienaber C, Katsuta H, *et al.* Carbonic anhydrase II-positive pancreatic cells are progenitors for both endocrine and exocrine pancreas after birth. *Proc Natl Acad Sci U S A* 2008; 105: 19915-19919.

8   Trezíse AEO, Buchwald M. In vivo cell-specific expression of the cystic fibrosis transmembrane conductance regulator. *Nature* 1991; 353: 434-437.

9   Beer RL, Parsons MJ, Rovira M. Centroacinar cells: At the center of pancreas regeneration. *Dev Biol* 2016; 413: 8-15.

10   Apte M V, Haber PS, Applegate TL, *et al.* Periacinar stellate shaped cells in rat pancreas: Identification, isolation, and culture. *Gut* 1998; 43: 128-133.

11   Gartner LP, HIatt JL. *Color Atlas and Text of Histology-sixth editon*. 2014.

12   Ducreux M, Cuhna AS, Caramella C, *et al.* Cancer of the pancreas: ESMO Clinical Practice Guidelines for diagnosis, treatment and follow-up. *Ann Oncol* 2015; 26: v56-v68.

13   Arnold M, Rutherford MJ, Bardot A, *et al.* Progress in cancer survival, mortality, and incidence in seven high-income countries 1995–2014 (ICBP SURVMARK-2): a population-based study. *Lancet Oncol* 2019; 20: 1493-1505.

14   Rhim AD, Mirek ET, Aiello NM, *et al.* EMT and dissemination precede pancreatic tumor formation. *Cell* 2012; 148: 349-361.

15   Makohon-Moore AP, Matsukuma K, Zhang M, *et al.* Precancerous neoplastic

cells can move through the pancreatic ductal system. *Nature* 2018; 561: 201-205.

16   Aichler M, Seiler C, Tost M, *et al.* Origin of pancreatic ductal adenocarcinoma from atypical flat lesions: A comparative study in transgenic mice and human tissues. *J Pathol* 2012; 226: 726-734.

17   Ren B, Liu X, Suriawinata AA. Pancreatic Ductal Adenocarcinoma and Its Precursor Lesions: Histopathology, Cytopathology, and Molecular Pathology. *Am J Pathol* 2019; 189: 9-21.

18   Nagtegaal ID, Odze RD, Klimstra D, *et al.* The 2019 WHO classification of tumours of the digestive system. *Histopathology* 2020; 76: 182.

19   McGinnis T, Bantis L, Madan R, *et al.* Survival outcomes of pancreatic intraepithelial neoplasm (PanIN) versus intraductal papillary mucinous neoplasm (IPMN) associated pancreatic adenocarcinoma. *J Clin Oncol* 2020; 9: 3102.

20   Feldmann G, Beaty R, Hruban RH, *et al.* Molecular genetics of pancreatic intraepithelial neoplasia. *J Hepatobiliary Pancreat Surg* 2007; 14: 224-232.

21   Bryant KL, Mancias JD, Kimmelman AC, *et al.* KRAS: Feeding pancreatic cancer proliferation. *Trends Biochem Sci* 2014; 39: 91-100.

22   Löhr M, Klöppel G, Maisonneuve P, *et al.* Frequency of K-ras mutations in pancreatic intraductal neoplasias associated with pancreatic ductal adenocarcinoma and chronic pancreatitis: A meta-analysis. *Neoplasia* 2005; 7: 17-23.

23   Kanda M, Matthaei H, Wu J, *et al.* Presence of somatic mutations in most early-stage pancreatic intraepithelial neoplasia. *Gastroenterology* 2012; 140: 730-733.

24   Raphael BJ, Hruban RH, Aguirre AJ, *et al.* Integrated Genomic Characterization of Pancreatic Ductal Adenocarcinoma. *Cancer Cell* 2017; 32: 185-203.

25   Guan M, Bender RJ, Pishvaian MJ, *et al.* Molecular and clinical characterization of BRAF mutations in pancreatic ductal adenocarcinomas (PDACs). *J Clin Oncol* 2018; 214-214.

26   Yonezawa S, Higashi M, Yamada N, *et al.* Precursor Lesions of Pancreatic Cancer. *Gut Liver* 2008; 2: 137.

27   Biankin A V, Biankin SA, Kench JG, *et al.* Aberrant p16INK4A and

DPC4/Smad4 expression in intraductal papillary mucinous tumours of the pancreas is associated with invasive ductal adenocarcinoma. *Gut* 2002; 50: 861-868.

28   Hingorani SR, Wang L, Multani AS, *et al.* Trp53R172H and KrasG12D cooperate to promote chromosomal instability and widely metastatic pancreatic ductal adenocarcinoma in mice. *Cancer Cell* 2005; 7: 469-483.

29   Morton JP, Timpson P, Karim SA, *et al.* Mutant p53 drives metastasis and overcomes growth arrest/senescence in pancreatic cancer. *Proc Natl Acad Sci U S A* 2010; 107; 246-251.

30   Iacobuzio-Donahue CA, Klimstra DS, Adsay NV, *et al.* Dpc-4 protein is expressed in virtually all human intraductal papillary mucinous neoplasms of the pancreas: Comparison with conventional ductal adenocarcinomas. *Am J Pathol* 2000; 157: 755-761.

31   Morris JP, Wang SC, Hebrok M. KRAS, Hedgehog, Wnt and the twisted developmental biology of pancreatic ductal adenocarcinoma. *Nat Rev Cancer* 2010; 10: 683–95.

32   Waters AM, Der CJ. KRAS: The critical driver and therapeutic target for pancreatic cancer. *Cold Spring Harb Perspect Med* 2018; 8: a031435.

33   Westphalen CB, Olive KP. Genetically engineered mouse models of pancreatic cancer. *Cancer J* (United States). 2012; 18: 502.

34   Hingorani SR, Petricoin EF, Maitra A, *et al.* Preinvasive and invasive ductal pancreatic cancer and its early detection in the mouse. *Cancer Cell* 2003; 4: 437-450.

35   Kopp JL, von Figura G, Mayes E, *et al.* Identification of Sox9-Dependent Acinar-to-Ductal Reprogramming as the Principal Mechanism for Initiation of Pancreatic Ductal Adenocarcinoma. *Cancer Cell* 2012; 22: 737-750.

36   Ray KC, Bell KM, Yan J, *et al.* Epithelial tissues have varying degrees of susceptibility to KrasG12D-initiated tumorigenesis in a mouse model. *PLoS One* 2011; 6: e16786.

37   Habbe N, Shi G, Meguid RA, *et al.* Spontaneous induction of murine pancreatic intraepithelial neoplasia (mPanIN) by acinar cell targeting of oncogenic Kras in adult mice. *Proc Natl Acad Sci U S A* 2008; 105: 18913-18918.

38   Guerra C, Schuhmacher AJ, Cañamero M, *et al.* Chronic Pancreatitis Is Essential for Induction of Pancreatic Ductal Adenocarcinoma by K-Ras

Oncogenes in Adult Mice. *Cancer Cell* 2007; 11: 291-302.

39   Giroux V, Rustgi AK. Metaplasia: Tissue injury adaptation and a precursor to the dysplasia-cancer sequence. *Nat Rev Cancer* 2017;17:594-604.

40   Storz P. Acinar cell plasticity and development of pancreatic ductal adenocarcinoma. *Nat Revies Gastroenterol Hepatol* 2017;14:296-304.

41   Liu J, Akanuma N, Liu C, *et al.* TGF-β1 promotes acinar to ductal metaplasia of human pancreatic acinar cells. *Sci Rep* 2016;6:1-11.

42   Garcia-Carracedo D, Yu CC, Akhavan N, *et al.* Smad4 loss synergizes with TGFα overexpression in promoting pancreatic metaplasia, PanIN development, and fibrosis. *PLoS One* 2015;10:e01250851

43   Korc M, Chandrasekar B, Yamanaka Y, *et al.* Overexpression of the epidermal growth factor receptor in human pancreatic cancer is associated with concomitant increases in the levels of epidermal growth factor and transforming growth factor alpha. *J Clin Invest* 1992;90:1352-1360.

44   Sandgren EP, Luetteke NC, Palmiter RD, *et al.* Overexpression of TGFα in transgenic mice: Induction of epithelial hyperplasia, pancreatic metaplasia, and carcinoma of the breast. *Cell* 1990;61:1121–35.

45   Neuhöfer P, Roake CM, Kim SJ, *et al.* Acinar cell clonal expansion in pancreas homeostasis and carcinogenesis. *Nature* 2021;597:715-719.

46   Ardito CM, Grüner BM, Takeuchi KK, *et al.* EGF Receptor Is Required for KRAS-Induced Pancreatic Tumorigenesis. *Cancer Cell* 2012;22:304-317.

47   Navas C, Hernández-Porras I, Schuhmacher AJ, *et al.* EGF Receptor Signaling Is Essential for K-Ras Oncogene-Driven Pancreatic Ductal Adenocarcinoma. *Cancer Cell* 2012; 22: 318-330.

48   Principe DR, Doll JA, Bauer J, *et al.* TGF-β: Duality of function between tumor prevention and carcinogenesis. *J Natl Cancer Inst* 2014;106.

49   Shi Y, Massagué J. Mechanisms of TGF-β signaling from cell membrane to the nucleus. *Cell* 2003;113:685–700.

50   Zhang YE. Non-Smad pathways in TGF-β signaling. *Cell Res* 2009;19:128–39.

51   Bardeesy N, Cheng KH, Berger JH, *et al.* Smad4 is dispensable for normal pancreas development yet critical in progression and tumor biology of pancreas cancer. *Genes Dev* 2006;20:3130-3146.

52   Leung L, Radulovich N, Zhu CQ, *et al.* Loss of canonical Smad4 signaling promotes KRAS driven malignant transformation of human pancreatic duct

epithelial cells and metastasis. *PLoS One* 2013;8:e84366.

53   Ijichi H, Chytil A, Gorska AE, *et al.* Aggressive pancreatic ductal adenocarcinoma in mice caused by pancreas-specific blockade of transforming growth factor-β signaling in cooperation with active Kras expression. *Genes Dev* 2006;20:3147-3160.

54   Adrian K, Strouch MJ, Zeng Q, *et al.* Tgfbr1 haploinsufficiency inhibits the development of murine mutant Kras-induced pancreatic precancer. *Cancer Res* 2009;69:9169-9174.

55   Chuvin N, Vincent DF, Pommier RM, *et al.* Acinar-to-Ductal Metaplasia Induced by Transforming Growth Factor Beta Facilitates KRASG12D-driven Pancreatic Tumorigenesis. *CMGH* 2017;4:263-282.

56   MacDonald BT, Tamai K, He X. Wnt/β-Catenin Signaling: Components, Mechanisms, and Diseases. *Dev Cell* 2009;17:9–26.

57   Gordon MD, Nusse R. Wnt signaling: Multiple pathways, multiple receptors, and multiple transcription factors. *J Biol Chem* 2006;281:22429-22433.

58   Zhang Y, Morris IV JP, Yan W, *et al.* Canonical Wnt signaling is required for pancreatic carcinogenesis. *Cancer Res* 2013;73:4909-4922.

59   Sano M, Driscoll DR, DeJesus-Monge WE, *et al.* Activation of WNT/β-Catenin Signaling Enhances Pancreatic Cancer Development and the Malignant Potential Via Up-regulation of Cyr61. *Neoplasia (United States)* 2016;18:785–94.

60   Morris IV JP, Cano DA, Sekine S, *et al.* β-catenin blocks Kras-dependent reprogramming of acini into pancreatic cancer precursor lesions in mice. *J Clin Invest* 2010;120:508–20.

61   Krah NM, De La O. JP, Swift GH, *et al.* The acinar differentiation determinant PTF1A inhibits initiation of pancreatic ductal adenocarcinoma. *Elife* 2015;4:e07125.

62   Shi G, Zhu L, Sun Y, *et al.* Loss of the Acinar-Restricted Transcription Factor Mist1 Accelerates Kras-Induced Pancreatic Intraepithelial Neoplasia. *Gastroenterology* 2009;136:1368-1378.

63   Hale MA, Swift GH, Hoang CQ, *et al.* The nuclear hormone receptor family member NR5A2 controls aspects of multipotent progenitor cell formation and acinar differentiation during pancreatic organogenesis. *Development* 2014;141:3123-3133.

64   Von Figura G, Morris IV JP, Wright CVE, *et al.* Nr5a2 maintains acinar cell differentiation and constrains oncogenic Kras-mediated pancreatic neoplastic initiation. *Gut* 2014;63:656-664.

65   Flandez M, Cendrowski J, Cañamero M, *et al.* Nr5a2 heterozygosity sensitises to, and cooperates with, inflammation in KRasG12V-driven pancreatic tumourigenesis. *Gut* 2014;63:647-655.

66   Cobo I, Martinelli P, Flández M, *et al.* Transcriptional regulation by NR5A2 links differentiation and inflammation in the pancreas. *Nature* 2018;554:533-537.

67   Hale MA, Kagami H, Shi L, *et al.* The homeodomain protein PDX1 is required at mid-pancreatic development for the formation of the exocrine pancreas. *Dev Biol* 2005;286:225-237.

68   Holland AM, Hale MA, Kagami H, *et al.* Experimental control of pancreatic development and maintenance. *Proc Natl Acad Sci U S A* 2002;99:12236-12241.

69   Rooman I, Heremans Y, Heimberg H, *et al.* Modulation of rat pancreatic acinoductal transdifferentiation and expression of PDX-1 in vitro. *Diabetologia* 2000;43:907-914.

70   Roy N, Takeuchi KK, Ruggeri JM, *et al.* PDX1 dynamically regulates pancreatic ductal adenocarcinoma initiation and maintenance. *Genes Dev* 2016;30:2669-2683.

71   Pierreux CE, Poll A V, Kemp CR, *et al.* The Transcription Factor Hepatocyte Nuclear Factor-6 Controls the Development of Pancreatic Ducts in the Mouse. *Gastroenterology* 2006;130:532-541.

72   Zhang H, Ables ET, Pope CF, *et al.* Multiple, temporal-specific roles for HNF6 in pancreatic endocrine and ductal differentiation. *Mech Dev* 2009;126:958-973.

73   Prévot PP, Simion A, Grimont A, *et al.* Role of the ductal transcription factors HNF6 and Sox9 in pancreatic acinar-to-ductal metaplasia. *Gut* 2012;61:1723-1732.

74   Lau HH, Ng NHJ, Loo LSW, *et al.* The molecular functions of hepatocyte nuclear factors – In and beyond the liver. *J Hepatol* 2018;68:1033-1048.

75   Wu G, Bohn S, Ryffel GU. The HNF1β transcription factor has several domains involved in nephrogenesis and partially rescues Pax8/lim1-induced kidney malformations. *Eur J Biochem* 2004;271:3715–28.

76   Rey-Campos J, Chouard T, Yaniv M, *et al.* vHNF1 is a homeoprotein that activates transcription and forms heterodimers with HNF1. *EMBO J* 1991;10:1445-1457.

77   Harries LW, Brown JE, Gloyn AL. Species-specific differences in the expression of the HNF1A, HNF1B and HNF4A genes. *PLoS One* 2009;4:e7850.

78   Poll A V, Pierreux CE, Lokmane L, *et al.* A vHNF1/TCF2-HNF6 cascade regulates the transcription factor network that controls generation of pancreatic precursor cells. *Diabetes* 2006;55:61-69.

79   Solar M, Cardalda C, Houbracken I, *et al.* Pancreatic Exocrine Duct Cells Give Rise to Insulin-Producing β Cells during Embryogenesis but Not after Birth. *Dev Cell* 2009;17:849–60.

80   Barbacci E, Reber M, Ott MO, *et al.* Variant Hepatocyte Nuclear Factor 1 is required for visceral endoderm specification. *Development* 1999;126:4795-4805.

81   Haumaitre C, Barbacci E, Jenny M, *et al.* Lack of TCF2/vHNF1 in mice leads to pancreas agenesis. *Proc Natl Acad Sci U S A* 2005;102:1490-1495.

82   De Vas MG, Kopp JL, Heliot C, *et al.* Hnf1b controls pancreas morphogenesis and the generation of Ngn3+ endocrine progenitors. *Development* 2015;142:871-882.

83   El-Khairi R, Vallier L. The role of hepatocyte nuclear factor 1β in disease and development. Diabetes, Obes. Metab. 2016;18:23–32.

84   Horikawa Y, Iwasaki N, Hara M, *et al.* Mutation in hepatocyte nuclear factor-1ß gene (TCF2) associated with MODY. *Nat Genet* 1997;17:384-385.

85   Brackenridge A, Pearson ER, Shojaee-Moradie F, *et al.* Contrasting insulin sensitivity of endogenous glucose production rate in subjects with hepatocyte nuclear factor-1β and -1α mutations. *Diabetes* 2006;55:405-411.

86   Bingham C, Hattersley AT. Renal cysts and diabetes syndrome resulting from mutations in hepatocyte nuclear factor-1β. Nephrol. Dial. Transplant. 2004;19:2703–8.

87   Shao A, Chan SC, Igarashi P. Role of transcription factor hepatocyte nuclear factor-1beta in polycystic kidney disease. *Cell Signal* 2020;71:109568.

88   Edghill EL, Bingham C, Ellard S, *et al.* Mutations in hepatocyte nuclear factor-1β and their related phenotypes. *J Med Genet* 2006;43:84–90.

89   Bockenhauer D, Jaureguiberry G. HNF1B-associated clinical phenotypes: the kidney and beyond. *Pediatr Nephrol* 2016;31:707-714.

90   Wang W, Hayashi Y, Ninomiya T, *et al.* Expression of HNF-1a and HNF-1β in various histological differentiations of hepatocellular carcinoma. *J Pathol* 1998;184:272–278.

91   Yu DD, Jing YY, Guo SW, *et al.* Overexpression of hepatocyte nuclear factor-1beta predicting poor prognosis is associated with biliary phenotype in patients with hepatocellular carcinoma. *Sci Rep* 2015;5:1-13.

92   Zhu JN, Jiang L, Jiang JH, *et al.* Hepatocyte nuclear factor-1beta enhances the stemness of hepatocellular carcinoma cells through activation of the Notch pathway. *Sci Rep* 2017;7:1-11.

93   Muglia VF, Prando A. Renal cell carcinoma: histological classification and correlation with imaging findings. *Radiol Bras* 2015;48:166-174.

94   Buchner A, Castro M, Hennig A, *et al.* Downregulation of HNF-1B in renal cell carcinoma is associated with tumor progression and poor prognosis. *Urology* 2010;76:507-e6.

95   Sun M, Tong P, Kong W, *et al.* HNF1B loss exacerbates the development of chromophobe renal cell carcinomas. *Cancer Res* 2017;77:5313-5326.

96   Walsh N, Zhang H, Hyland PL, *et al.* Agnostic Pathway/Gene Set Analysis of Genome-Wide Association Data Identifies Associations for Pancreatic Cancer. *J Natl Cancer Inst* 2019;111:557-567.

97   Klein AP, Wolpin BM, Risch HA, *et al.* Genome-wide meta-analysis identifies five new susceptibility loci for pancreatic cancer. *Nat Commun* 2018;9:1-11.

98   Hoskins JW, Jia J, Flandez M, *et al.* Transcriptome analysis of pancreatic cancer reveals a tumor suppressor function for HNF1A. *Carcinogenesis* 2014;35:2670-2678.

99   Diaferia GR, Balestrieri C, Prosperini E, *et al.* Dissection of transcriptional and cis -regulatory control of differentiation in human pancreatic cancer . *EMBO J* 2016;35:595-617.

100   Janky R, Binda MM, Allemeersch J, *et al.* Prognostic relevance of molecular subtypes and master regulators in pancreatic ductal adenocarcinoma. *BMC Cancer* 2016;16:1-15.

101   Quilichini E, Fabre M, Dirami T, *et al.* Pancreatic Ductal Deletion of Hnf1b Disrupts Exocrine Homeostasis, Leads to Pancreatitis, and Facilitates

Tumorigenesis. *CMGH* 2019;8:487-511.

102 Coffinier C, Gresh L, Fiette L, *et al.* Bile system morphogenesis defects and liver dysfunction upon targeted deletion of HNF1β. *Development* 2002;129:1829–38.

103 Kopinke D, Brailsford M, Pan FC, *et al.* Ongoing Notch signaling maintains phenotypic fidelity in the adult exocrine pancreas. *Dev Biol* 2012;362:57-64.

104 Jackson EL, Willis N, Mercer K, *et al.* Analysis of lung tumor initiation and progression using conditional expression of oncogenic K-ras. *Genes Dev* 2001;15:3243-3248.

105 Stemmer M, Thumberger T, Del Sol Keyer M, *et al.* CCTop: An intuitive, flexible and reliable CRISPR/Cas9 target prediction tool. *PLoS One* 2015;10:e0124633.

106 Ferreira RMM, Sancho R, Messal HA, *et al.* Duct- and Acinar-Derived Pancreatic Ductal Adenocarcinomas Show Distinct Tumor Progression and Marker Expression. *Cell Rep* 2017;21:966-978.

107 Daniluk J, Liu Y, Deng D, *et al.* An NF-κB pathway-mediated positive feedback loop amplifies Ras activity to pathological levels in mice. *J Clin Invest* 2012;122:1519–28.

108 Collins MA, Bednar F, Zhang Y, *et al.* Oncogenic Kras is required for both the initiation and maintenance of pancreatic cancer in mice. *J Clin Invest* 2012;122:639-653.

109 Jochheim LS, Odysseos G, Hidalgo-Sastre A, *et al.* The neuropeptide receptor subunit RAMP1 constrains the innate immune response during acute pancreatitis in mice. *Pancreatology* 2019;19:541-547.

110 Rooman I, Real FX. Pancreatic ductal adenocarcinoma and acinar cells: A matter of differentiation and development? *Gut* 2012;61:449-458.

111 Shi G, Direnzo D, Qu C, *et al.* Maintenance of acinar cell organization is critical to preventing Kras-induced acinar-ductal metaplasia. *Oncogene* 2013;32:1950-1958.

112 Pinho A V, Rooman I, Reichert M, *et al.* Adult pancreatic acinar cells dedifferentiate to an embryonic progenitor phenotype with concomitant activation of a senescence programme that is present in chronic pancreatitis. *Gut* 2011;60:958-966.

113 Maiti B, Li J, De Bruin A, *et al.* Cloning and characterization of mouse E2F8, a

novel mammalian E2F family member capable of blocking cellular proliferation. *J Biol Chem* 2005;280:18211-18220.

114   Deng Q, Wang Q, Zong WY, *et al.* E2F8 contributes to human hepatocellular carcinoma via regulating cell proliferation. *Cancer Res* 2010;70:782-791.

115   Zhang AMY, Magrill J, de Winter TJJ, *et al.* Endogenous Hyperinsulinemia Contributes to Pancreatic Cancer Development. *Cell Metab* 2019;30:403-404.

116   Liou GY, Döppler H, Necela B, *et al.* Macrophage-secreted cytokines drive pancreatic acinar-to-ductal metaplasia through NF-KB and MMPs. *J Cell Biol* 2013;202:563-577.

117   R. J, M.M. B, J. A, *et al.* Prognostic relevance of molecular subtypes and master regulators in pancreatic ductal adenocarcinoma. *BMC Cancer* 2016;16:1-15.

118   Deer EL, González-Hernández J, Coursen JD, *et al.* Phenotype and genotype of pancreatic cancer cell lines. *Pancreas* 2010;39:425.

119   Kornfeld JW, Baitzel C, Könner AC, *et al.* Obesity-induced overexpression of miR-802 impairs glucose metabolism through silencing of Hnf1b. *Nature* 2013;494:111-115.

120   Long Z, Cao M, Su S, *et al.* Inhibition of hepatocyte nuclear factor 1b induces hepatic steatosis through DPP4/NOX1-mediated regulation of superoxide. *Free Radic Biol Med* 2017;113:71-83.

121   Falasca M, Selvaggi F, Buus R, *et al.* Targeting Phosphoinositide 3-Kinase Pathways in Pancreatic Cancer – from Molecular Signalling to Clinical Trials. *Anticancer Agents Med Chem* 2012;11:455-463.

122   Oki S, Ohta T, Shioi G, *et al.* Ch IP -Atlas: a data-mining suite powered by full integration of public Ch IP -seq data . *EMBO Rep* 2018;19:e46255.

123   Sablina AA, Hector M, Colpaert N, *et al.* Identification of PP2A complexes and pathways involved in cell transformation. *Cancer Res* 2010;70:10474-10484.

124   Grabliauskaite K, Hehl AB, Seleznik GM, *et al.* P21WAF1/Cip1 limits senescence and acinar-to-ductal metaplasia formation during pancreatitis. *J Pathol* 2015;235:502-514.

125   Sarker RS, Steiger K. A critical role for Akt1 signaling in acute pancreatitis progression. *J Pathol* 2020;251:1–3.

126   Zhu L, Shi G, Schmidt CM, *et al.* Acinar cells contribute to the molecular heterogeneity of pancreatic intraepithelial neoplasia. *Am J Pathol*

2007;171:263-273.

127 Van Heek NT, Meeker AK, Kern SE, *et al.* Telomere shortening is nearly universal in pancreatic intraepithelial neoplasia. *Am J Pathol* 2002;161:1541-1547.

128 Hong SM, Heaphy CM, Shi C, *et al.* Telomeres are shortened in acinar-to-ductal metaplasia lesions associated with pancreatic intraepithelial neoplasia but not in isolated acinar-to-ductal metaplasias. *Mod Pathol* 2011;24:256-266.

129 Seeley ES, Carrière C, Goetze T, *et al.* Pancreatic cancer and precursor pancreatic intraepithelial neoplasia lesions are devoid of primary cilia. *Cancer Res* 2009;69:422-430.

130 Nammo T, Yamagata K, Hamaoka R, *et al.* Expression profile of MODY3/HNF-1α protein in the developing mouse pancreas. *Diabetologia* 2002;45:1142–53.

131 Kalisz M, Bernardo E, Beucher A, *et al.* HNF1A recruits KDM6A to activate differentiated acinar cell programs that suppress pancreatic cancer. *EMBO J* 2020;39:e102808.

132 He P, Yang JW, Yang VW, *et al.* Krüppel-like Factor 5, Increased in Pancreatic Ductal Adenocarcinoma, Promotes Proliferation, Acinar-to-Ductal Metaplasia, Pancreatic Intraepithelial Neoplasia, and Tumor Growth in Mice. *Gastroenterology* 2018;154:1494-1508.

133 Collisson EA, Sadanandam A, Olson P, *et al.* Subtypes of pancreatic ductal adenocarcinoma and their differing responses to therapy. *Nat Med* 2011;17:500-503.

134 Lamouille S, Xu J, Derynck R. Molecular mechanisms of epithelial-mesenchymal transition. *Nat Rev Mol Cell Biol* 2014;15:178-196.

135 Smith B, Bhowmick N. Role of EMT in Metastasis and Therapy Resistance. *J Clin Med* 2016;5:17.

136 Wang J, He C, Gao P, *et al.* HNF1B-mediated repression of SLUG is suppressed by EZH2 in aggressive prostate cancer. *Oncogene* 2020;39:1335-1346.

137 Rekin's Janky, Maria Mercedes Binda, Joke Allemeersch, *et al.* Prognostic relevance of molecular subtypes and master regulators in pancreatic ductal adenocarcinoma. *BMC Cancer* 2016;16:1-15.

138 Aiello NM, Maddipati R, Norgard RJ, *et al.* EMT Subtype Influences Epithelial Plasticity and Mode of Cell Migration. *Dev Cell* 2018;45:681-695.

139   Milan M, Balestrieri C, Alfarano G, *et al.* FOXA 2 controls the cis -regulatory networks of pancreatic cancer cells in a differentiation grade-specific manner . *EMBO J* 2019;38:e102161.

Acknowledgments